AD-A155 031 A REVIEW OF THE PHYSICS AND RESPONSE MODELS FOR BURNOUT OF SEMICONDUCTOR DEVICES(U) LAWRENCE LIVERMORE NATIONAL LAB CA W J ORVIS ET AL. DEC 84 UCRL-53573 1/1

UNCLASSIFIED W-7405-ENG-48 F/G 9/1 NL

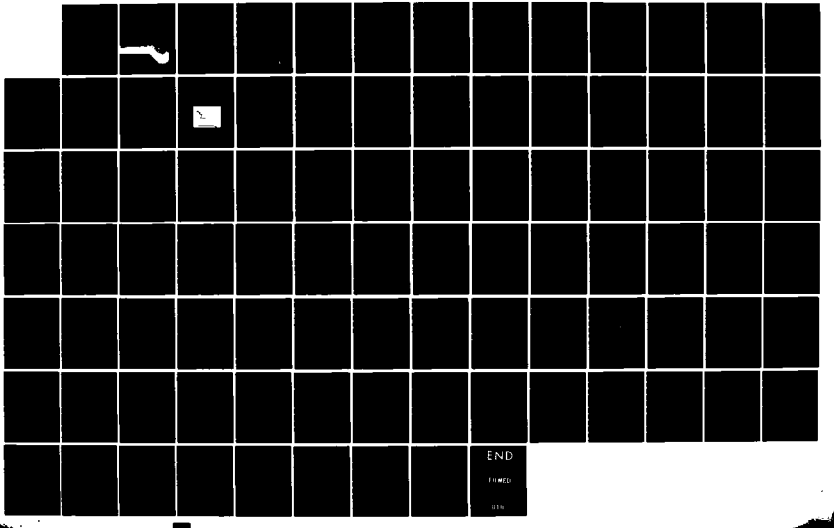

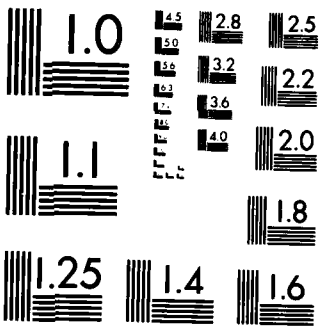

MICROCOPY RESOLUTION TEST CHART
NATIONAL BUREAU OF STANDARDS-1963-A

UCRL-53573

A Review of the Physics and Response Models for Burnout of Semiconductor Devices

Final Report

W. J. Orvis

G. H. Khanaka

J. H. Yee

December 1984

Lawrence Livermore National Laboratory

DISCLAIMER

UCRL-53573
Distribution Category UC-38

A Review of the Physics and Response Models for Burnout of Semiconductor Devices

Final Report

W. J. Orvis

G. H. Khanaka

J. H. Yee

Manuscript date: December 1984

LAWRENCE LIVERMORE NATIONAL LABORATORY
University of California • Livermore, California • 94550

A REVIEW OF THE PHYSICS AND RESPONSE MODELS FOR BURNOUT OF SEMICONDUCTOR DEVICES*

W. J. Orvis, G. H. Khanaka, J. H. Yee

ABSTRACT

Physical mechanisms that cause semiconductor devices to fail from electrical overstress--particularly, EMP-induced electrical stress--are described in light of the current literature and the authors' own research. A major concern is the cause and effects of second breakdown phenomena in p-n junction devices. Models of failure thresholds are evaluated for their inherent errors and for their ability to represent the relevant physics. Finally, the response models that relate electromagnetic stress parameters to appropriate failure-threshold parameters are discussed.

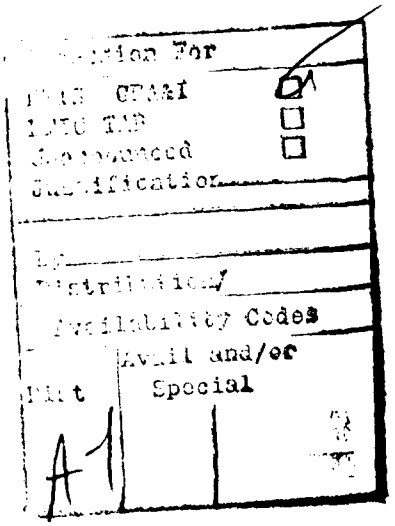

*Work performed under the auspices of the U. S. Department of Energy by the Lawrence Livermore National Laboratory under contract number W-7405-ENG-48. This work was funded by the Defense Nuclear Agency through the Air Force Weapons Laboratory.

CONTENTS

ILLUSTRATIONS

I INTRODUCTION

Systems analysts and electronic designers are often charged with assessing the survivability of electronic systems in an electrical overstress (EOS) environment. Such an assessment involves comparing the failure thresholds for the system in question with the expected EOS threat. Several inherent problems prevent this from being a straightforward engineering task:

- It is difficult to obtain accurate theoretical or experimental values of the failure thresholds for any particular electronic device.
- Real EOS stress parameters must be compared with the idealized stresses used in experimentally or theoretically derived failure threshold data. Overly conservative estimates can result in an over-hardened system, unnecessarily increasing costs, delaying schedules, and degrading system performance. On the other hand, underestimating the threshold limits can result in a system that is vulnerable to EOS-induced failures.

To characterize an electronic system it is first necessary to characterize its individual components. The factors that affect the failure thresholds in semiconductor components include variations in manufacturing processes, non-uniform test methods, variations among devices of different types (and even among devices of the same type), and the existence of many possible failure mechanisms.

The characterization is further complicated by the wide range of electromagnetic environments that cause EOS effects:

- Electromagnetic pulse (EMP).
- Nuclear electromagnetic pulse (NEMP).
- Lightning electromagnetic pulse (LEMP).
- Electromagnetic interference (EMI).
- Electrostatic discharge (ESD).
- Intersystem and intrasystem electromagnetic compatibility (EMC).
- System-generated electromagnetic pulse (SGEMP or STP).
- Other transient radiation-induced electromagnetic effects (TREE).

Four of these environments are compared in Fig. 1 (from Pierce, Ref. 1). Note that Fig. 1 shows only some representative voltages for different types of pulses and that the available currents or powers will also differ. Figure 2 (from Durgin, Ref. 2) compares the spectral contents of several different types of EOS.

Most experimental failure thresholds are obtained by applying a series of high-voltage square pulses across a device's terminals (Ref. 3-5). (There are exceptions: Tasca has conducted EMP experiments with different pulse shapes, including triangular and damped sine waves; see Ref. 3. Other researchers have used a resistance-capacitance network to simulate the human body for ESD testing; see Refs. 6, 7.) In all of these experiments, pulse voltage and length were varied to determine the delay time to failure and the failure power or energy. Data that are based, in most cases, on square-pulse excitation must then be related to the decidedly non-square pulse stresses shown in Fig. 1. A further complication is that the data vary tremendously, even among devices from the same wafer, although the variation is much larger among devices from different wafers and among devices from different manufacturers (see Fig. 3, Ref. 8).

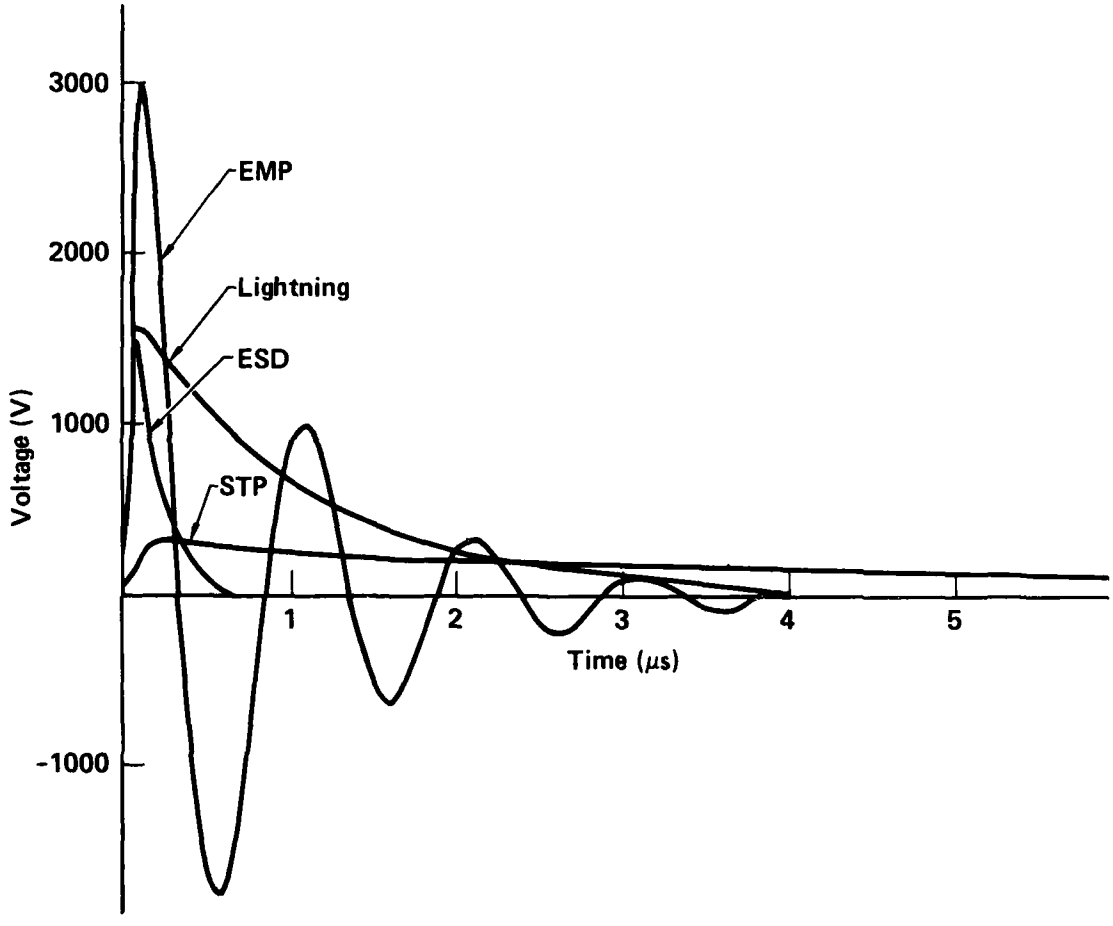

Figure 1. A comparison of several EOS threats (after Ref. 1).

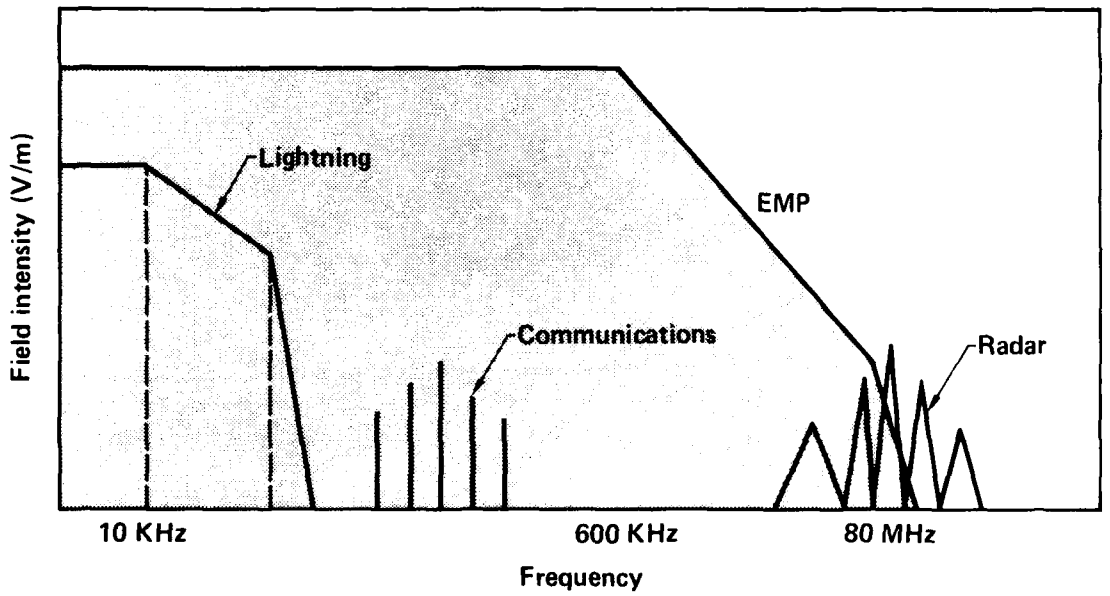

Figure 2. A comparison of the spectral content of several EOS threats (after Ref. 2).

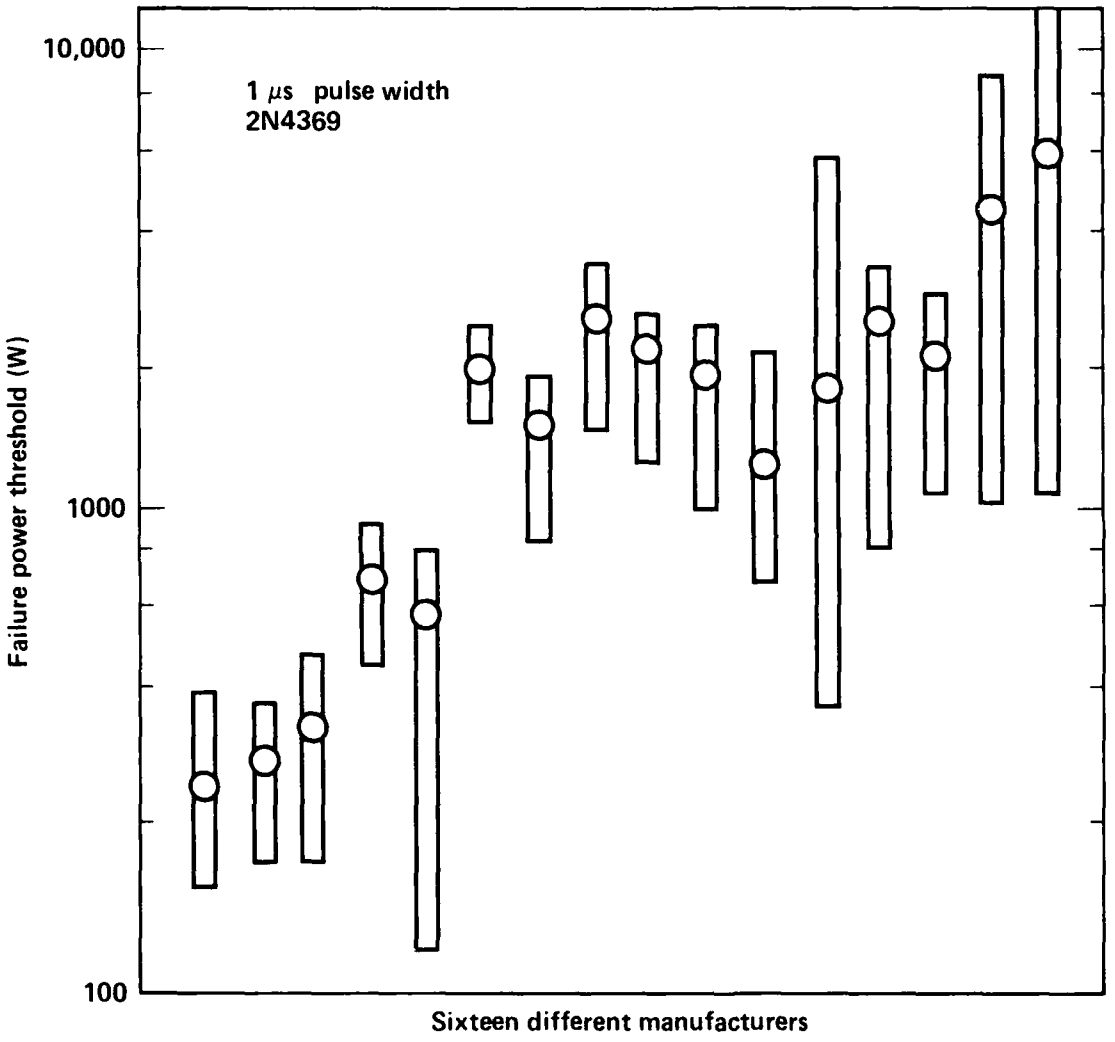

Figure 3. Failure power threshold variability vs manufacturers for 2N4369 transistors (after Ref. 8).

Test data are difficult to access because they have been gathered by a number of government agencies and private companies. Three databases--VZAP, GIDEP, and SCORCH--have been established to obtain and catalog this information (Ref. 9). VZAP is maintained by the Reliability Analysis Center at the Rome Air Development Center at Griffiss Air Force Base in New York, GIDEP is part of the Government-Industry Data Exchange Program managed by the Naval Material Command, and SCORCH is managed by the Air Force Weapons Laboratory at Kirtland AFB in New Mexico.

Normal semiconductor device operation is described with the electron- and hole-continuity equations and Poisson's equation. To describe semiconductor operation during a high-voltage transient, the heat-flow equation and the thermal and high-field dependencies of the coefficients of the equations must be included. This results in a set of coupled, nonlinear, stiff*, partial differential equations for semiconductor device operation and heat flow.
The electron- and hole-continuity equations,

$$\frac{\partial n}{\partial t} = G - U + (1/q)\nabla J_n \tag{1}$$

and

$$\frac{\partial p}{\partial t} = G - U - (1/q)\nabla J_p \tag{2}$$

where

$$J_n = qn\mu_n E + qD_n\nabla n \tag{3}$$

and

$$J_p = qp\mu_p E - qD_p\nabla p \tag{4}$$

are the electron- and hole-current density equations.
Poisson's equation is

$$\nabla^2\varphi = -q(p - n + N)/\varepsilon, \tag{5}$$

and the heat flow equation is

$$\rho c\frac{\partial T}{\partial t} = \nabla\cdot(K\nabla T) + |J\cdot E| \ , \tag{6}$$

$D_n(\|E\|,T,N)$	Electron diffusion coefficient
$D_p(\|E\|,T,N)$	Hole diffusion coefficient
E	Electric field
$G(\|E\|,T,n,p)$	Avalanche generation term
$J = J_n + J_p$	Total carrier current density
J_n	Electron current density
J_p	Hole current density
$K(T)$	Thermal conductivity
$N = N_D - N_A$	Net positive doping density

*Stiff equations describe phenomena of interest that occur over drastically different timescales.

any other times, the models will give erroneous results because of the large changes in the material parameters at elevated temperatures (Ref. 28).

T. Misawa-- In 1966, Misawa performed an analytical solution to Eqs. 1 through 5 (Ref. 29). To perform this solution, Misawa assumed one-dimensional equations, ignored all electrical diffusion, and ignored all recombination effects. He assumed constant avalanche generation near the breakdown voltage and then performed a small-signal, plane-wave analysis on the resulting equations. The resulting solution describes the operation of a semiconductor junction, biased near the breakdown voltage, before any significant amount of heat is generated.

$$E = C_1 e^{igx} + C_2 e^{-igx} + \frac{2\alpha - i\omega}{g^2} J \quad , \tag{24}$$

$$J_n = \frac{i}{2}(g - \omega) C_1 e^{igx} - \frac{i}{2}(g - \omega) C_2 e^{-igx} - \frac{\alpha' J'}{g^2} J \quad , \tag{25}$$

and

$$J_p = -\frac{i}{2}(g - \omega) C_1 e^{igx} + \frac{i}{2}(g - \omega) C_2 e^{-igx} - \frac{\alpha' J'}{g^2} J \quad , \tag{26}$$

where

$$g = (\omega^2 - 2\alpha' J' + i2\omega\alpha)^{1/2} \quad , \tag{27}$$

$$C_1 = \frac{1}{\Delta} \begin{bmatrix} J_{ns} + \dfrac{\alpha' J'}{g^2} J & -\dfrac{i}{2}(g + \omega) \\ J_{ps} + \dfrac{\alpha' J'}{g^2} J & \dfrac{i}{2}(g - \omega) e^{-ig} \end{bmatrix} \quad , \tag{28}$$

$$C_2 = \frac{1}{\Delta} \begin{bmatrix} \dfrac{i}{2}(g - \omega) & J_{ns} + \dfrac{\alpha' J'}{g^2} J \\ -\dfrac{i}{2}(g + \omega) e^{ig} & J_{ps} + \dfrac{\alpha' J'}{g^2} J \end{bmatrix} \quad , \tag{29}$$

and

$$\Delta = (1/4)[(g + \omega)^2 e^{ig} - (g - \omega)^2 e^{-ig}] \quad . \tag{30}$$

In Eqs. 25 through 30, the primed components are the steady-state DC parts of the equation, and the other variables are the small-signal AC values. The angular frequency of the applied small signal is ω with a wave vector g. Also, α is the constant avalanche coefficient, α' is the rate of change of α with respect to the electric field, J_{ps} is the injection current boundary condition on the p side, and J_{ns} is the injection current boundary condition on the n side. Note that all of the variables have been normalized (see Ref. 29).

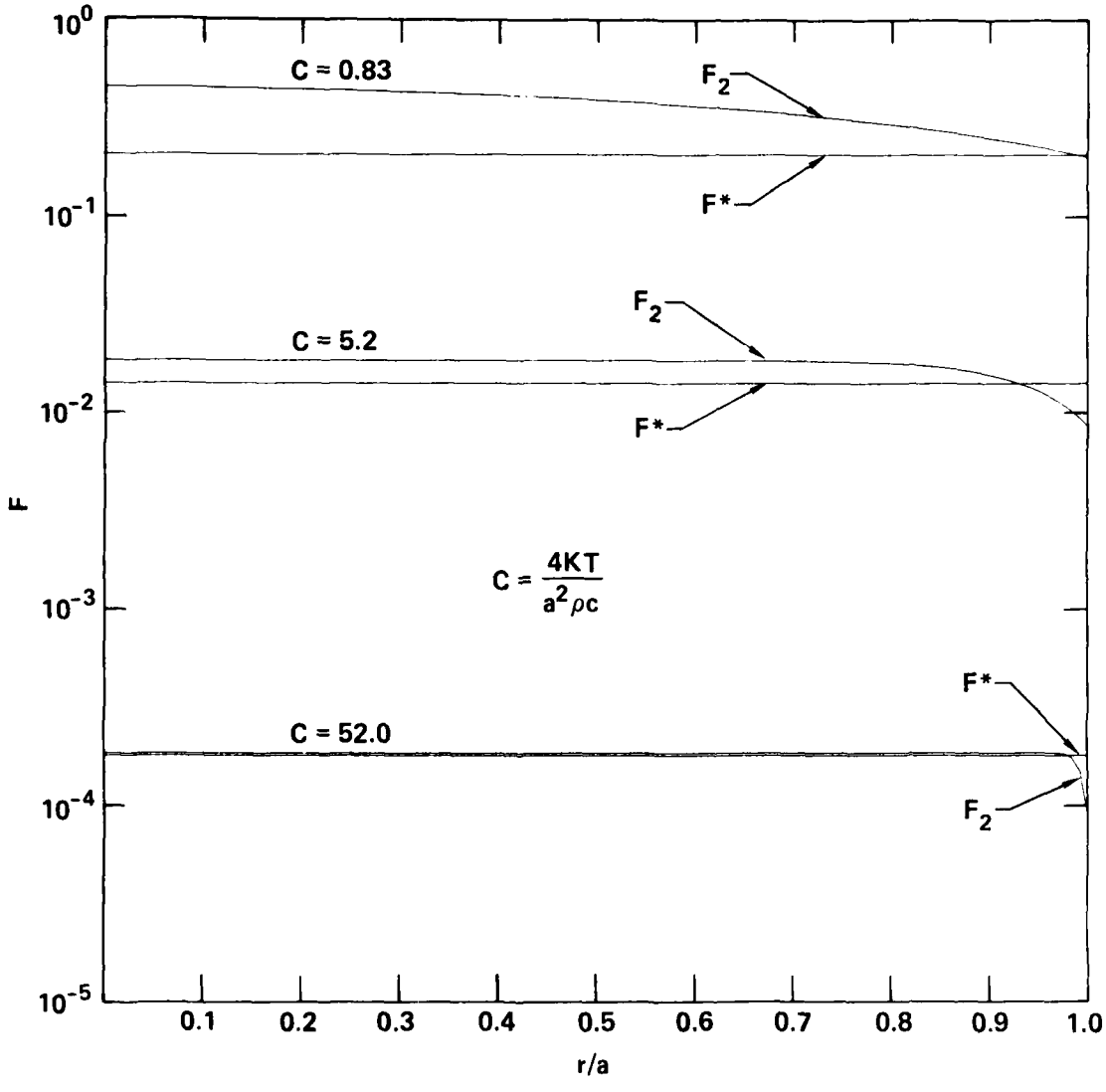

Figure 8. A comparison of Eq. 19 (F_2) with the approximation Eq. 20 (F^*).

$$F_2 = \frac{2kt}{a^2}\left[1 - \frac{2a}{r} i^2\mathrm{erfc}\left(\frac{a-r}{2\sqrt{kt}} \right) + \frac{2a}{r} i^2\mathrm{erfc}\left(\frac{a+r}{2\sqrt{kt}} \right) \right.$$

$$\left. - \frac{4\sqrt{kt}}{r} i^3\mathrm{erfc}\left(\frac{a-r}{2\sqrt{kt}} \right) + \frac{4\sqrt{kt}}{r} i^3\mathrm{erfc}\left(\frac{a+r}{2\sqrt{kt}} \right) \right] . \quad (19)$$

Tasca then defines a less complicated form for F^* that approximates F_1 and F_2 at the center of the sphere and at a point about 0.9 of the way to the edge of the sphere.

$$F^* = \frac{\frac{4Kt}{a^2\rho c}}{2 + 3\left(\frac{4Kt}{a^2\rho c} \right)^{1/2} + \frac{4Kt}{a^2\rho c}} . \quad (20)$$

Tasca does not give any physical or mathematical justification for Eq. 20. However, note that it has the powers of t that are expected from the experimental evidence. Figure 8, which compares Eq. 19 with Eq. 20, indicates that Eq. 20 is a fair estimate for the other more complicated equations.

Tasca inserts Eq. 20 into Eq. 16 and notes that the heat rate per unit volume is

$$Q = P/[(4/3)\pi a^3] . \quad (21)$$

Tasca then obtains his power-failure curve:

$$P = (T_m - T_j)\left(\frac{4}{3}\pi a^3 \rho c t^{-1} + 4\pi a^2 \sqrt{\rho c K} t^{-1/2} + \frac{8}{3}\pi a K \right) . \quad (22)$$

This power-failure equation is based on a spherical hot spot (an unrealistic shape). Therefore, Tasca first ignores the last term, which he identifies as a steady-state failure power, and then identifies the volume and surface parts of the equation to get

$$P = (\rho c V t^{-1} + s\sqrt{\rho c K} t^{-1/2})(T_m - T_j) , \quad (23)$$

where V is volume of the hot spot and s is its surface area. Tasca assumes that this general equation will apply to any device geometry, with appropriate geometric area and volume coefficients. More specifically, he assumes a cylindrical geometry, with the length of the cylinder equal to the depletion width and the radius of the cylinder equal to the radius of the constriction site.

Eq. 23 has the same trend as the Wunsch-Bell model, containing a term in t^{-1} for short delay times and a term in $t^{-1/2}$ for longer delay times. Both terms have been combined in one equation, in contrast with the Wunsch-Bell model that has a separate equation for each separate region.

Electrical models-- Electrical models are solutions of Eqs. 1 through 5, ignoring Eq. 6, the heat flow equation. Since heating is ignored, these models can give reasonable results only at low power levels (where heating is insignificant) or during the early times of a high-power pulse (before a device has a chance to heat up). At

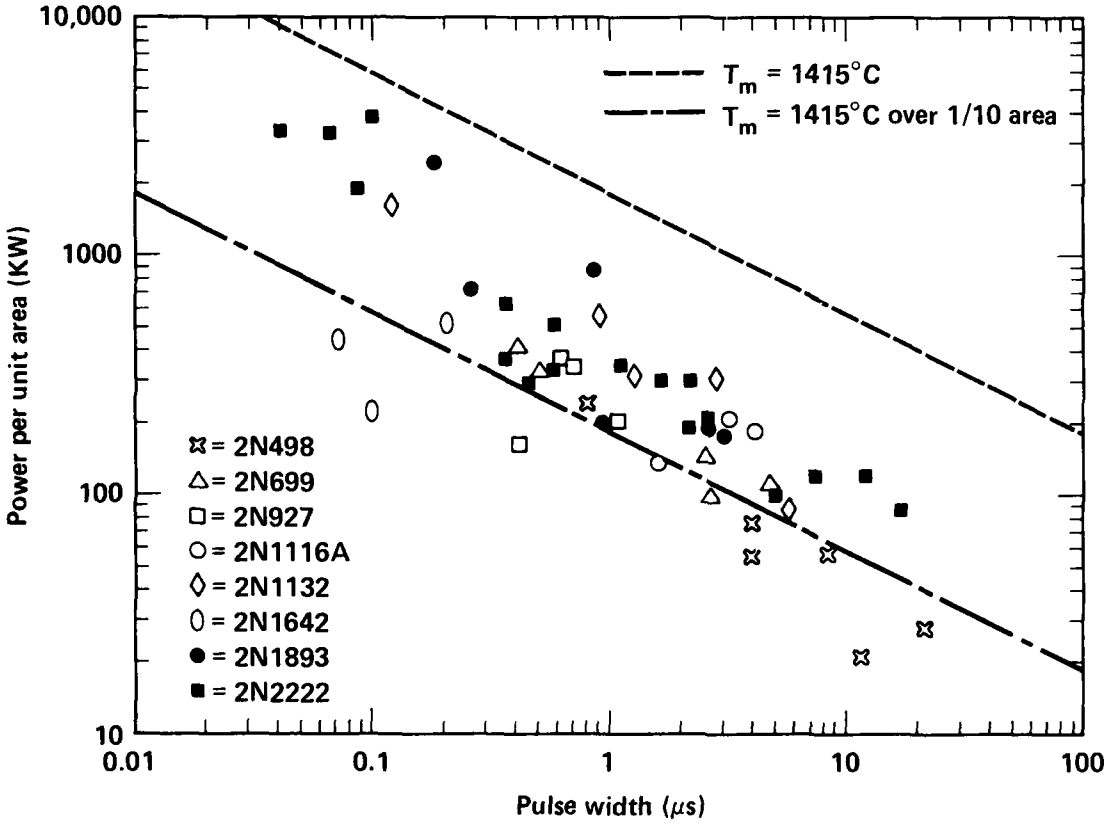

Figure 7. Wunsch-Bell model failure-threshold powers compared with experimental data.

$$\rho c \frac{\partial T}{\partial t} = P/V \ . \tag{13}$$

The resulting solution:

$$P/V = \rho c (T_m - T_j) t^{-1} \ . \tag{14}$$

Wunsch and Bell compared their equation to a number of experimental data points (Fig. 7) and found that the average of the data lies about an order of magnitude below the theoretical line, although the $t^{-1/2}$ trend of the data compares well. They overcome this problem by assuming that the current flows through a current filament that covers only 10% of the device's junction area. This modification gives much better agreement with the experimental data and is well justified by experimental observations (Ref. 21), although the spread of the data is still quite large.

D. M. Tasca-- On the basis of his own experimental research and experience with the Wunsch-Bell model, Tasca (Ref. 26) developed an analytical model that combined the short and long pulse formulas. Tasca assumes spherical symmetry in an infinite region. Heat is generated in a finite sphere by the applied electrical power and flows uniformly outward from the sphere to infinity. This results in a radial form of the heat-flow equation,

$$\rho c \frac{\partial T}{\partial t} = K \frac{1}{r^2} \frac{\partial}{\partial r} \left(r^2 \frac{\partial T}{\partial r} \right) + Q \ , \tag{15}$$

where Q is the heat generation rate inside the sphere and is zero outside the sphere. Solution of this equation is performed in a manner described by Carslaw and Jaeger (Ref. 27), giving the temperature rise at a radius r in a sphere of radius a for a given pulse length t:

$$\Delta T = T_m - T_j = \frac{a^2 Q}{2K} F^* \ , \tag{16}$$

where

$$\left.\begin{aligned} F^* &= F_1, \ r = 0 \\ &= F_2, \ 0 < r < a \end{aligned}\right\} \ , \tag{17}$$

$$F_1 = 1 + \left(\frac{2kt}{a^2} - 1 \right) \operatorname{erf}\left(\frac{a}{2\sqrt{kt}} \right) - 2 \frac{\sqrt{kt}}{\sqrt{\pi a^2}} \exp\left(\frac{-a^2}{4kt} \right) \ , \text{ and} \tag{18}$$

where k, the thermal diffusivity, is given by

$$k = K/\rho c \quad . \tag{8}$$

The three solutions of this equation are then matched at their boundaries (x = 0 and x = 1) and at infinity (the outer layers are assumed to extend to infinity). At the boundary between region one and region two (x = 0) an infinitely thin heat source is assumed to generate heat equal to the applied electrical power (P). Using Laplace transforms, the solution at x = 0 is found to be

$$P = K_d t^{-1/2} \quad , \tag{9}$$

where K_d is a damage constant.

The damage constant K_d has the analytical value

$$K_d = A(\pi)^{1/2}[K_1/(k_1)^{1/2} + K_2/(k_2)^{1/2}](T_m - T_j)/2 \quad , \tag{10}$$

where K_1 and K_2 are the thermal conductivities in regions one and two and k_1 and k_2 are the thermal diffusivities defined by Eq. 8 for regions one and two. The junction cross-sectional area is A, the melting temperature is T_m, and the ambient junction temperature is T_j.

Since this model was developed for separating surface breakdown effects from bulk breakdown effects, it is rarely used to predict device failure thresholds.

D. C. Wunsch and R. R. Bell-- In 1968, Wunsch and Bell (Ref. 20) developed what is now known as the Wunsch-Bell model. This model and its derivatives are the basis for most second breakdown device-failure research and analysis since that time. Its development is similar to that performed by Davies and Gentry above; however, the device geometry is much simpler.

Wunsch and Bell assume a single, one-dimensional material stretching to infinity in both directions. Using this material, they solve the one-dimensional form of the heat-flow equation (Eq. 7), by assuming that a heat source at some point x = a is equal to the input electrical power. The solution follows the same form as Davies and Gentry, but without the complexity of matching boundary conditions of three different materials. The solution is similar to that found by Davies and Gentry with a slightly different damage constant. Wunsch and Bell also removed the device area from the damage constant in an attempt to develop a more universal damage equation that would depend only on device materials. In their formulation, the power failure equation is

$$P/A = (\pi K \rho c)^{1/2}(T_m - T_j)t^{-1/2} \quad . \tag{11}$$

The damage constant, K_d, for this equation can be seen to be

$$K_d = (\pi K \rho c)^{1/2}(T_m - T_j) \quad . \tag{12}$$

Note that the Davies and Gentry model reduces to the Wunsch-Bell model if the numerical subscripts in Eq. 10 are removed. Wunsch and Bell use this model in the range of 0.1 to 20 μs. For shorter delay times, assuming that no heat flow exists, they assert that the power failure threshold is proportional to t^{-1} rather than to $t^{-1/2}$. The basis for this assertion can easily be seen by integrating

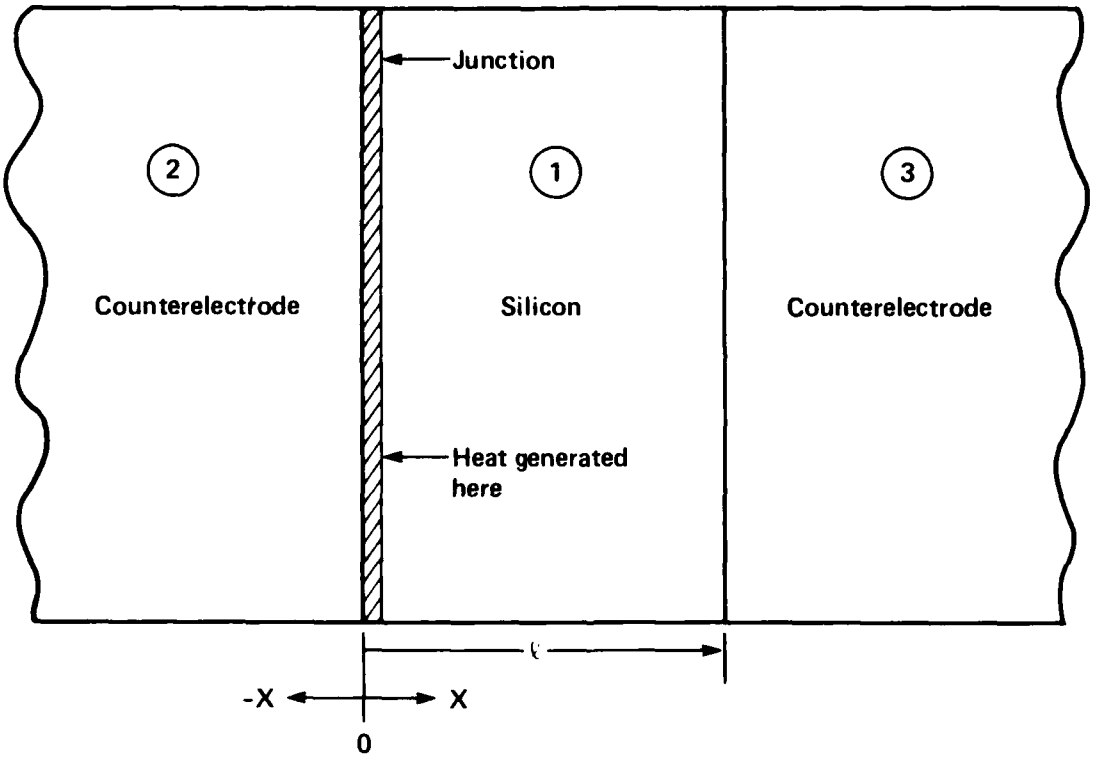

Figure 6. Device structure used for the Davies and Gentry thermal model.

III FAILURE MODELS

Three different models of second breakdown failure are described in the literature: analytical, empirical, and numerical. When Eqs. 1 through 6 can be sufficiently simplified, analytical solutions are possible. Empirical models are used when some equation can be made to fit the experimental data, irrespective of the physics involved. Numerical models are used to solve Eqs. 1 through 6 with much more of the physics intact than is possible with the analytical models.

In addition, these types can be further broken down into thermal, electrical, and electrothermal models. Placement in this second set of categories is determined by which equations are solved and which are either ignored or simplified to triviality. Thermal models solve only Eq. 6 (the heat flow equation) and ignore all of the others. Electrical models solve Eqs. 1 through 5 (the carrier continuity equations and Poisson's equation) and ignore Eq. 6. Electrothermal models, as the name implies, solve all six equations.

In this section we describe the different failure models in detail. The different models are grouped by types as described above, and models of a particular type are described together. In addition, the last section describes metallization failure models. Note that we do not exhaustively list all semiconductor models and semiconductor breakdown models in existance today. However, we do include all of the more common models.

Analytical Second Breakdown Models

Analytical models are complete, closed-form solutions of Eqs. 1 through 6. Because these equations are complex, no analytical solutions exist for the complete, unsimplified set of equations, even when they are reduced to one-dimensional forms. Most analytical models are based on solutions of the one-dimensional form of the heat flow equation. These models ignore all of the electrical equations. Therefore, most analytical models are thermal models.

Thermal Models-- The analytical thermal models are based on a one-dimensional solution of the heat flow equation. All electronic equations are ignored, except for a factor that includes the rate at which heat is generated by the device current. In general, heat is assumed to be generated in an infinitely thin junction region and to then flow outward in an infinite, one-dimensional medium. The heat-generating excitation is assumed to be a single square pulse of electrical energy. These restrictions make the problem amenable to analytic solutions; however, they severely restrict the models' validity. Models of this type are called Wunsch or Wunsch-Bell models, even though the original analytic solution was performed by Davies and Gentry.

R. L. Davies and F. E. Gentry-- In 1964, Davies and Gentry (Ref. 12) investigated the effects of surface breakdown on device geometry. To separate the surface effects from the bulk breakdown effects, they developed a simple, three-layer thermal model (Fig. 6). A one-dimensional form of the heat flow equation (Eq. 6) is solved in each of the three regions:

$$\frac{\partial T}{\partial t} = k\frac{\partial^2 T}{\partial x^2} \quad . \tag{7}$$

further increasing the temperature. If this runaway is not quickly halted (by stopping power to the device), the resulting high temperatures will damage or destroy the device. These high currents can also melt (with ohmic heating) the metallization stripes that supply power to the semiconductor.

Current-mode second breakdown occurs at higher applied power levels and involves much higher currents than does thermal-mode second breakdown. Normally, the doping density controls the electric field in the space charge (depletion) region, since the density of charge carriers is much less than the doping density. At high applied voltages, large numbers of charge carriers are generated by avalanche (impact) ionization and injected into the space charge region. When the density of charge carriers exceeds the doping density, the charge carriers, rather than the doping density, will control the electric field in that region. The high density of charge carriers then forces the electric field from the center of the space charge region to the edges. These higher fields enhance avalanche generation at the edges and produce the so-called "double injection" of charge carriers from the edges of the space charge region into its center. If charge carriers are injected faster than conduction processes can remove them, then more of the electric field will be driven from the space charge region to its edges, further increasing the double injection. The resulting runaway tremendously increases the current density, causing a significant amount of heating in the device. Heating will suppress avalanche generation and could shut down the current-mode second breakdown. However, at sufficiently high power levels, the runaway will increase faster than heating can suppress it, maintaining the second breakdown. Eventually the temperatures will reach levels that degrade or destroy the device. As with thermal-mode second breakdown, the high currents involved can also degrade and destroy the metallization stripes elsewhere in the device.

Another phenomenon that happens in conjunction with second breakdown, and is generally considered synonymous with second breakdown, is the formation of current and thermal filaments (Refs. 20, 21). Filaments form when the high currents no longer flow uniformly over the whole junction, but concentrate in a small area. This concentration of current (and heating) enhances the processes described above and results in hot spots in the semiconductor device. Several experimenters have observed these hot spots (Refs. 21-25). When a hot spot reaches about 1000 K, the device's operation will be severely degraded as a result of alloying and impurity migration. When the temperature reaches 1688 K the silicon will melt, resulting in a short through the junction or in the ejection of material, as shown in Fig. 4.

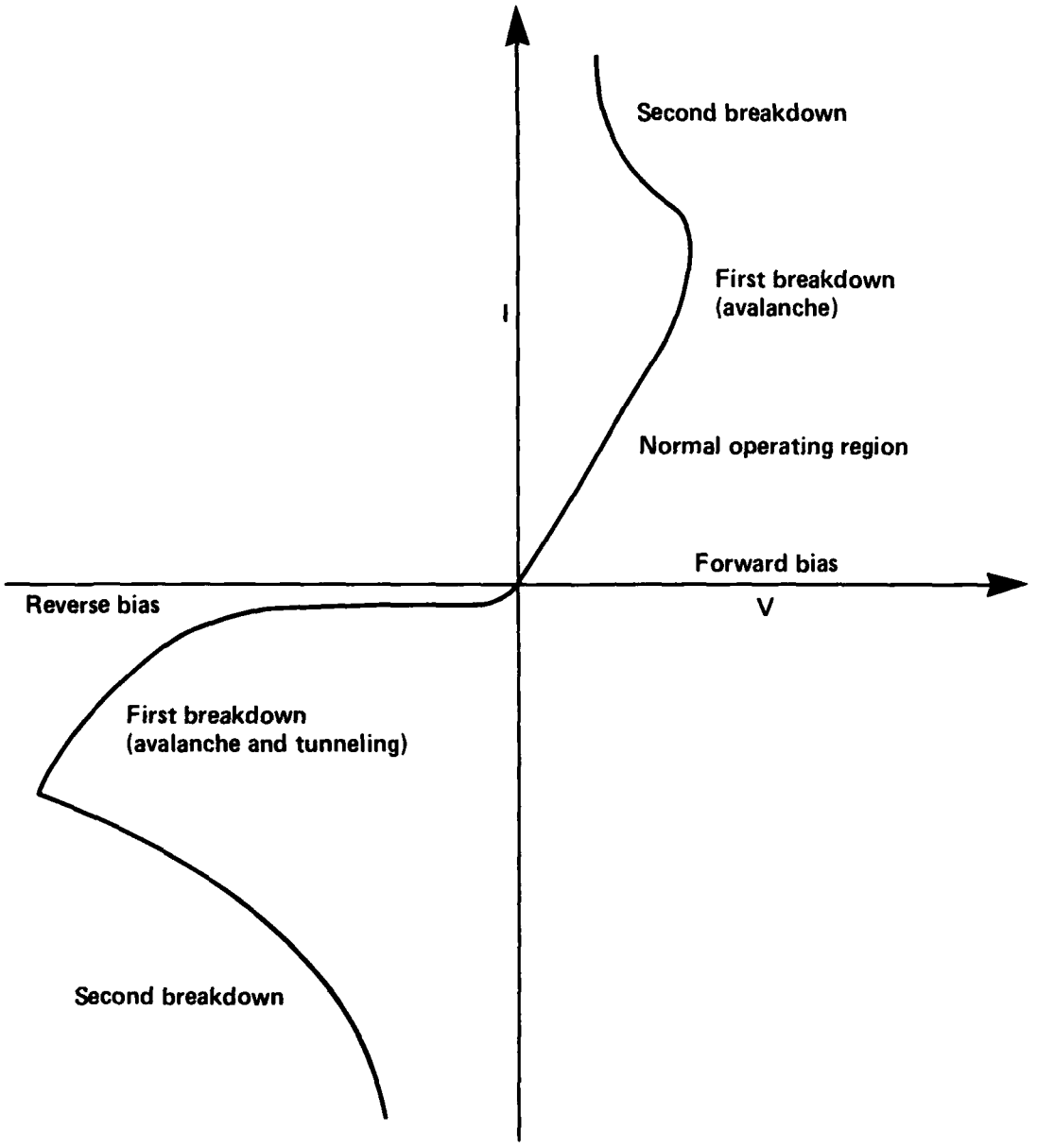

Figure 5. Current vs voltage characteristic curve for a p-n junction, showing breakdown regions.

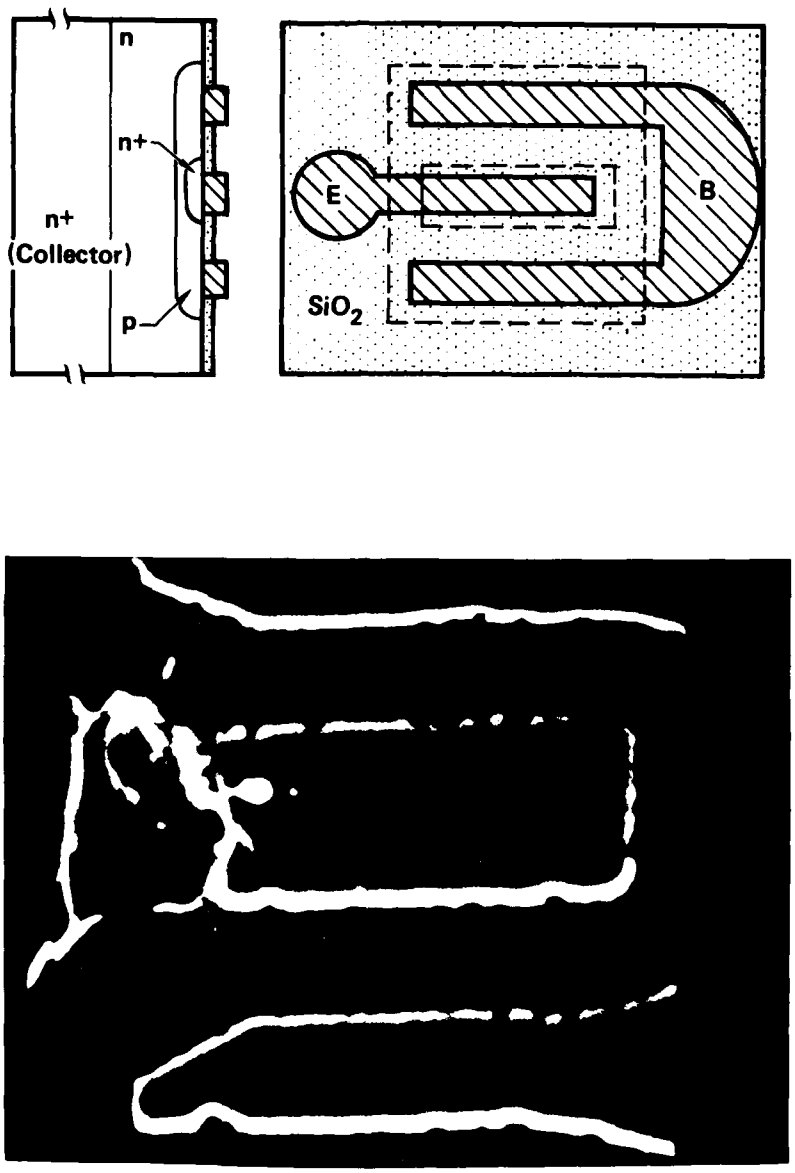

Figure 4. Thermal ejection of material from the junction of an electrically overstressed 2N918 transistor. The hole is in the emitter finger and penetrates deep into the device. The outside contacts shown are the base fingers, and the collector comes out the bottom.

surface, the field distribution on the surface can be controlled by proper design (Ref. 12). For a surface of unknown nature, however, no general theory exists to explain how the field on the surface can be reduced. High fields at the surface not only cause surface breakdown, but also can cause ionized surface impurities to migrate. Reducing the field at the surface also reduces the probability of ion migration, thus making the device more stable (Ref. 10).

Another source of surface breakdown is surface tracking caused by dust (especially metal dust) deposited on the surface. Metal dust sometimes acts like a thin metal film that can cause shorts in the device. When two closely spaced metal dust particles are in an electric field, they can enhance the electric field that is between them much as a sharp point enhances the electric field in a conductor. The high localized fields can then initiate surface breakdown in a device where the average field is well below the breakdown field. In general, several mechanisms can also cause surface breakdown; for example, the bonds of atoms at the surface can be broken with high fields which often occur in organic dielectrics (Ref. 13).

Failures in the dielectric region of the device consist of high-voltage breakdown (punch-through), which is caused by high transient fields in the material or by thermal and mechanical damage from hot spots in the adjacent silicon.

Unique to MOS is an oxide layer that insulates the metallization from the doped silicon. The conductivity of the silicon is modulated by the field developed across the oxide layer by a voltage applied to the metallization. Breakdown and failure in this oxide layer is called MOS oxide breakdown. Physically, oxide breakdown results from enhanced electric fields near inhomogeneities and voids. These enhanced fields cause localized breakdown in the oxide at much lower applied fields than would normally be expected to cause breakdown (Ref. 14).

Failures in a semiconductor device's active junction region usually result from localized melting and subsequent recrystallization of the silicon or from actual thermal ejection of material from the junction's surface (Fig. 4, Ref. 15). This heating is caused by a high current density through the junction, which in turn results from thermally or electrically generated second breakdown.

The two modes of second breakdown are thermal mode and current mode (Refs. 10, 16, 17). Which mode takes place is a function of the power of the incident EOS. The two modes can be distinguished by their different rates of development. Current-mode second breakdown develops much faster than thermal-mode second breakdown (usually in nanoseconds, compared with microseconds for thermal-mode second breakdown.) Second breakdown can be distinguished from other forms of breakdown, such as avalanche breakdown, by the negative resistance region that it imparts to the current versus voltage curve (Fig. 5). This curve shows a rapid transition to a high current and generally damaging mode of operation. A number of authors have investigated the physics of second breakdown (Refs. 3, 10, 15, 16, 18, 19, 20, Bibliography), and the description that follows is based on these references and the experience of the authors in their own research.

In thermal-mode second breakdown, which is thought to predominate below a certain threshold power, the high current from avalanche breakdown heats the device. When the temperature reaches about 600 to 800 K, thermal generation of charge carriers becomes significant, and the device goes into a thermal-current runaway. In thermal-current runaway, the increasing temperature generates more charge carriers, decreasing the device's resistivity. Decreasing the resistivity allows a larger current to flow,

II PHYSICAL MECHANISMS OF DEVICE FAILURE

Semiconductor devices, when subjected to EOS testing, exhibit a number of physical failure mechanisms, which are described in the reports on the modeling and testing of semiconductor devices listed in the Bibliography at the end of this report. Almost any part of a semiconductor device can be involved in its failure:

- Metallization and lead wires can be melted off. Electromigration can cause metal film conductors to become thinner, eventually leading to open circuits.
- Electrical breakdown, which leads to localized high temperatures, can occur in the dielectric or oxide regions of a device or across the surface of the device.
- Second breakdown, which results in high currents and temperatures, can occur in the active junction region.

According to one study (Ref. 1), breakdown in the junction region is the cause for about 90% of failures in bipolar devices, with metallization failures accounting for the other 10%. For metal oxide semiconductor (MOS) devices, the same study indicates that 63% failed from metallization failure and 27% failed from oxide breakdown.

Metallization and lead-wire failures generally occur when the local metal temperature is elevated to the melting point. This heating can result from high current densities in the metal or from hot silicon (because of a high current density elsewhere) in the vicinity of the metal. Failure of the metallization or lead wires usually consists of a separation in the trace or wire (somewhat like burning out a fuse) that leads to an open circuit. The high currents that cause these failures probably result from breakdown or failure elsewhere in the device. Therefore, metallization and lead-wire failure may be a result rather than a cause of device failure.

Electromigration is a term applied to the transport of mass in metals when the metals are stressed at high current densities. This effect, which has been known for several decades, has been observed in both molten and solid metals (Ref. 11). Recently, electromigration has been recognized as a potential wear-out failure mode in semiconductor devices whose metal film conductors are of inadequate cross-sectional area. This phenomenon has stimulated investigation of mass transport in metal films. The failure is an electrical open circuit apparently due to the loss of conductor metal (Ref. 10).

When the electric field between two etched conduction paths on a semiconductor or insulator exceeds the breakdown limit of the intervening materials, an arc can short the strips together by forming a channel of melted metal. The result can be a short circuit. This breakdown mechanism will become more important as feature sizes in integrated circuits continue to decrease; eventually, even small voltages will suffice to create enormous electric fields within devices.

The surface conditions of a p-n junction influence the electrical characteristics of the device (Ref. 12). This is because the surface recombination process, which depends on surface conditions, acts as a sink for free carriers. A device's surface can be damaged mechanically or electrically. One cause of surface damage is high-field surface breakdown. For semiconductor devices, this high field occurs near the intersection of the space charge (junction) region and the surface. For an ideal

N_D	Donor density
N_A	Acceptor density
T	Absolute temperature
$U(T,n,p)$	Recombination term
c	Heat capacity
n	Electron density
p	Hole density
q	Magnitude of the charge on an electron
t	Time
ε	Permittivity
$\mu_n(\|E\|,T,N)$	Electron mobility
$\mu_p(\|E\|,T,N)$	Hole mobility
ρ	Mass density
φ	Electrostatic potential

Primarily because of the coupling and non-linearity, these equations have no analytic solutions, even in one dimension. Stiffness causes the numerical solutions of the equations to be prohibitively expensive. Therefore, authors generally simplify these equations to reduce them to a form that is solvable, either analytically or numerically. This simplification is generally so severe as to considerably limit the validity of the models (Ref. 10). A number of models are currently in use, although none of them explains the tremendous variability in the data shown in Fig. 3. Most models are also based on square-pulse excitations, which again causes problems relating real stresses to failure thresholds.

Once a component has been evaluated, it must be modeled as an equivalent circuit that can be used in one of the large electronic-circuit simulation codes. This conversion is done so that the larger systems of electronics can be evaluated for EOS sensitivity.

This report is organized in six sections:

- In section II, the physical processes that lead to failure of a semiconductor component are discussed.
- In section III, the different failure models used to predict the failure power (or energy) thresholds are discussed.
- In section IV, an error analysis is performed on these models.
- In section V, the expected error is compared with the spread of the experimental data about the theoretical curves.
- In section VI, actual stress parameters and methods used to relate them to the experimental or theoretical failure data are discussed.
- Finally, in addition to the references, a large bibliography of papers and reports concerning EOS-induced failures and semiconductor modeling has been included.

For the most part, the models dealt with in this report are concerned with second breakdown and second breakdown effects. Although several metallization models will be described, they will not be analysed in this report.

This model will not be of much use for determining breakdown power thresholds and threshold delay times since it is valid only in that area of the current versus voltage curve near the breakdown voltage. However, it does show negative resistance in that region with no thermal effects, indicating that it may be the beginning of current-mode second breakdown.

Empirical Second Breakdown Models

Empirical, second breakdown, failure models are based on the ability to fit experimental failure data to a particular equation, without considering the physics involved in the process. As it turns out, these models are developed by the same authors who developed the analytical equations, in an attempt to better fit the experimental data. In most cases, they used their experience with the analytical models to assume a particular form of the empirical model equation that would closely follow the trends of the experimental data. The empirical models are therefore essentially thermal models, although, by nature, they are not based on any particular physics.

D. C. Wunsch and R. R. Bell-- Using the form of their analytical model, Wunsch and Bell derived an empirical equation for the power-failure threshold (Ref. 20). The impetus for this development was the large deviation of the experimental data from the analytical curve, although the trend of this curve is essentially correct (Fig. 7). The empirical model is obtained by the straightforward use of Eq. 11 with the damage constant determined by a curve fit to the experimental data. Curves of this type are the basis for most of the empirical models described here:

$$P/A = K_d t^{-1/2} \quad . \tag{31}$$

Figure 9 from Ref. 20 shows the results of these curve fits for several types of electronic components. This figure also includes analytical curves for failure over the whole junction and failure occurring over only one-tenth of the junction area.

D. M. Tasca, J. C. Peden, J. L. Andrews, and S. J. Stokes, III-- In 1973, Tasca, Peden, and Andrews (Ref. 3) attempted to fit a curve of the form

$$P = At^{-C} + Bt^{-D} \quad . \tag{32}$$

In 1976, Tasca and Stokes (Ref. 30) used their experience with analytical models and curve-fit experimental data to develop the following equation:

$$P = K_{d1} t^{-1} + K_{d2} t^{-1/2} \quad . \tag{33}$$

Using Eq. 33 as a base, they related the failure power and delay time to these device parameters: the surge impedance and the pulse currents (in both forward and reverse directions) and the device impedance (in the reverse direction only). Regression techniques are used to fit the equations to the experimental data.

B. Kalab-- Kalab (Ref. 5) fits Eq. 33 to several sets of experimental data. He notes that it does not fit well at short pulse widths (<100 ns) where current-mode rather then thermal-mode second breakdown becomes prevalent.

H. B. O'Donnell and D. M. Tasca-- In 1977, O'Donnell and Tasca extended

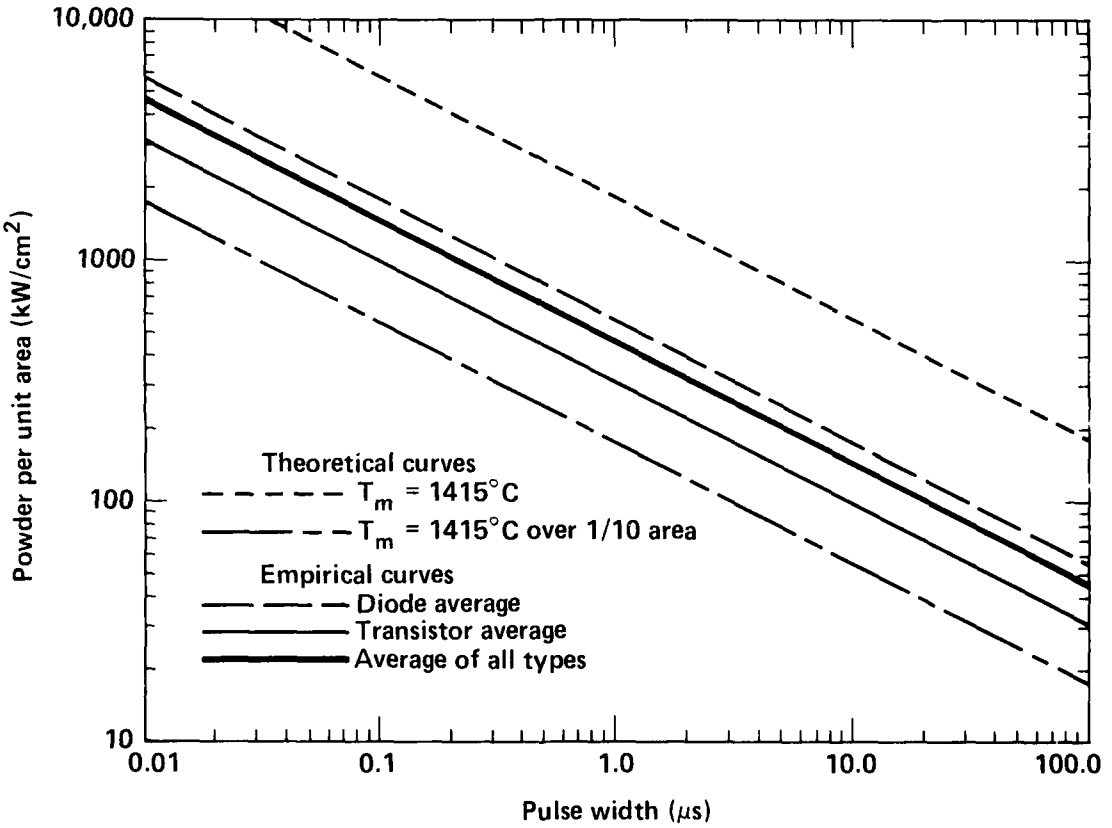

Figure 9. Empirical Wunsch-Bell model failure-threshold powers compared with experimental data (after Ref. 20).

Tasca's work (described above) to integrated circuits by using the following general thermal-failure equation (Ref. 31):

$$P = At^{-B} \quad , \tag{34}$$

where A and B are both constants to be determined by a curve fit. Actually, they tested four different forms of the equation: the average power expression above; an average current expression,

$$I = Ct^{-D} \quad ; \tag{35}$$

a surge impedance equation,

$$Z = Et^{-F} \quad ; \tag{36}$$

and a regression fit of all of the analytical model parameters,

$$P = A(t_{pd})^{B}(C_A)^{C}(\Theta_{JA})^{D}(V_b)^{E}(t)^{F} \quad , \tag{37}$$

where t_{pd} is the propagation delay, C_A is the junction capacitance, θ_{JA} is the thermal resistance of the junction, V_b is the breakdown voltage, and A, B, C, D, E, and F are constants to be determined by a regression fit to the experimental data.

D. R. Alexander et al.-- Alexander (Ref. 32) performs a similar analysis to O'Donnell's, by empirically fitting integrated-circuit failure data to the general failure equation (Eq. 34). On the assumption that $B = -1/2$, he also tries to use junction resistance and capacitance, breakdown voltage, and thermal resistance to estimate the junction area and the damage constant.

Numerical Second Breakdown Models

Numerical models, the most complex second breakdown failure models, employ several numerical techniques to simplify and solve Eqs. 1 through 6. The numerical models attempt to model the complete, time-dependent operation of the semiconductor device throughout the application of the EOS rather than to just predict the final results, as the analytical and empirical models do. Therefore, numerical models are best suited to provide insight and knowledge about the actual physical processes taking place in a semiconductor device during an EOS. This insight can lead to design rules for circuits and devices that can possibly enhance system survival during an EOS.

Thermal Models-- As indicated before, thermal models solve only Eq. 6, with little allowance made for the electronic effects.

H. M. Olson-- In 1977, Olson (Ref. 33) developed a thermal diffusion model that calculates the steady-state temperature of a one-dimensional cylindrical junction with heat flow perpendicular to current flow. It is basically a Green's function solution of the heat flow equation (Eq. 6). Heat generation is determined from the applied voltage and an empirical-temperature and field-dependent electrical conductivity. Since this is a steady-state solution to the heat flow equation, it is useful only for determining the steady-state failure power, which is not very useful for pulse-failure modeling.

A. Baruah and B. B. Budenstein-- Baruah and Budenstein have developed a two-dimensional model for modeling thin film silicon-on-sapphire (SOS) diodes (Ref. 21). The heat flow equation is solved in two dimensions with essentially an explicit finite difference. The electrical effects are taken into account as if the thin film were composed of a set of independent, parallel circuits. Each circuit is composed of a number of resistors and an ideal p-n junction in series (Fig. 10). The value of each resistor is determined with the empirical resistivity versus temperature curve (Fig. 11) and the geometry of the device.

This model produces interesting results concerning thermal effects and hot-spot formation. However, it is limited to thin-film, abrupt-junction, SOS diodes. Since the electrical effects are based entirely on the steady-state resistivity, the model's electrical behavior is suspect during an electrical transient. Plus, because of the lack of any other electronic considerations, it cannot show the effects of current-mode second breakdown.

N. Kusnezov and J. S. Smith-- Kusnezov and Smith (Ref. 34, 35) developed a model similar to that developed by Baruah. In one or two dimensions, they perform a two-step process:

- In the first step, the device is modeled as a grid of resistors, with each resistance fixed by the local temperature. This model is then solved to give the heat dissipation rate at each grid point.
- The second step is to put the heat dissipation rates into a heat-transfer code and allow that code to run for a specific length of time (e.g., 5 ns), assuming that the heat dissipation rate is a constant at each grid point. At the end of that run, new model temperatures are calculated at each grid point and used to set the resistances used in step one. These two steps alternate, to move the problem ahead in time.

As with Baruah's model, this model relies on the steady-state electrical resistance versus temperature curve to control all electronic effects. This reliance makes the transient electrical effects suspect and precludes simulating any current-mode second breakdown effects.

Electrical Models-- Numerical electrical models solve more detailed versions of Eqs. 1 through 5 but totally ignore thermal generation and transport in the device. Also, the original purpose of most numerical electrical models was to model device operations over normal voltage ranges. Thus, they cannot handle the effects of the high electric fields generated during an EOS. These effects consist of such things as field-dependent mobility, velocity saturation, and avalanche generation.

K. Kano and H. J. Reich-- In 1964, Kano and Reich developed a simple, one-dimensional model of a p-n junction to handle injection levels higher than those the analytical models could handle accurately (Ref. 36). Though these are higher injection levels, they are nowhere near the levels needed for EOS analysis.

T. Misawa-- Building on his analytical, steady-state model (Ref. 29), Misawa solves the steady-state equations numerically by straightforward numerical integration (Ref. 37). He also generates a solution for a small AC signal on the steady-state solution. However, these solutions suffer from the same problem as the analytic models described earlier: because they are steady-state models, they cannot predict transient failure thresholds and delay times.

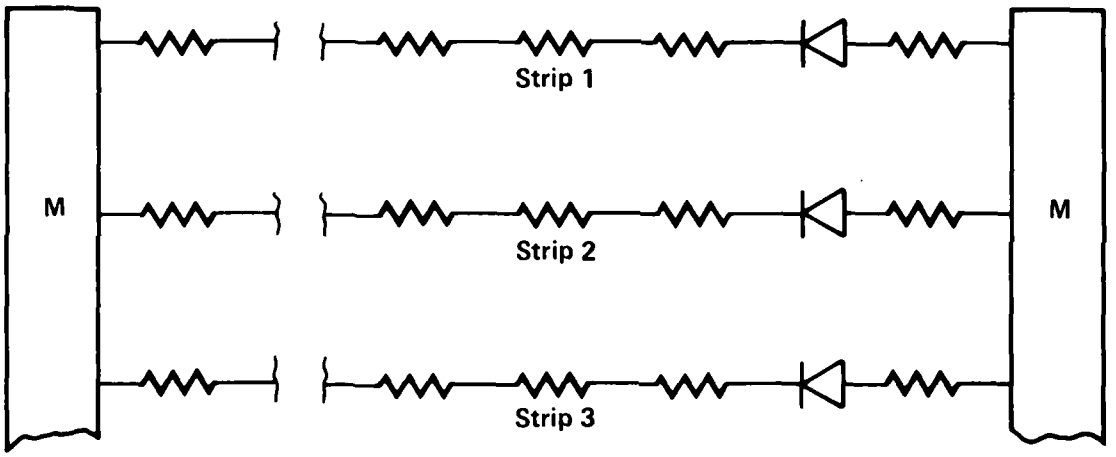

Figure 10. Electrical model used by Baruah and Budenstein.

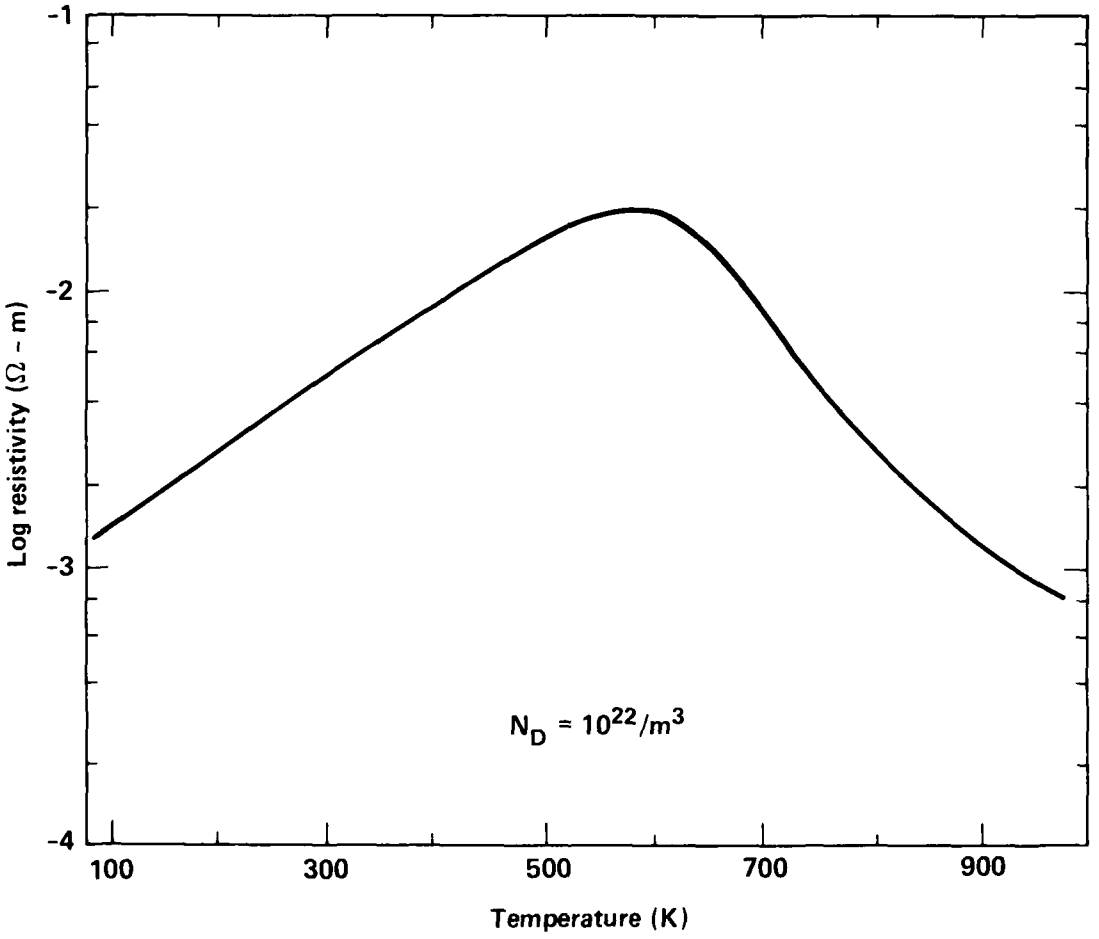

Figure 11. Resistivity vs temperature used by Baruah and Budenstein (after Ref. 21).

V. A. J. Van Lint, J. H. Alexander, D. K. Nichols, and P. R. Ward-- In 1967, Van Lint et al. developed a numerical computer model that solves all of the electronic equations for a simple p-n junction with what appears to be an iterated finite difference (Ref. 38). Their model has generation and recombination terms, and they indicate that the generation term can handle avalanche generation, although they give no details. This code could probably be used to model the initial phase of current-mode second breakdown, before any significant heating has taken place. However, it was designed to investigate the effects of injection (caused by ionizing radiation) on a device in the normal operating range, rather than EOS effects.

M. W. Muller and H. Guckel-- Muller and Guckel have developed a numerical model to look for steady-state current filaments in semiconductor devices (Ref. 39). Their one-dimensional code only considers the intrinsic region of a p^+-i-n^+ device. The code includes high-field avalanche generation but ignores recombination and any thermal effects. Since it is a steady-state code, it will not be useful for determining failure-power thresholds and delay times; however it could be useful for investigating current filament formation.

H. C. Bowers-- Bowers has generated a model similar to that developed by Muller and Guckel (described above) for a more complex device (Ref. 40). Where Muller and Guckel's model considers only the intrinsic region of a p^+-i-n^+ diode, Bowers' model also includes the p^+ and n^+ boundary regions. Again, since this is also a steady-state model, it cannot predict failure-power thresholds and delay times.

L. R. Razouk and G. W. Neudeck-- Razouk and Neudeck have developed a one-dimensional, electrical model for use at high current densities (Refs. 41, 42). The model solves all of the electronic equations by implicit finite differences and Newton-Raphson iteration. The model includes approximations for the high-field properties of the material parameters and assumes an external circuit that delivers a specified current pulse. This model appears to contain all of the electrical effects required for EOS analysis of devices excited with a constant current pulse. The model lacks any thermal effects, which makes the solution suspect after a short time because it operates at high current densities, which would cause significant heating.

E. M. Buturla, P. E. Cottrell, B. M. Grossman, and K. A. Salsburg-- As part of their work in computer-aided design (CAD), Buturla et al. developed a complex, finite-element code to model semiconductor devices in one, two, or three dimensions (Ref. 43). The code is designed to model semiconductor devices and integrated circuits during normal operation, and thus it has no high-field capability (avalanche generation, carrier velocity saturation, etc.) nor does it consider any thermal effects.

This code gives very detailed, time-dependent information about the operation of a semiconductor device. It could possibly be modified to include high-field and thermal effects, but not without considerable difficulty. This difficulty would arise because adding thermal effects requires the simultaneous solution of another differential equation (the heat flow equation), which is strongly coupled to all of the other equations through the temperature dependence of the material parameters (mobility, avalanche generation, diffusion, etc.). Also, some form of dynamic gridding would be needed to accomodate the dynamic nature of the charge carrier profiles, the electric field, and the temperature profile. Note that these problems are not unique to this model, but must be dealt with by all semiconductor, EOS, failure models.

G. D. Hachtel, M. H. Mack, R. R. O'Brien, and B. Speelpenning-- Hachtel et al. have developed a general-purpose, finite-element, partial differential equation solver for semiconductor-like problems (Refs. 44, 45). Their results are similar to those generated by Buturla, but with a more general program. This model is also used to analyze semiconductor devices and integrated circuits during normal operation.

Because the partial differential equation solver is a general program, it may be less difficult to add another differential equation (the thermal equation) to the set being solved; however, all other problems and difficulties described for Buturla's model would also be relevant here.

Electrothermal models-- An electrothermal model is an attempt made to combine all of the electrical and thermal effects into a single model. These models solve the complete set of equations for semiconductor device operation at high fields and high temperatures in an attempt to truly predict EOS effects and failure thresholds.

S. P. Gaur and D. H. Navon-- In 1976, Gaur and Navon developed a two-dimensional, steady-state model of power transistors (Ref. 46). The model solves steady-state versions of Eqs. 1 through 6 for a transistor-like device at normal operating conditions. The model solves these equations by finite differencing them and then iterating the equations until they converge. The model is steady-state only and does not have high-field capability (no avalanche or velocity saturation), so it will not be useful in determining failure-power thresholds and delay times.

W. D. Raburn and W. H. Causey-- Raburn and Causey have developed a one-dimensional, time-dependent model of the operation of an abrupt p-n junction (Ref. 28). The model solves all of the equations and has a high field capability. The equations are solved by first differencing them with a Crank-Nicolson formulation, then linearizing the set of difference equations with a first-order Taylor series. This set of linear equations can then be solved with standard matrix techniques. The model assumes that the external circuit consists of only a constant current source.

The model seems to give reasonable results for times greater then 10 ns, showing thermal-mode second breakdown; however, it does not show any current-mode effects, possibly because it assumes a constant current source.

K. Koyanagi, K. Hane, and T. Suzuki-- Koyanagi et al. have developed a model for the high-voltage operation of a transistor (Ref. 16). The model assumes that the transistor is operating at a high voltage (carrier velocity is saturated) and thus is not able to predict any low-voltage effects. The numerical solution is performed only over the n region of an abrupt junction, n^+-p-n-n^+ structure. The external circuit consists of a constant voltage source, or (as discussed in Ref. 47) a voltage source and a resistor in series.

This model shows either thermal-mode or current-mode second breakdown, depending on the applied voltage. Since it is one dimensional it cannot simulate current filaments, though hot spots can form from uneven heating in the device structure. Since it can only model a single region in a semiconductor device, and because it cannot model low-field regions correctly, this model can give only qualitative results concerning the operation of a semiconductor device during an EOS.

A. L. Ward-- For a number of years, Ward has been modeling the operation of semiconductor devices during EOS transients (Ref. 19). He solves a complete, one-dimensional set of the electrical and thermal equations with an explicit finite

difference. He ignores the electrical diffusion term by making the numerical diffusion inherent in difference equations equivalent to the electrical diffusion. He ignores the thermal diffusion by only considering short times, before any significant diffusion can take place. The external circuit can consist of a voltage source and a resistor in series. Using this model, Ward has done several parameter studies concerning second breakdown sensitivity.

J. H. Yee, W. J. Orvis, L. C. Martin, and J. C. Peterson-- The next two models described were developed by the authors of this report. The first model is very similar to that developed by Koyanagi, a one-dimensional model of the n region of an n^+-p-n-n^+ transistor-like structure (Ref. 18). The work was extended beyond that performed by Koyanagi to include part of the p region and to consider more effects of the external circuit.

W. J. Orvis, J. H. Yee, G. H. Khanaka, and D. L. Lair-- The second model developed by the authors is a general, one-dimensional, p-n junction device model (Refs. 10, 15, 18). The method considers a complete, one-dimensional device, from metal contact to metal contact, including the highly doped ohmic contact regions. The model solves a complete set of the electrical and thermal equations without neglecting any terms. The range of the material parameters includes high and low electric fields and high and low temperatures, which is necessary to model a complete device, because of the large variation of electric field and temperature in a particular problem. The model will accept any reasonable doping profile between the fixed metal contacts and gives reasonable results at high and low applied voltages in either direction. The external circuit consists of a voltage source and a resistor in series.

This is a one-dimensional device model, which means that it cannot simulate current filament formation, which can be a significant limitation, since filaments are observed in almost all failure situations. This model does show current-mode and thermal-mode second breakdown. Its temperature profiles resemble those measured experimentally by Knight and Budenstein (Ref. 48), although no definitive comparison has been performed yet between the experimental data and the model results for a specific device.

Metallization Failure Models

Because metallization failure is a leading cause of failure in MOS-type devices, several authors have tried to model metallization failure for these devices. These are primarily thermal models, with parameters that are very similar to those for analytical thermal models for second breakdown failures.

D. M. Tasca-- In conjunction with his investigations of semiconductor device failure, Tasca also investigated the failures of the interconnections on integrated circuits (Ref. 26). In a later report, he included experimental evidence concerning interconnection failures (Ref. 3).

Tasca's metallization failure model follows from a fairly simple derivation. He assumes that a length of wire w has a rectangular cross section of area A. The wire is assumed to be formed of a uniform, homogeneous material. He neglects skin effects, assumes a uniform current density, and neglects all heat loss and heat flow in the material. Then, the differential energy input to the metallization by a current I is

$$dQ = \frac{I^2 r_e w}{A}\, dt \quad , \tag{38}$$

where Q is the energy and r_e is the resistivity. Then, assuming no heat loss or heat flow, the differential temperature increase of the material is

$$dT = \frac{dQ}{c\rho wA} = \frac{I^2 r_e}{A^2 c\rho}\, dt \quad , \tag{39}$$

where ρ is the mass density. This equation must then be integrated to determine the heat input required to increase the temperature of the metal from ambient to the melting point. If one assumes that the resistivity and the heat capacity vary linearly with the temperature and performs the integration the result is t_1, the time required for the device to reach the melting temperature,

$$t_1 = \frac{C_1 A^2}{I^2} \quad , \tag{40}$$

where C_1 is a constant (equal to $2.87 \cdot 10^8$ s-A^2/cm^4 for aluminum, according to Tasca, Ref. 26). To this time must be added the amount of time, t_2, required to deliver an amount of energy, Q_f, equal to the heat of fusion, H, of the material. The energy of the heat of fusion is

$$Q_f = HcwA = \frac{I^2 r_m w t_2}{A} \quad , \tag{41}$$

where r_m is the resistivity at the melting point. Solving this equation for t_2 yields

$$t_2 = \frac{C_2 A}{I^2} \quad , \tag{42}$$

where C_2 is a constant (equal to $9.25 \cdot 10^7$ s-A^2/cm^4 for aluminum). Combining these two times ($t_1 + t_2$) yields the pulse length required to melt the metallization. If we solve that sum for the current,

$$I = \frac{C_3 A}{\sqrt{t}} \quad , \tag{43}$$

where C_3 is a constant (equal to $1.95 \cdot 10^4$ A-s$^{1/2}$/cm^2 for aluminum), we have a failure-current threshold versus pulse-width curve for metallization failures.

D. G. Pierce-- Pierce describes two types of metallization failure models (Ref. 49): One, attributed to Wunsch (Ref. 50), breaks the pulse-width dependence of the failure curve into three separate regions. The first region ($< 1\ \mu s$) is for short pulses and corresponds to adiabatic heating in the metal, with the current proportional to $t^{-1/2}$. The second region ($1\ \mu s < t < 100\ \mu s$) is for quasi-adiabatic heating, with the current proportional to $t^{-1/4}$. The third region, for long pulses, corresponds to steady-state heating of the wire and constant currents (Fig. 12).

The second model described by Pierce is attributed to Smith (Ref. 51). In this model, the thermal equations describing heat flow in a metal trace overlaying a silicon-dioxide layer and a silicon substrate are solved numerically (Fig. 13). Note that the transition between the three regions is much smoother than is shown in the Wunsch model (Fig. 12).

Pierce develops his own analytical model, in which he assumes uniform current flow in the metallization, with one-dimensional heat flow from the metallization through the oxide layer and into a constant-temperature-substrate heat sink. He solves the one-dimensional heat-flow equations in the metallization and the oxide

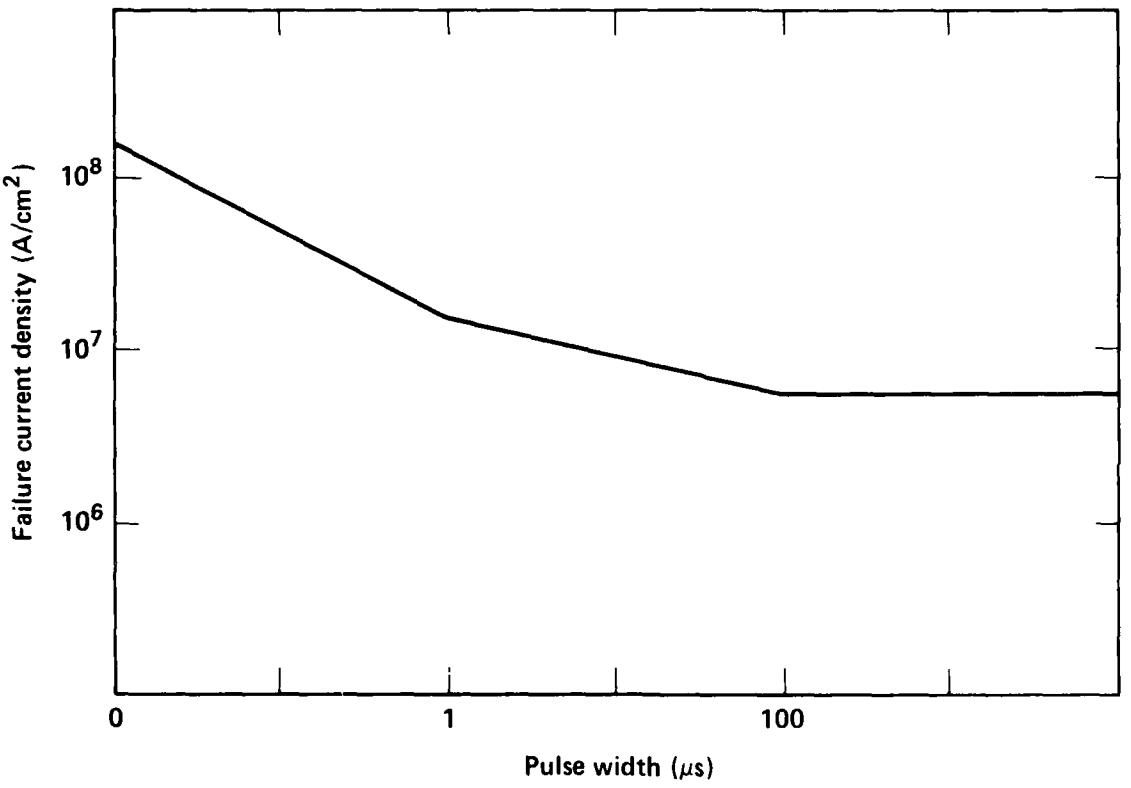

Figure 12. Wunsch model of aluminum metallization failure (after Pierce, Ref. 49).

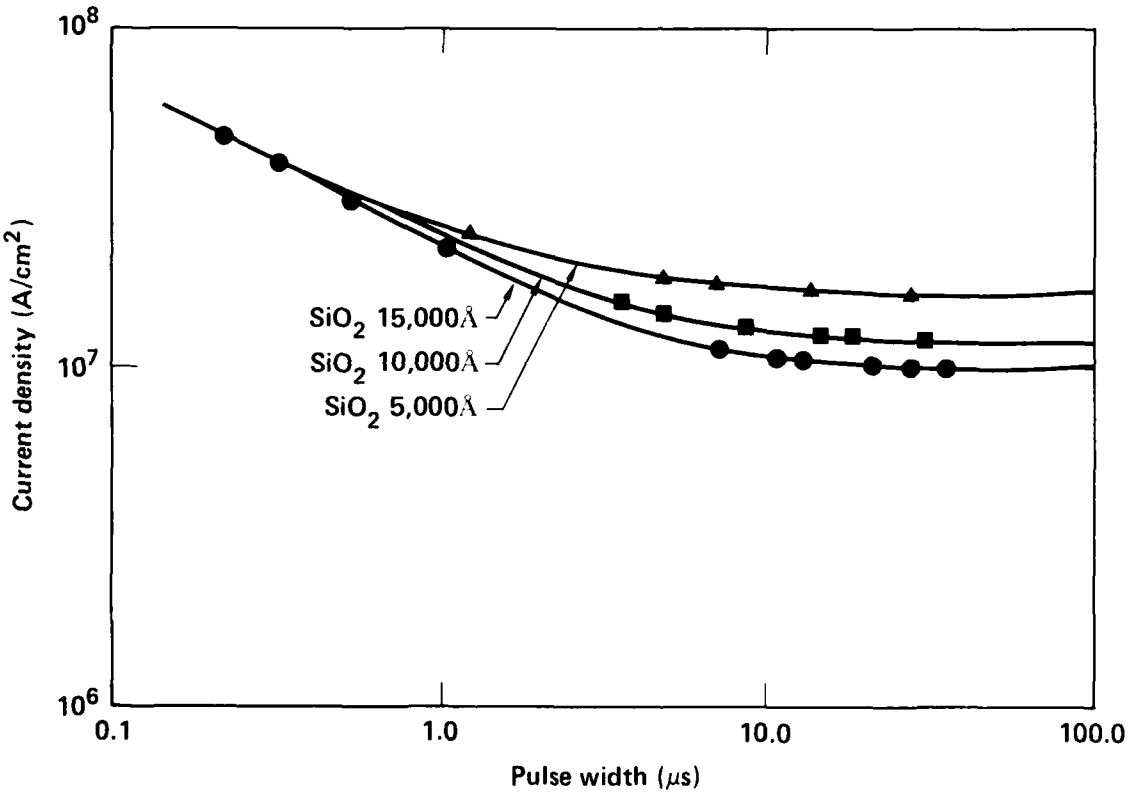

Figure 13. Smith's numerical model of metallization failure. The failure current density is for an aluminum trace over various thicknesses of SiO_2, laid on a Si substrate (after Pierce, Ref. 49).

ayer, matching the solutions at the boundary layer. The resulting equation gives the emperature rise at the metal-oxide interface as a function of the applied current ulse magnitude and pulse length:

$$T_m - T_j = \frac{1}{r_t}\left[\left[\frac{1}{1 - \frac{K_m}{K_{ox}} B^{1/2}\delta\tan(B^{1/2}l)} - 1\right]\right] \times$$

$$\sum_n \frac{2Ak_m\delta^2 l^2\exp(\gamma_n^2 k_{ox}t/\delta^2)}{l^2 k_{ox}\gamma_n^2[1 + 2\alpha_n csc(2\alpha_n)] + \delta^2 k_m\alpha_n^2[1 - 2\gamma_n csch(2\gamma_n)]}, \quad (44)$$

where the γ_n are the positive roots of

$$\frac{K_m\delta\alpha_n}{K_{ox}l\gamma_n}\tanh(\gamma_n)\tan(\alpha_n) = 1 \quad (45)$$

and

$$\alpha_n = \left[Bl^2 - \gamma_n^2\frac{k_{ox}l^2}{k_m\delta^2}\right]^{1/2}, \quad (46)$$

where $A = J^2 r_e/K_m$, $B = r_t A$, r_t is the temperature coefficient of the resistivity; K_m, K_{ox} are the thermal conductivities of the metallization and the oxide; and k_m, k_{ox} are the thermal diffusivities of the metallization and the oxide. Figure 14 plots threshold failure current versus pulse length. Note that the curve shape is quite similar to the numerical results in Fig. 13. Pierce also has similar results for constant voltage and constant power pulses, as well as the constant current case shown here.

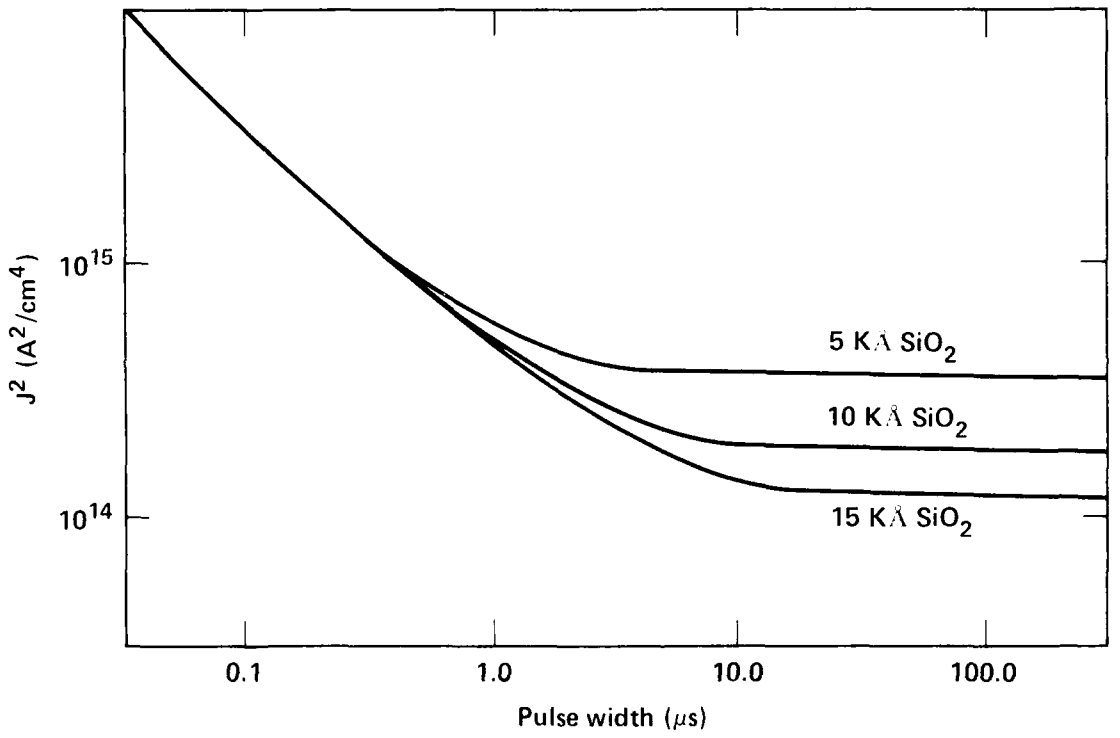

Figure 14. Pierce's model of metallization failure. A 5000-Angstrom aluminum metallization over various thicknesses of oxide (after Pierce, Ref. 19).

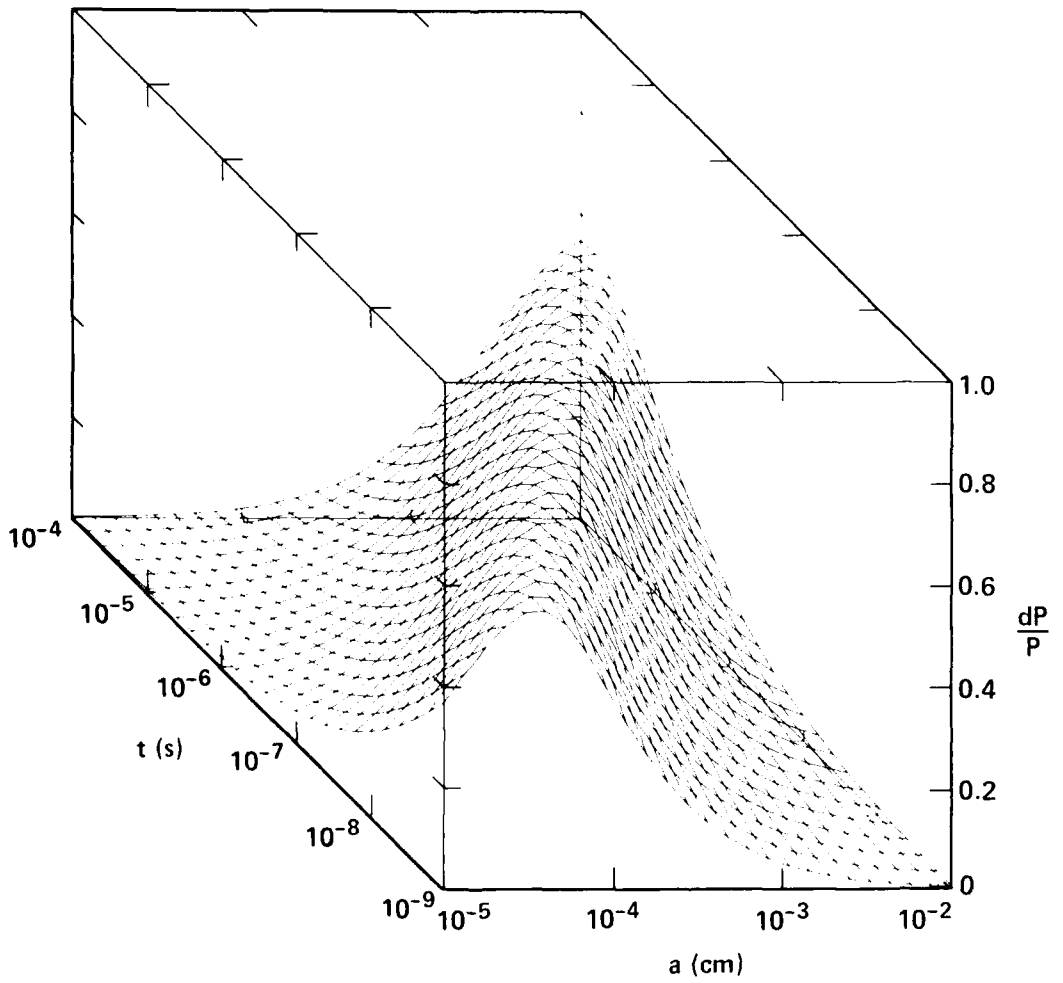

Figure 22. Error resulting from the Tasca approximation vs the pulse length and the radius of the hot spot.

amounts to a random error of about ±0.05.

If these adjusted values are put into the the error analysis, the following table results:

	Bias error	Random error
Pulse length		±0.1
Failure temperature		±0.36
K and c		±0.06
Active area		±0.01
Infinite device	-0.0035	±0.0035
One-dimensional device	-0.11	±0.11
Uniform breakdown	-0.3	±0.3
Multiple hot-spots		±0.05
No current-mode breakdown	?	
Total bias error (SUM)	-0.41	
Total random error (RSS)		±0.50

Tasca's Extensions-- Tasca extended the Wunsch-Bell model by adding a t^{-1} term for the short pulse region and a constant term for long pulses. He solves Eq. 15 analytically for a spherically symmetric heat source (Eq. 16) and then generalizes that to a cylindrical heat source (Eq. 23). In the process, he approximates the analytical solution with Equation 20. Figure 22 shows the error induced in the failure power by using this approximation as a function of the pulse length and the radius of the hot spot. The maximum error is 0.55 with a minimum of 0, indicating a bias error of 0.275 with a random component of ±0.275.

Next, Tasca ignores the constant, long-pulse term in Eq. 22. Figure 23 shows the error induced by neglecting that term versus the pulse length and the radius of the hot spot. Note that this term is only large at long times and for small hot spots, so for hot spots greater than 10 μm in radius, there will be negligible error.

This leaves Eq. 23, which Tasca assumes applies to cylindrical as well as spherical hot spots, with only a change in the surface area and volume terms. The error induced by this approximation is not known; a three-dimensional solution in cylindrical coordinates is required for comparison. The volume and surface area of a cylinder are written as

$$V = \pi R^2 W \tag{55}$$

$$s = 2\pi RW + 2\pi R^2 \ , \tag{56}$$

where W is the depletion width and R is the radius of the hot spot. Using abrupt junction approximations, the depletion width and the breakdown voltage (V_b) are approximated by Tasca with

$$W = \left(\frac{2\epsilon V_b}{qN} \right)^{1/2} \text{ and} \tag{57}$$

$$V_b^{1.43} = 3.4 \cdot 10^{18}/N, \text{ respectively,} \tag{58}$$

where ϵ is the permittivity; N is the doping density in cm^{-3}; V_b, the breakdown

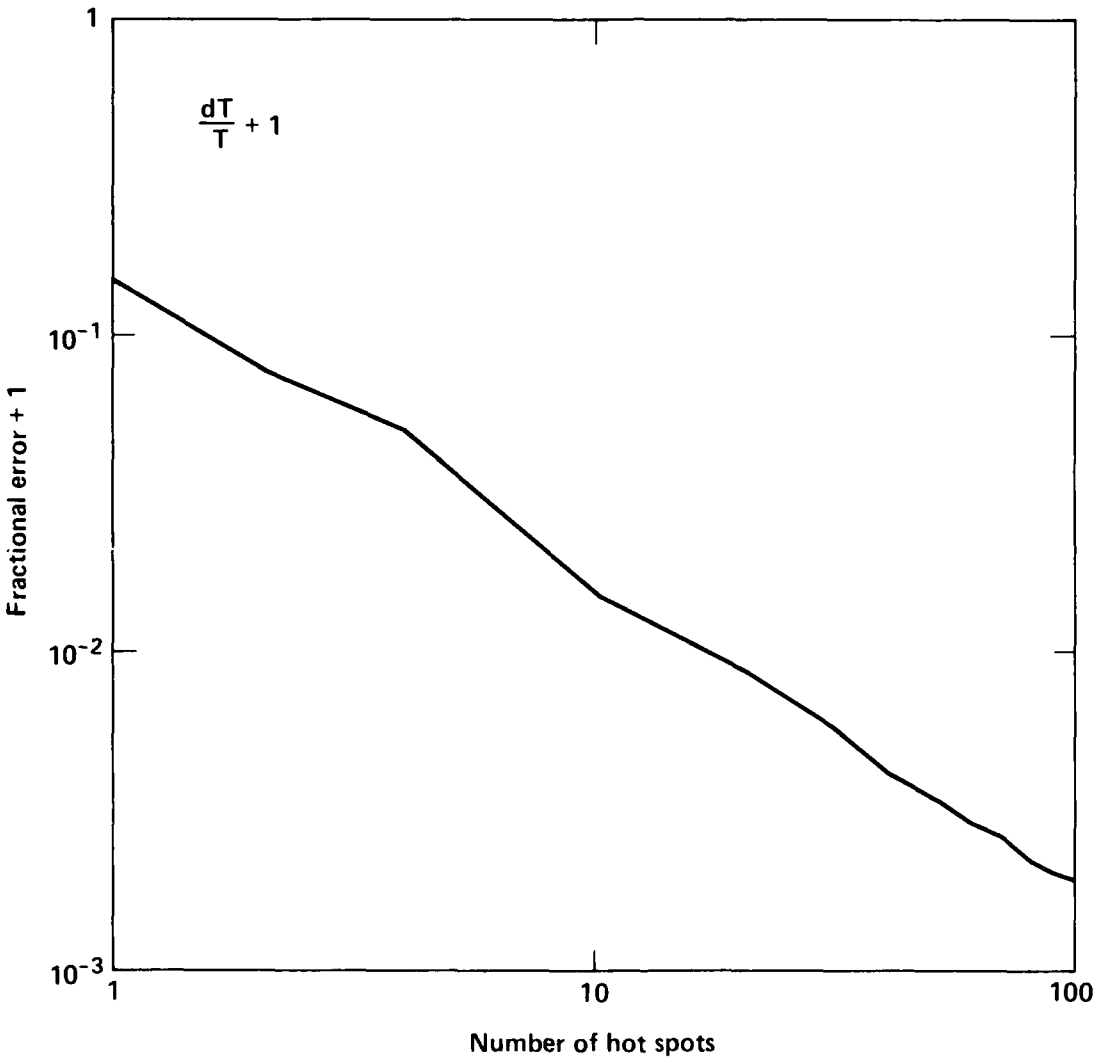

Figure 21. Fractional error vs number of hot spots covering a total area of 10% of the junction area.

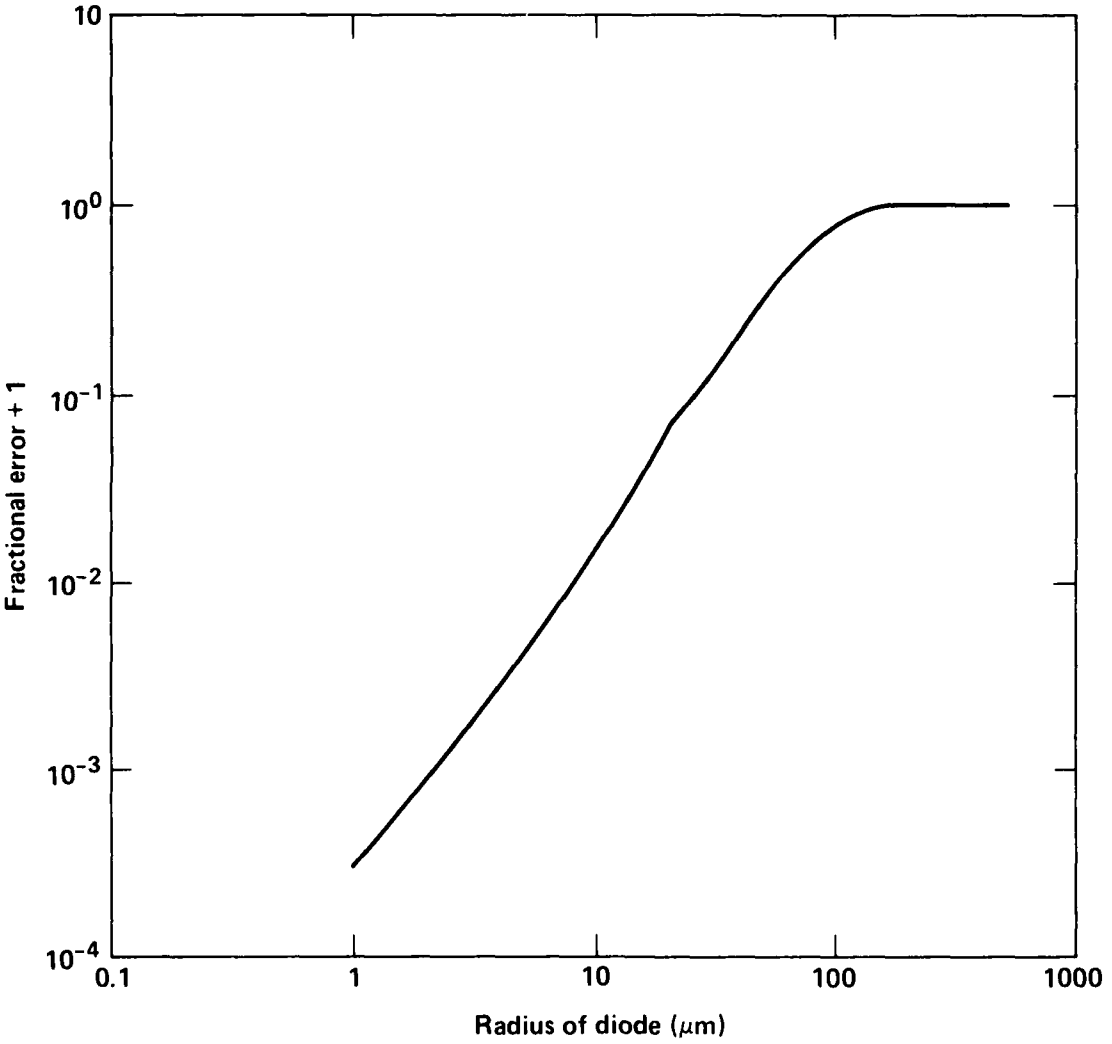

Figure 20. Fractional error in the temperature caused by assuming a one-dimensional material.

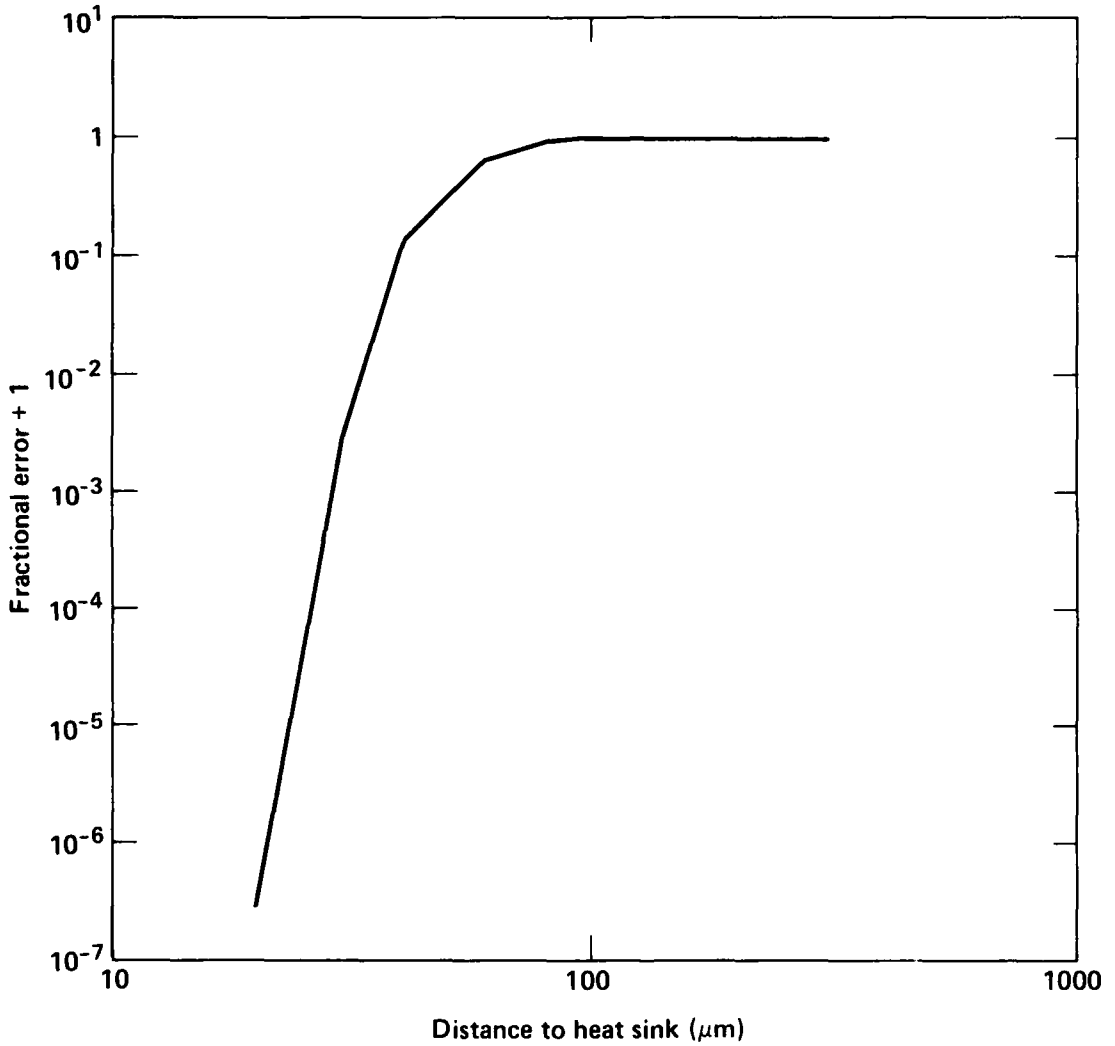

Figure 19. Fractional error in the temperature caused by assuming an infinite medium.

$$\text{Fractional error} = (1/2)\left(\frac{K(T) - K(950)}{K(950)} + \frac{c(T) - c(950)}{c(950)} \right) . \qquad (54)$$

If we assume that we can be reasonably smart about picking a temperature that gives us the correct values of thermal conductivity and heat capacity (say within 100 K), then the error from those terms will be around 0.06 rather then 0.47.

Fig. 19 shows the error induced in the temperature by the assumption of an infinite material. The figure shows the error induced as a function of the distance to a perfect heat sink. Because of the range of small values of the error, the error has been plotted as the log of the fractional error plus 1. This makes the figure a plot of the ratio of the true value to the model value rather than a plot of the ratio of the error to the model value (fractional error). This figure indicates that--for devices with geometries that have a heat sink more than 100 μm from the heat generating region and for a timespan of 20 μs or less--the device can be considered infinite in extent. For smaller devices (or longer times) the error will rapidly become significant; however, the thickness of a signal diode (one of the smaller discrete semiconductor components) is on the order of 100 μm, which is within this region.

The error due to the assumption of a one-dimensional device versus the radius of the heat generating region is shown in Fig. 20. This figure indicates that, for devices with heat generating regions with radii of more than 150 μm there will be negligible error induced in 20 μs by assuming one-dimensional geometry. For a signal diode, the junction region has a radius of approximately 100 μm, which means that some error (-0.11 $\pm$0.11) will result from this assumption.

The estimates of the portion of a device that is involved in second breakdown range from 10% (Wunsch-Bell) to 100%. However, Wunsch-Bell's estimate significantly overestimates the bias in the failure threshold. If the area of the device involved in second breakdown is assumed to range from 40 to 100% of the active device area, then the estimate has a bias error of -0.3 with a random component of $\pm$0.3 .

Breakdown can actually happen at several points. The change in the error estimate can be estimated by using the curve of error versus the radius of the heated region (Fig. 20). Figure 21 is generated by (1) assuming that the total area of all heated regions amounts to 10% of the total device area and (2) calculating the error for each of the heated regions, using Fig. 20 to determine the error per region. This error is then multiplied by the total number of heated regions and is plotted on Fig. 21. Removing the -0.9 bias due to the current flowing through only 10% of the active device area gives an estimate of the error due to multiple hot spots. This

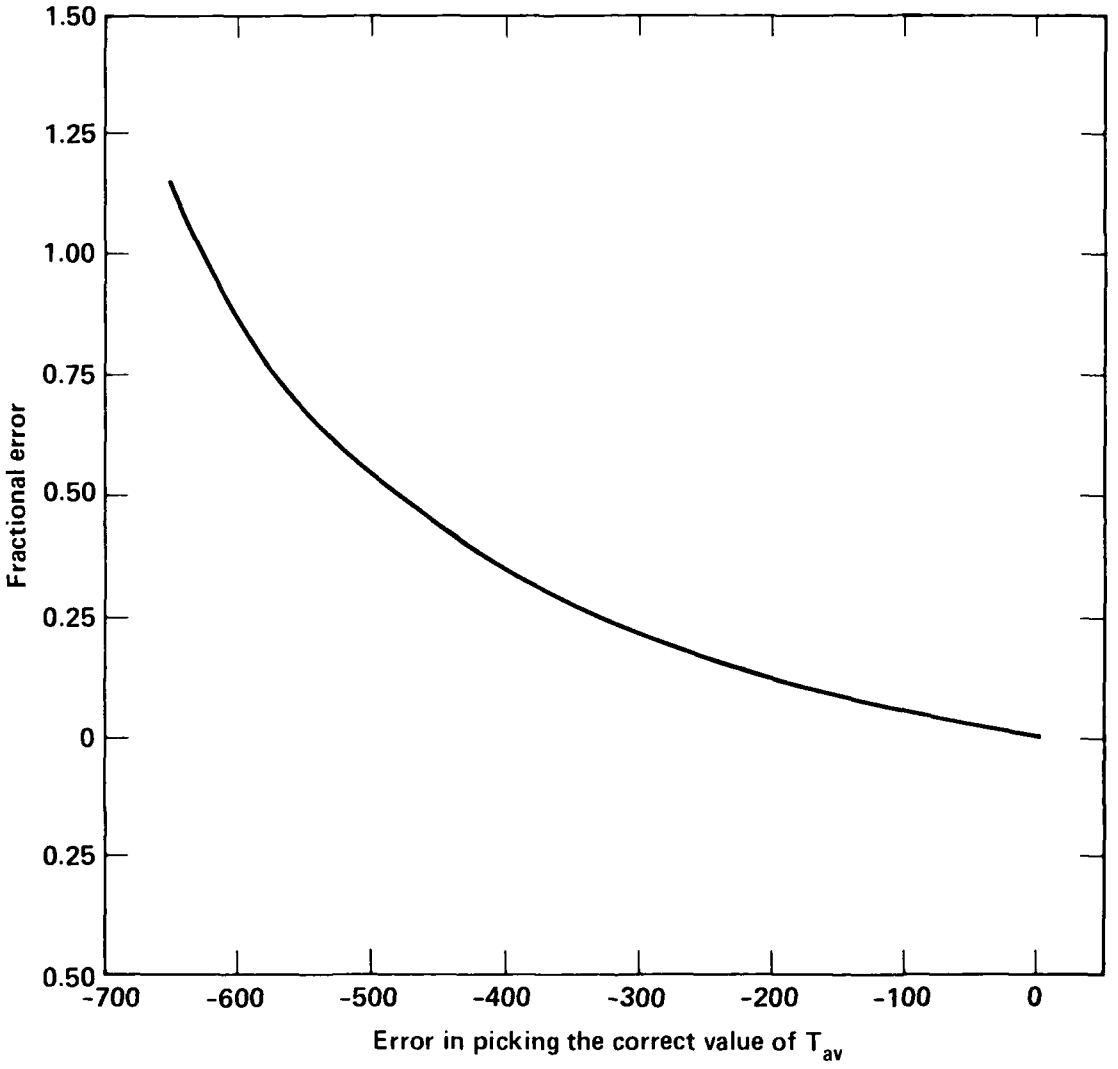

Figure 18. Fractional error in the thermal conductivity and the heat capacity caused by picking the wrong temperature to use to calculate the average values.

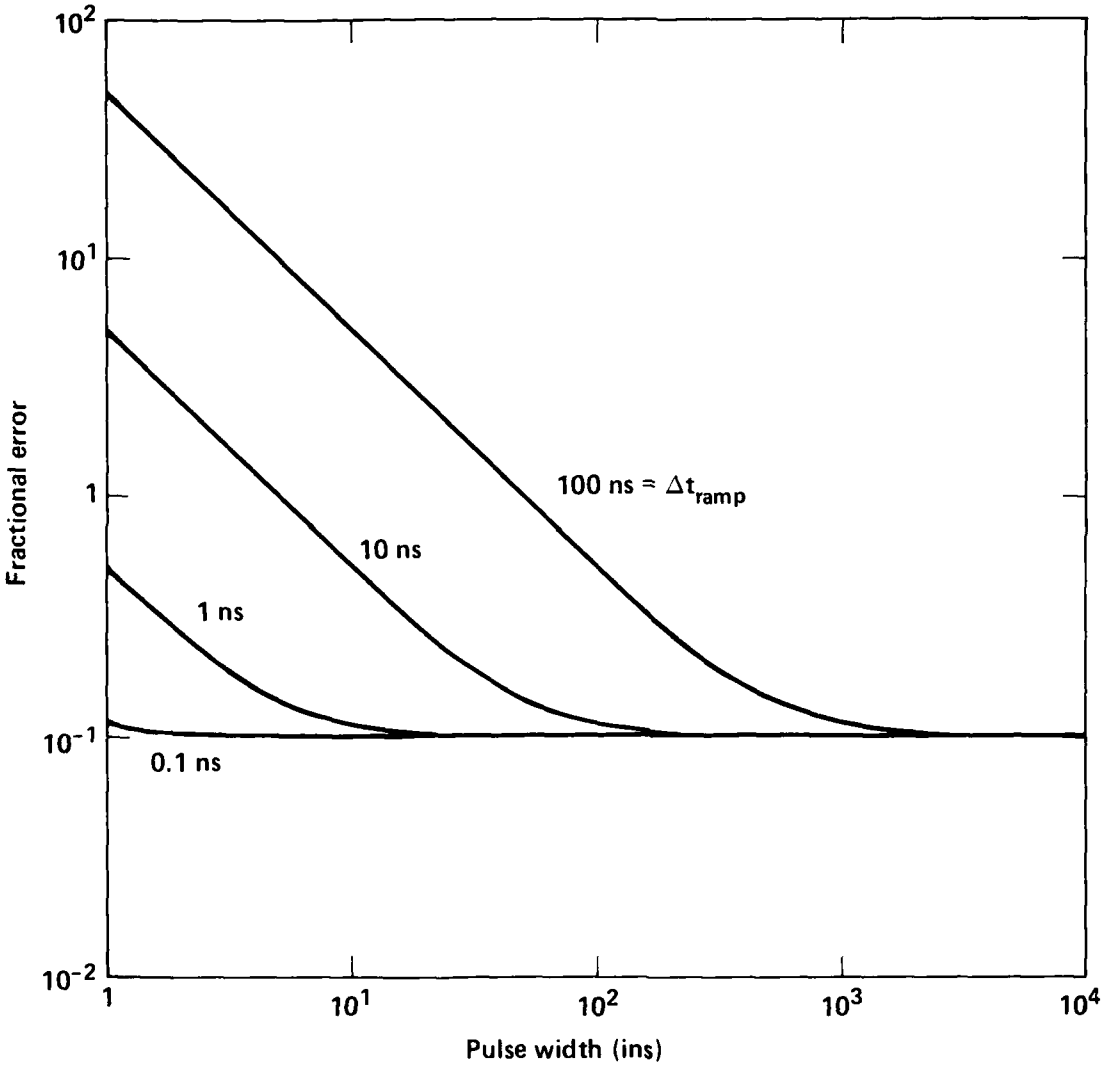

Figure 17. Pulse width error vs pulse width and pulse rise time.

Combining these errors will estimate the total error in the Wunsch-Bell type models.

	Bias error	Random error
Pulse length		±0.1
Failure temperature		±0.36
K and c		±0.47
Active area		±0.01
Infinite device	-0.0035	±0.0035
One-dimensional device	-0.11	±0.11
Uniform breakdown	-0.9	
No current-mode breakdown	?	
Total bias error (SUM)	-1.01	
Total random error (RSS)		±0.61

Note that this rough estimate of the total error exceeds 100% of the value predicted by the model. Experimental data (Fig. 7) indicate that most of the data is within one order of magnitude below the model values, indicating a bias error of -0.4 to -0.5. This apparent discrepancy between the experimental variation and the calculated error indicates that the error has probably been overestimated. Therefore, the various sources of error will be examined more closely.

By looking more closely at the pulse length error, you will note that it can be defined by the following equation

$$-(1/2)\frac{dt}{t} = -(1/2)\left[\left(\frac{\Delta t_{ramp}}{t} \right)^2 + \left(0.2 \right) \right]^{1/2} , \qquad (53)$$

where we assume a 20% error in the data read from the oscilloscope, and Δt_{ramp} is the ramp width or rise time of the square pulse. This equation is plotted in Fig. 17 versus the pulse width and for several values of the ramp width. As can be seen, if the rise time of the pulse is less than 1 ns or the pulse length is long, then the error is limited by the reading error off the oscilloscope.

The error in the failure temperature depends on the definition of device failure. The temperature chosen by Davies and Gentry (948 K) generally indicates a predisposition to failure rather than actual failure induced by reaching the melting point (1688 K) of the device. Failure may also be induced at intermediate temperatures (around 1000 K) by changing the doping diffusions that define a device. In any event, temperatures in this range will degrade but not necessarily cause it to fail.

The values for thermal conductivity and heat capacity are generally chosen by picking some average temperature value and then using values of thermal conductivity and heat capacity at that point. If we assume that some temperature value will give values of thermal conductivity and heat capacity that correctly predict failure power for a given pulse length, then Fig. 18 will give the fractional error if the chosen temperature was in error. This curve assumes that 950 K is the correct value and gives errors in terms of deviations from that value. The curve extends only in the minus direction, since good heat-capacity data was available only up to 1000 K. The deviations are calculated with:

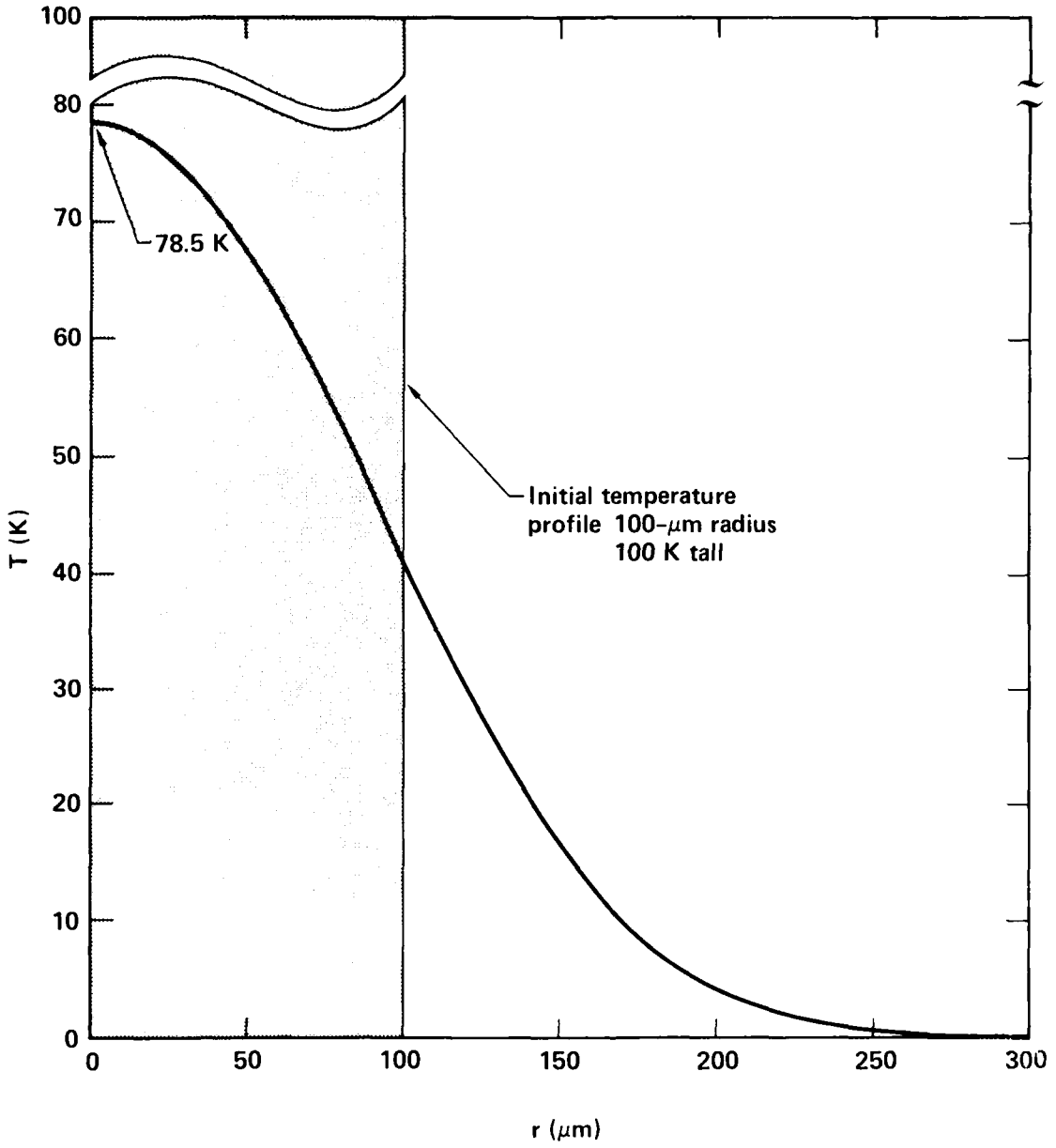

Figure 16. Radial heat flow for 20 μs for an initially heated 200-μm region in an effectively infinite (2000-μm diameter) space.

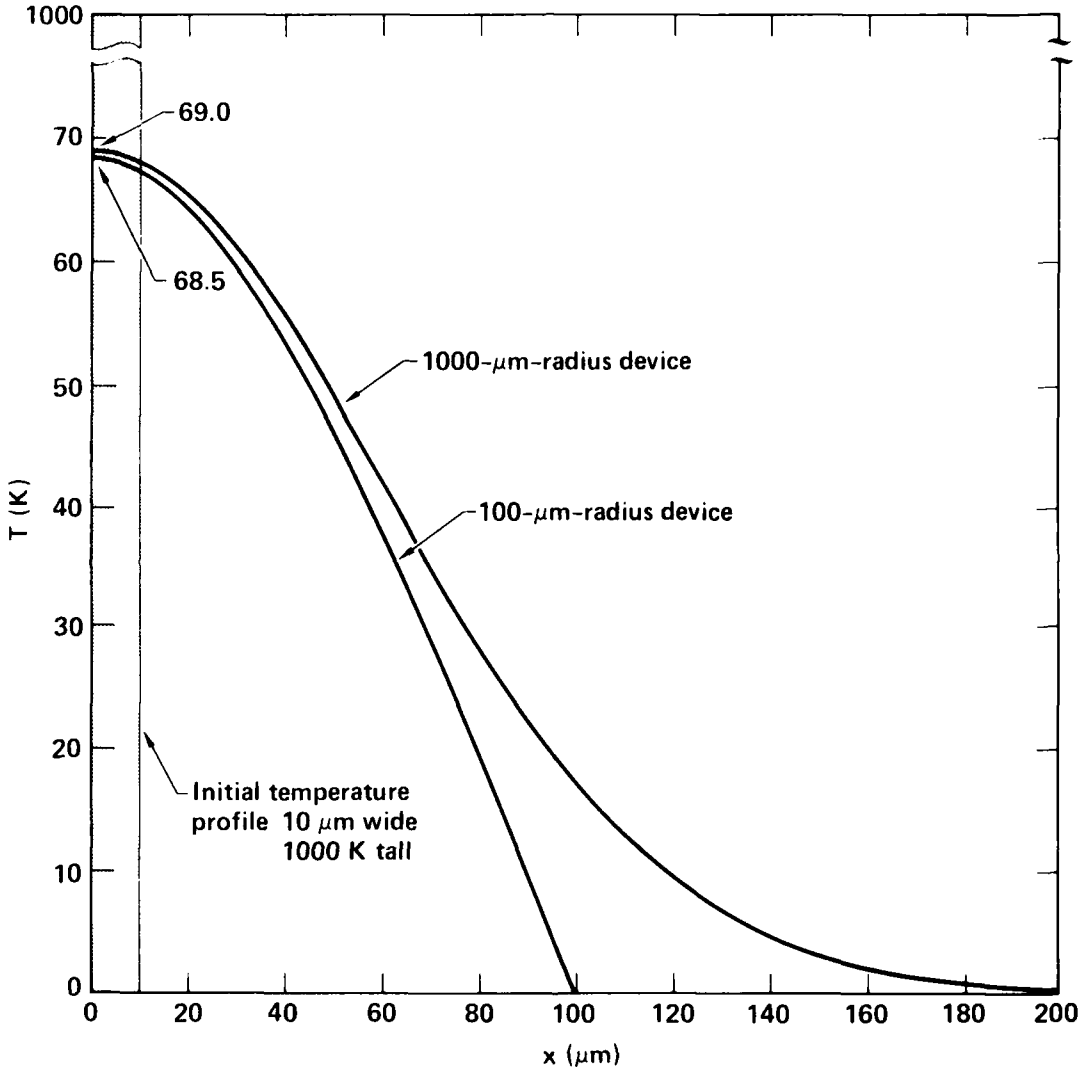

Figure 15. Axial heat flow for 20 μs for a 100-μm device compared with an effectively infinite (1000-μm) device.

The last term concerns the variation in the active device area. For a particular device type and for a single run by a single manufacturer, the variation should be less than 1%. However, different manufacturers use different device designs, and single manufacturers continually improve their designs; the result is a variation of from 10 to 20% in the active device area. Assuming that a designer knows this and picks his devices from a single run of a single manufacturer, this error will be ±0.01. If the designer does not take this into consideration, then this error needs to be adjusted accordingly.

The next step is to add in those fractional errors induced by the approximations and assumptions. It was assumed that the device was infinite in extent and made wholly of silicon. If heat was actually flowing into a heat sink, then the actual value of the temperature would be reduced. The one-dimensional heat flow equation was solved to numerically estimate this error. The initial condition consisted of a temperature pulse at the origin. The simulation was run twice: once with a heat sink at 100 μm (the thickness of a small signal diode) from the origin, and once with a heat sink 1000 μm from the origin (effectively at infinity). Both runs were continued for 20 μs (the extent of the range of the model), and then the temperatures at the origin were compared (Fig. 15). The resulting fractional error will range from 0 for short times to the following value at 20 μs:

$$\frac{68.5 - 69.0}{69.0} \approx -0.007 \ , \tag{52}$$

which is comparatively small. The final error estimate is a bias error of −0.0035 with a random component of ±0.0035 .

The next approximation is that of a one-dimensional device, assuming no heat flow in a radial direction. If a 200-μm-diameter cylindrical region is initially at some elevated temperature, and if the radial form of the heat flow equation is solved numerically for 20 μs, then the temperature at the center of the cylindrical region will be reduced to 0.78 of the initial temperature (Fig. 16). This results in a bias error of −0.11 with a random component of ±0.11 .

The Wunsch-Bell model assumes uniform breakdown over the whole junction. However, breakdown generally occurs in localized filaments and hot spots. Wunsch-Bell indicates that if the power actually goes through 10% of the junction area, then the failure curve will be moved down by one order of magnitude. If all failures are a result of a single filament formation that is 10% of the junction area, then this would indicate a bias error of −0.9 .

The Wunsch-Bell model does not account for any electrical effects occurring in the device. So, current-mode second breakdown is totally ignored. Current-mode second breakdown is a high-voltage/short-pulse effect that tends to decrease the failure power in the sub-10-ns range, which is below the range (50 ns to 20 μs) of the model.

Ignoring other electronic effects should not appreciably affect the model as long as it is realized that the model applies to on' ermal-mode second breakdown failures.

$$\frac{dP/A}{P/A} = -(1/2)\frac{dt}{t} + \frac{dT_m}{(T_m - T_j)} + (1/2)\left(\frac{dK}{K} + \frac{dc}{c}\right) - \frac{dA}{A} \quad . \tag{48}$$

The expected fractional error is found by taking the root sum square of the independent terms in this equation and then adding to that, values to account for the effect of the assumptions and approximations. Bias errors, which have a definite direction, are summed directly and separately.

The first term is associated with the measurement of the width of the input square voltage pulse. The model assumes zero rise time, while in reality there is a finite rise time on the order of a nanosecond. In the range of this model (50 ns to 20 μs), this has a maximum fractional error of 1/50 or 0.02. The final point is normally estimated from an oscilloscope trace, which has an estimated measurement error of 20% or a fractional measurement error of 0.2 (Ref. 52). Since these errors are independent, they are combined with a root sum square, to give the value of the term to be

$$(1/2)\frac{dt}{t} = (1/2)[(0.02)^2 + (0.2)^2]^{1/2} = \pm 0.10 \quad . \tag{49}$$

Other errors are induced because real EOS pulses do not come in nice square pulses. We will discuss these errors in Section VI (stress parameters).

The second term is associated with the error in the temperature (T_m) used to determine when the device fails. Values for this parameter range from 948 K (according to Davies and Gentry) to 1688 K (according to Wunsch and Bell) with an average of 1318 K. Accordingly, the maximum value of this term is

$$\frac{dT_m}{(T_m - T_j)} = \frac{1688 - 1318}{1318 - 298} = \pm 0.36 \quad . \tag{50}$$

The third term contains the dependent errors in thermal conductivity and heat capacity, which are due primarily to errors in the temperature. Both of these material parameters are assumed to be constant, where in fact they change with temperature. The average temperature is (1688 + 300)/2 = 994 K. Using data at 300 K and 994 K from Wolf (Ref. 53) the magnitude of this term can be estimated:

$K(300) = 1.57$ kW/m-K
$K(994) = 0.33$ kW/m-K
$K(ave) = (1.57 + 0.33)/2 = 0.95$ kW/m-K
$c(300) = 0.69$ kJ/kg-K
$c(994) = 1.0$ kJ/kg-K
$c(ave) = (0.69 + 1.0)/2 = 0.85$ kJ/kg-K

$$(1/2)\left(\frac{dK}{K} + \frac{dc}{c}\right) = (1/2)\left(\frac{0.33 - 1.57}{0.95} + \frac{1.0 - 0.69}{0.85}\right) = \pm 0.47 \quad . \tag{51}$$

The upper half width has been estimated to be the same as the lower half width, but might in fact be different, owing to the difference in the characters of the thermal-conductivity and heat-capacity curves between 994 and 1688 K. The upper half width is not calculated because there is insufficient data for the heat capacity in that temperature range.

IV ERROR ANALYSIS

In the last section, the different types of second breakdown failure models were identified, categorized, and described. In this section, model types will be analysed as much as possible in terms of their different sources of error. All errors will be stated as fractions of the model value, so as to be directly comparable to modeling results. All errors will be the 95% confidence limits (3σ) of a normal distribution (i.e., if the errors are distributed normally, then the probability that the true value is within 3σ of the model value is 95%, where σ is the standard deviation). Dependent errors are combined as a simple sum (SUM), and independent errors are combined using a root sum square (RSS) to allow for the probable cancellation of an error's effects. A number of the errors described will be bias rather than random errors. These errors are combined as a direct sum.

Two types of error can be applied to these modeling efforts. The first type is due to the approximations and assumptions made to simplify the model to a solvable form. The second type of error is due to measurement inaccuracies in experimentally derived quantities. Generally, one or the other type of error will dominate for a particular model type.

Analytical Second Breakdown Models

The analytical models are based on very simplified versions of Eqs. 1 through 6. In fact, most modeling ignores the first five equations and only solves a simple version of Eq. 6. Many assumptions and approximations are made, such as assuming infinite one-dimensional materials and neglecting the functional dependencies of many material parameters.

Of the analytical models discussed in section III, only the Wunsch-Bell or Wunsch models are really usable for large-scale failure-threshold analysis and interpolation of experimental data. This category includes Davies and Gentry's model and the Tasca model, which is an extension of Wunsch-Bell. The limited temporal domain of Misawa's model makes it useless for failure-threshold analysis. Therefore, the emphasis of this analysis will be on the Wunsch-Bell type of models.

Thermal Models-- The thermal models useful for device-failure modeling are primarily those of the Wunsch-Bell type, including Tasca's extensions of the Wunsch-Bell model.

Wunsch-Bell Type Models-- Wunsch-Bell models are based on the one-dimensional solution of the heat flow equation (Eq. 6), and all coefficients in the equation are assumed constant. These models include those developed by Davies and Gentry (Ref. 12), Wunsch and Bell (Ref. 20), and Tasca (Ref. 26). The resulting solution has the form

$$P/A = (\pi k \rho c)^{1/2}(T_m - T_j)t^{-1/2} \quad . \tag{47}$$

The fractional error in this equation can be obtained by taking the differential of the equation and then dividing that differential by the equation:

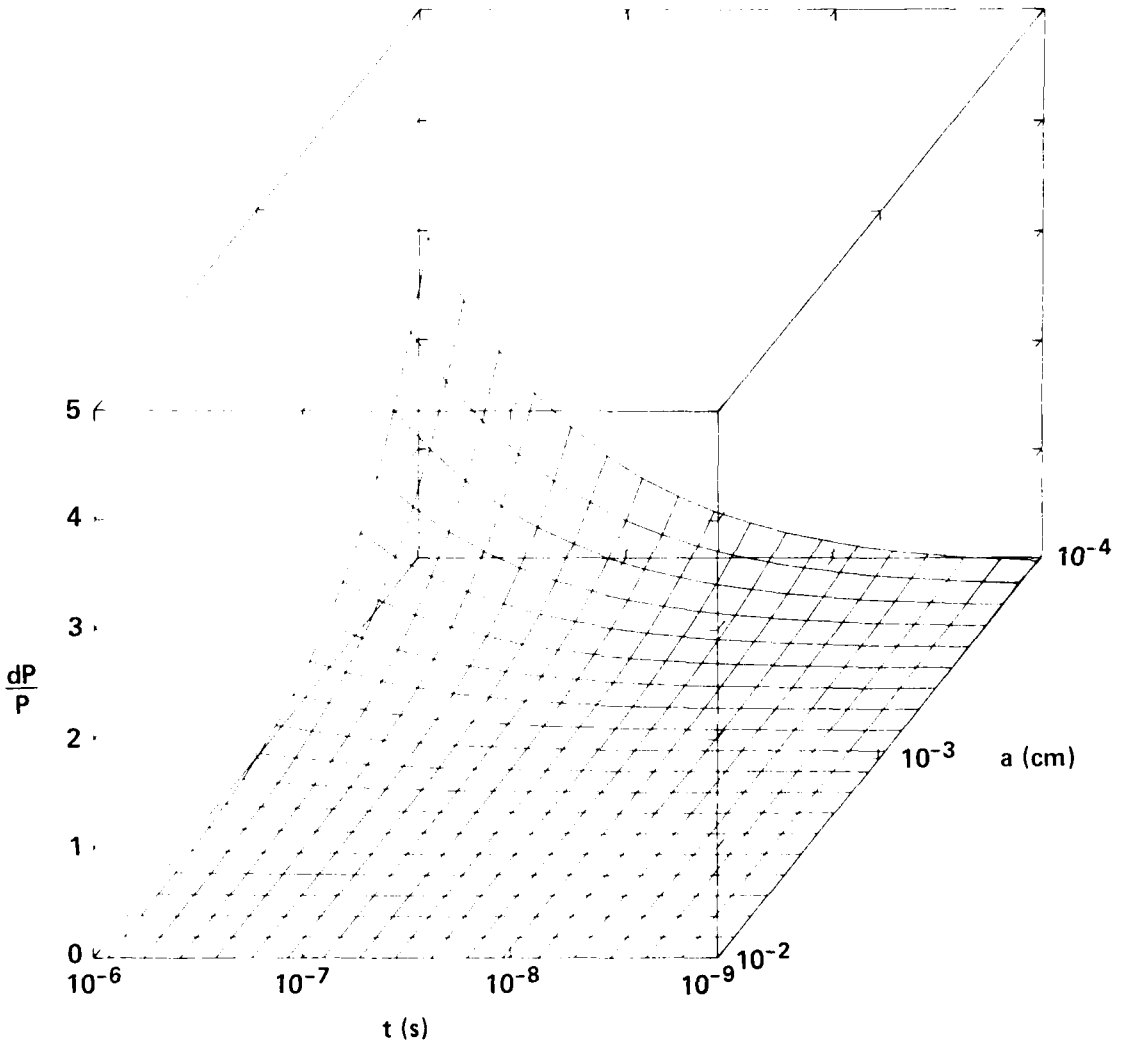

Figure 23. Error resulting from neglecting the long-pulse term vs the pulse length and the radius of the hot spot.

voltage, is greater than 6 V and the junction is reverse biased. These four equations can then be inserted in Eq. 23 giving

$$\frac{P}{A} = (T_m - T_j)\left[\frac{1.97\times10^{-6}\,R\rho c V_b^{1.215} t^{-1}}{2(R + 1.97\times10^{-6}V_b^{1.215})} + \sqrt{\rho c K}\,t^{-1/2}\right] . \tag{59}$$

Equation 59 will have two different error regions, depending on which term in the equation dominates. Figure 24 shows the parameter values where each of the two terms is dominant.

The t^{-1} term can also be split into two parts, depending on whether the V_b part or the R part dominates. Figure 25 shows the split of this term.

Looking now at the failure equation in these three regions, three different failure-power densities can be defined: P_1 where t^{-1} and R are dominant, P_2 where t^{-1} and V_b are dominant, and P_3 where $t^{-1/2}$ is dominant. The error differentials for these terms are

$$\frac{\partial P_1/A}{P_1/A} = -\frac{\partial t}{t} + \frac{\partial T}{T} + \frac{\partial c}{c} + 1.215\frac{\partial V_b}{V_b} - \frac{dA}{A} , \tag{60}$$

$$\frac{\partial P_2/A}{P_2/A} = -\frac{\partial t}{t} + \frac{\partial T}{T} + \frac{\partial c}{c} + \frac{\partial R}{R} - \frac{dA}{A} , \text{ and} \tag{61}$$

$$\frac{\partial P_3/A}{P_3/A} = -(1/2)\frac{\partial t}{t} + \frac{\partial T}{T} + (1/2)\left(\frac{\partial K}{K} + \frac{\partial c}{c}\right) - \frac{dA}{A} . \tag{62}$$

The other errors due to the assumptions must be added to these terms as was done in the Wunsch-Bell case. The errors must also be estimated for the terms in R and V_b. Tasca picks two values for the hot spot radius: 0.5 of the junction radius, and 0.3 of the junction radius. This suggests an error in R of ±0.1 of the junction radius, and the error term is

$$\frac{\partial R}{R} = \frac{0.1}{0.3} = \pm 0.33 . \tag{63}$$

The breakdown voltage in a reverse-biased p-n junction can normally be assumed to be equal to the applied voltage at the point that the junction just starts to break down. Actually, the IR drop across the bulk material should be subtracted from the applied voltage to yield the voltage across the junction. However, the small currents flowing in a reverse-biased junction just before breakdown will make that contribution negligible. The device's breakdown voltage will normally be measured with an oscilloscope, with the requisite error described previously.

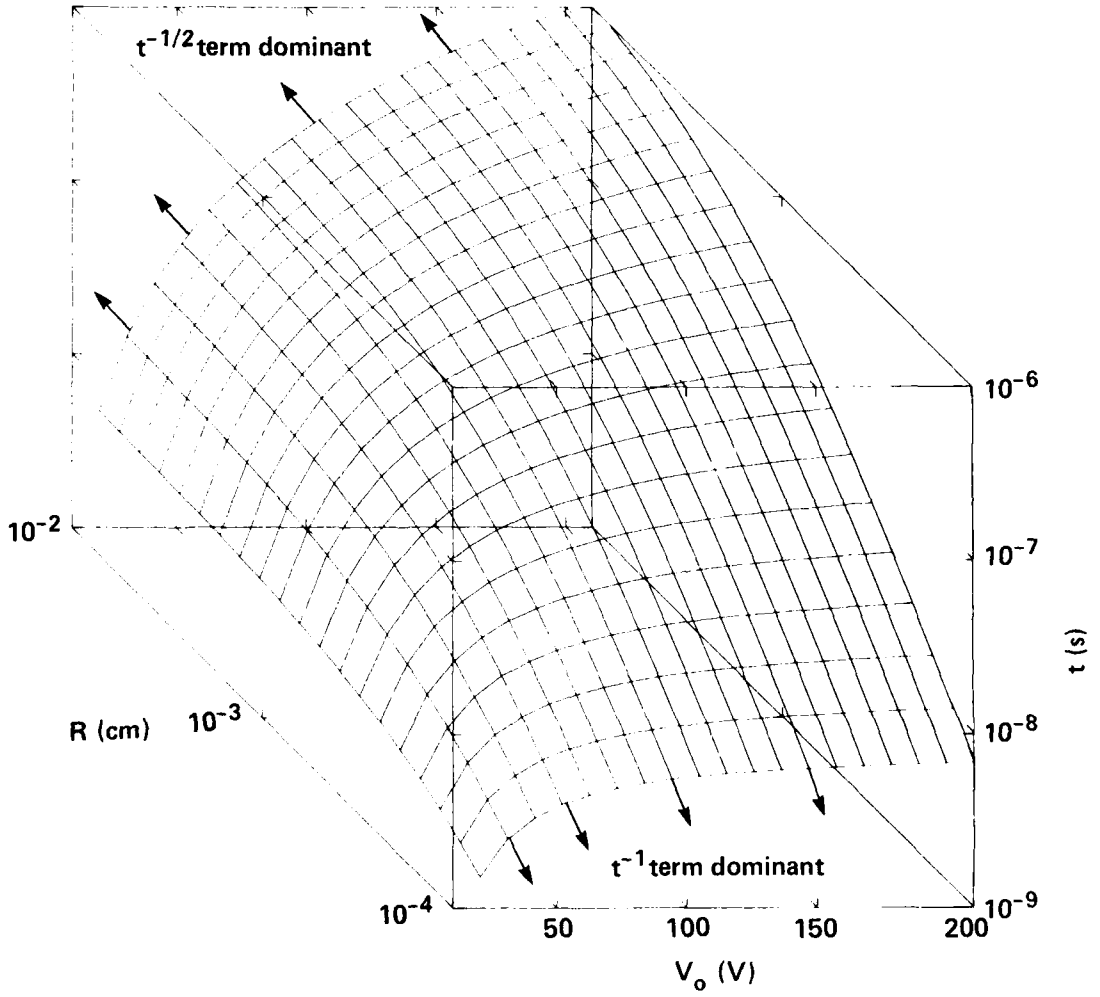

Figure 24. Dominant region in parameter space for the two terms in Tasca's equation.

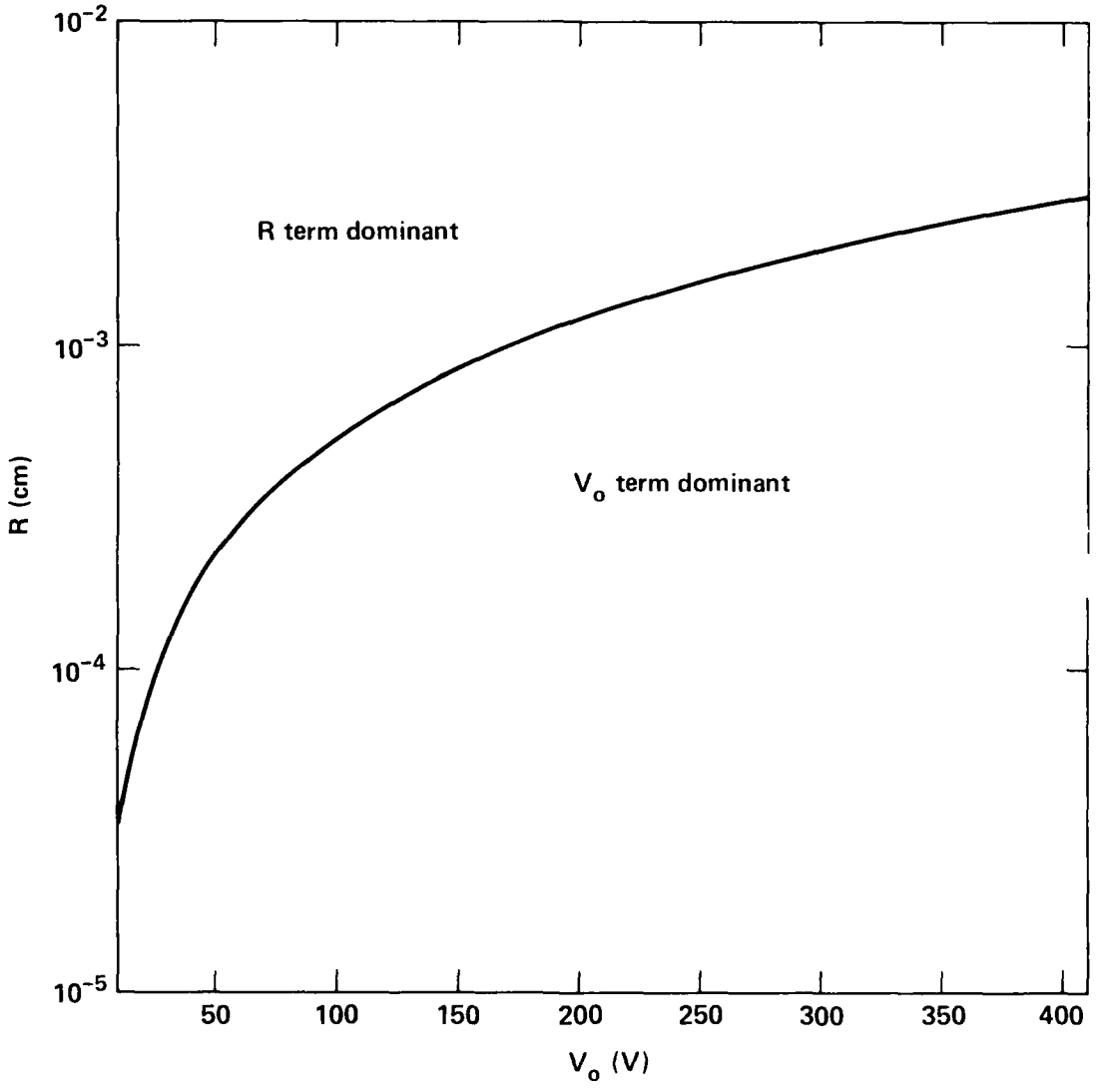

Figure 25. Splitting of the t^{-1} term in Tasca's equation.

Now, the total probable error is summed for each of the three regions.

For region one, where t^{-1} and V_b are dominant, the errors are

	Bias error	Random error
Pulse length		±0.2
Failure temperature		±0.36
Heat capacity		±0.06
Active area		±0.01
Breakdown voltage		±0.2
Infinite device	-0.0035	±0.0035
Equation approximation	0.275	±0.275
Spherical to cylindrical switch	?	?
No current-mode breakdown	?	?
Total bias error (SUM)	0.27	
Total random error (RSS)		±0.54

For region two, where t^{-1} and R are dominant, the errors are

	Bias error	Random error
Pulse length		±0.2
Failure temperature		±0.36
Heat capacity		±0.06
Active area		±0.01
Hot-spot radius		±0.33
Infinite device	-0.0035	±0.0035
Equation approximation	0.275	±0.275
Spherical to cylindrical switch	?	?
No current-mode breakdown	?	?
Total bias error (SUM)	0.27	
Total random error (RSS)		±0.60

And finally, for region three, where $t^{-1/2}$ is dominant, the errors are

	Bias error	Random error
Pulse length		±0.1
Failure temperature		±0.36
K and c		±0.06
Active area		±0.01
Infinite device	-0.0035	±0.0035
Equation approximation	0.275	±0.275
Spherical to cylindrical switch	?	?
No current-mode breakdown	?	?
Total bias error (SUM)	0.27	
Total random error (RSS)		±0.47

Empirical Models

The empirical models, being extensions of the analytical models mentioned previously, will have similar error estimates to those models, minus the bias errors that would be removed by the empirical curve fitting of the data. A few models have made the power of t and its coefficients adjustable. Because the error equations are

differential, this factor will be multiplied by the error and should be included in that manner. In general, the values for the power of t do not appreciably differ from the values in the analytical models, so the calculated errors will not be that different.

Numerical Second Breakdown Models

The numerical thermal models can describe heat flow in a diode. However, as Wunsch and Bell have shown, in one dimension that problem can be solved analytically. The numerical thermal models can produce three-dimensional solutions, but without the electronic effects their results will not be much more accurate than the analytical thermal models. This can be seen by examining the error induced in the Wunsch-Bell model by assuming a one-dimensional device. The improvement in accuracy is not worth the large increase in complexity encountered in going from the simple analytical equation to the numerical model.

The numerical electrical models can describe some pre-second breakdown electrical effects; this is especially true for those models that can handle high electric fields. However, without the thermal effects, these models lack one of the most important parameters associated with second breakdown.

Of all of the numerical models described in this report, only the time-dependent electrothermal models can really be useful in determining power failure thresholds and delay times. None of the models described have been compared with experimental data, other than in a qualitative way. This will make it difficult to ascribe error tolerances to these models with any degree of confidence.

The pulse length error associated with the analytical models also applies here, as the pulse lengths must still be read from an oscilloscope for comparison to the model results. The rise-time part of this error can be neglected, since a time-dependent model can be made to duplicate any rise time; however, this is only a small fraction of the total pulse length error and will not change its magnitude.

The failure-temperature error is not applicable to the numerical models, since the magnitude of a particular failure-temperature variable is not used to determine where failure occurs. Normally, the time-dependent, electrical, and thermal results are reviewed to determine where failure would have occurred.

Since these models all have temperature-dependent thermal conductivities and heat capacities, the error induced by assuming a single constant value will be eliminated. The remaining error attributable to these parameters is that inherent in the experimental data used to define those values. If the errors are assumed to be independent and equal to about 10%, then the cumulative error will be ± 0.14 . Other parameters that affect the power, and which are derived from experimental data, are the mobility (μ_n and μ_p) and the avalanche coefficients. Since power is proportional to the square of the current, and current is proportional to the mobility, the fractional error in the power will be equal to twice the fractional error in the mobility. If we again assume 10% error, this will amount to ± 0.2 . The avalanche coefficient is also approximately proportional (to first order) to the current. If the avalanche coefficient is also assumed to have 10% error, another ± 0.2 is added to the fractional error in the power. The root sum square of these errors amounts to ± 0.32. More error may also be induced by these terms in the high-field or

high-temperature regime of device operation since, in many such cases, no test data exist and the coefficients used are extrapolations from known values.

The infinite device errors do not apply here, since the models have definite extents and heat sinks. The one-dimensional device errors will apply, since all of these models assume one-dimensional geometry. This limitation will also prevent them from showing current filament formation; however, the effective device area can be adjusted to compensate for most uniform breakdown errors.

Because the models solve electronic as well as thermal equations and can model current-mode second breakdown, no error will be associated with the absence of a current-mode second breakdown term. Combining all of these errors for the numerical, electrothermal models yields:

	Bias error	Random error
Pulse length		±0.1
Active area		±0.01
Multiple hot-spots		±0.05
Experimental parameters		±0.32
One-dimensional device	-0.11	±0.11
Total bias error (SUM)	-0.11	
Total random error (RSS)		±0.36

V EXPERIMENTAL COMPARISONS

Many experimental comparisons have been made with the Wunsch-Bell type of analytical models, since these models are most popular for engineering analysis. Few significant comparisons have been made between other models and any experimental data; this is the case with even the numerical models that come so much closer to the real physics of the situation.

Analytical Models

Figure 26 from Ref. 1 compares data points for a number of different devices with the Wunsch-Bell model. The upper line on the figure is the Wunsch-Bell model (assuming uniform breakdown of the whole junction), and the lower curve is drawn with the assumption that the breakdown occurs only over one-tenth of the junction area. The projected error analysis from the last section for the upper curve was a bias error of -0.41 and a random component of ±0.50 . These errors compare well with the scatter in the data. The lower curve attempts to take out much of the bias error by assuming that the failure actually occurs in a filament that covers only one tenth of the junction area. This curve overshoots the bias error, suggesting that the actual failure area covers something like 30 to 50% of the junction rather then 10%.

Figure 27 from Ref. 26 compares the Tasca model with some experimental data for a 1N914 diode. There are two sets of curves on the figure: one set assumes that failure occurs when the device temperature reaches melting and that the radius of the failure region is 30% of the junction radius. The other set assumes that failure occurs when the temperature reaches the intrinsic temperature (approximately 900 K) and that the radius of the failure region is 50% of the junction radius. These two sets of curves are split into an upper curve and a lower curve on the basis of the upper and lower limits of the junction area given in the manufacturer's literature. The short-pulse-error estimates for this model have a bias error of 0.27 and random components of ±0.54 and ±0.60. For longer pulses, the bias is also 0.27 with a random component of ±0.47 . At a pulse length of 30 ns, the curves range between 49 and 631 μJ. If an average junction area is assumed, then the value would be 340 μJ. Biasing this up by 0.27 and adding a random component of ±0.47 yields a value of 432 ±160 μJ, or a range of data from 272 to 592 μJ. This brackets the data relatively well, but misses a few of the lower-energy data points, indicating that the bias error is possibly a little bit large.

Empirical Models

The empirical models, for the most part, are based on the form of the analytical thermal models described above. As such, they have the same error bounds as the analytical thermal models minus the bias errors. They would compare with experimental data as well as do the analytical thermal models.

Alexander, Karaskiewicz, and Enlow (Ref. 4) have performed a rather detailed statistical analysis of device topologies and processing methods. The tabular listing in Fig. 28 details some of their results for several topologies and processing methods. The figure shows the failure data for one process/topology combination and a curve fit to that data. The upper and lower lines are the 95% confidence limits of

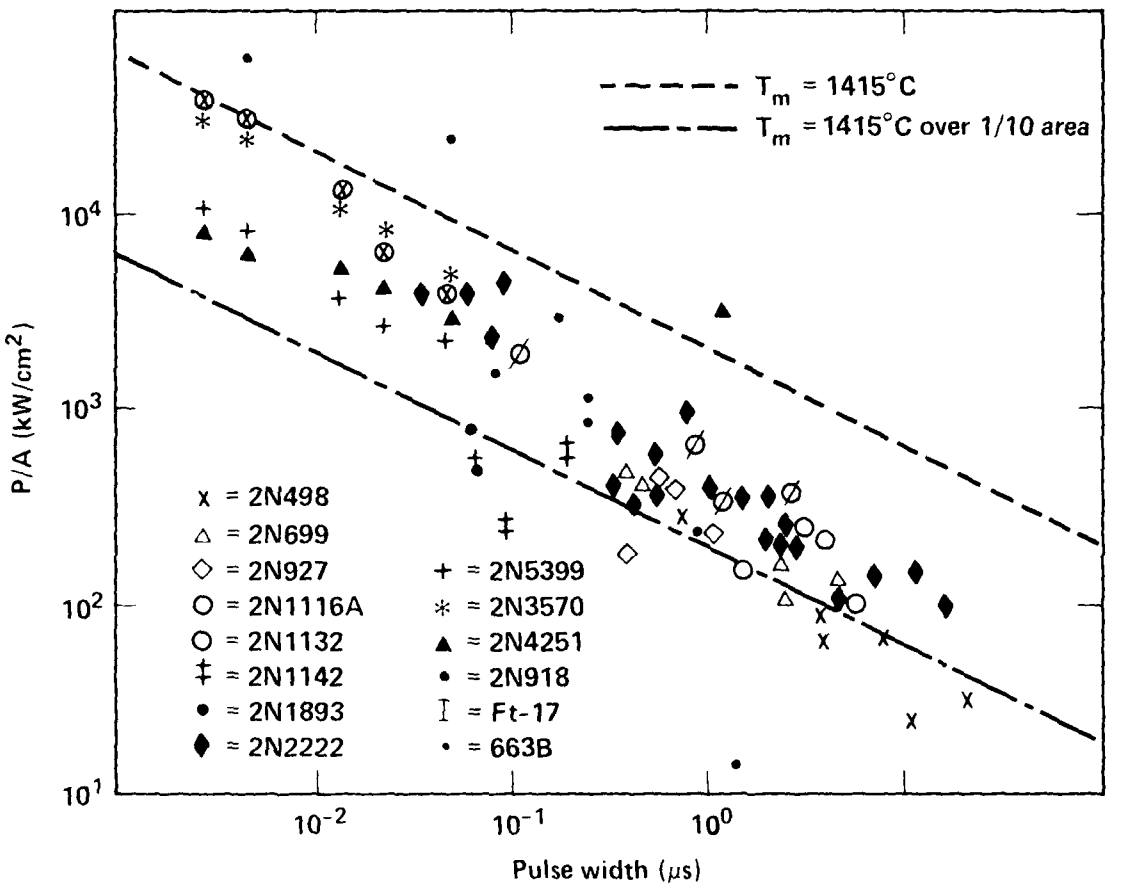

Figure 26. Wunsch-Bell failure model compared with a variety of different experimental data values (after Ref. 1).

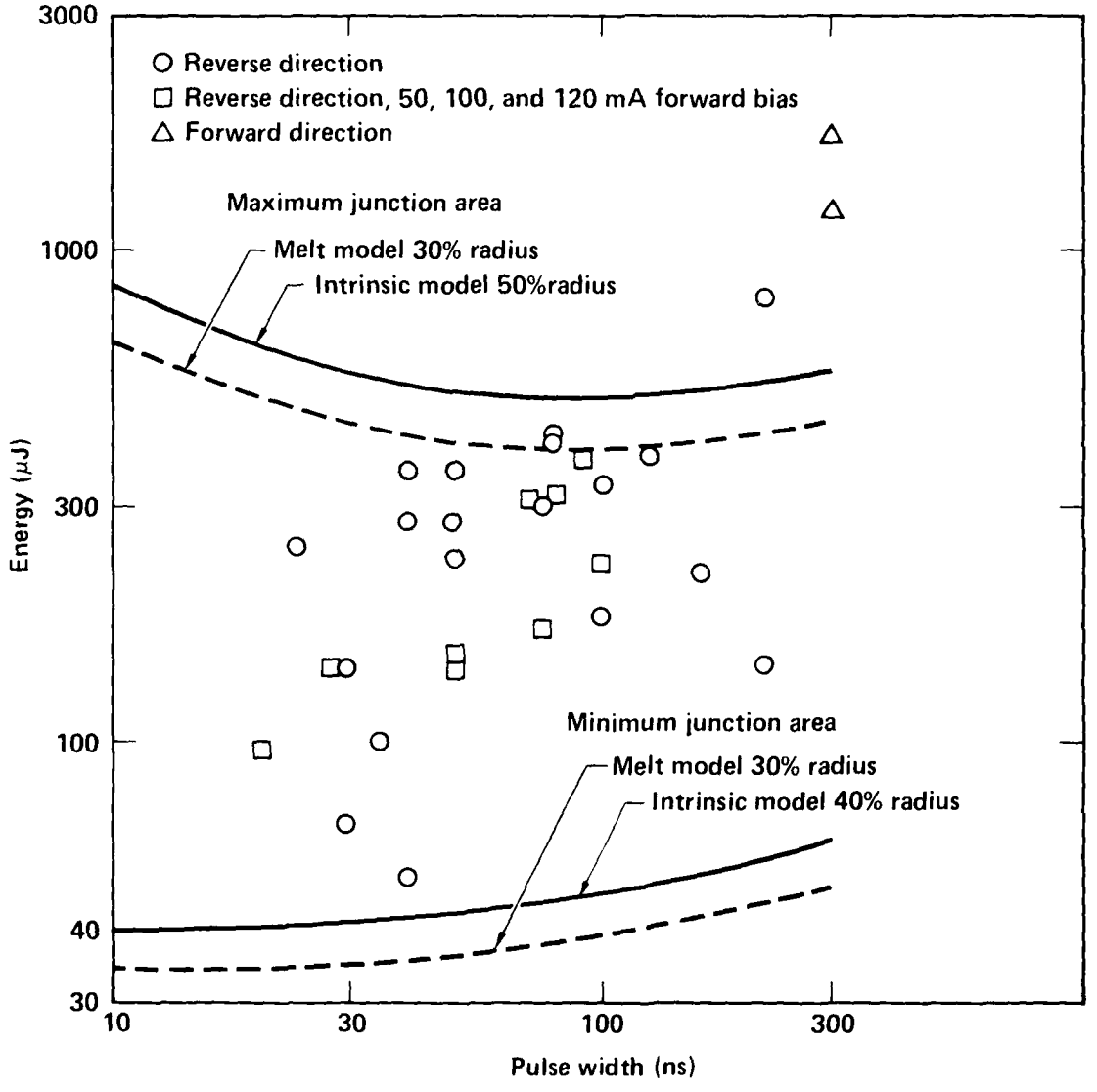

Figure 27. Tasca model compared with some data for a 1N914 diode (after Ref. 26).

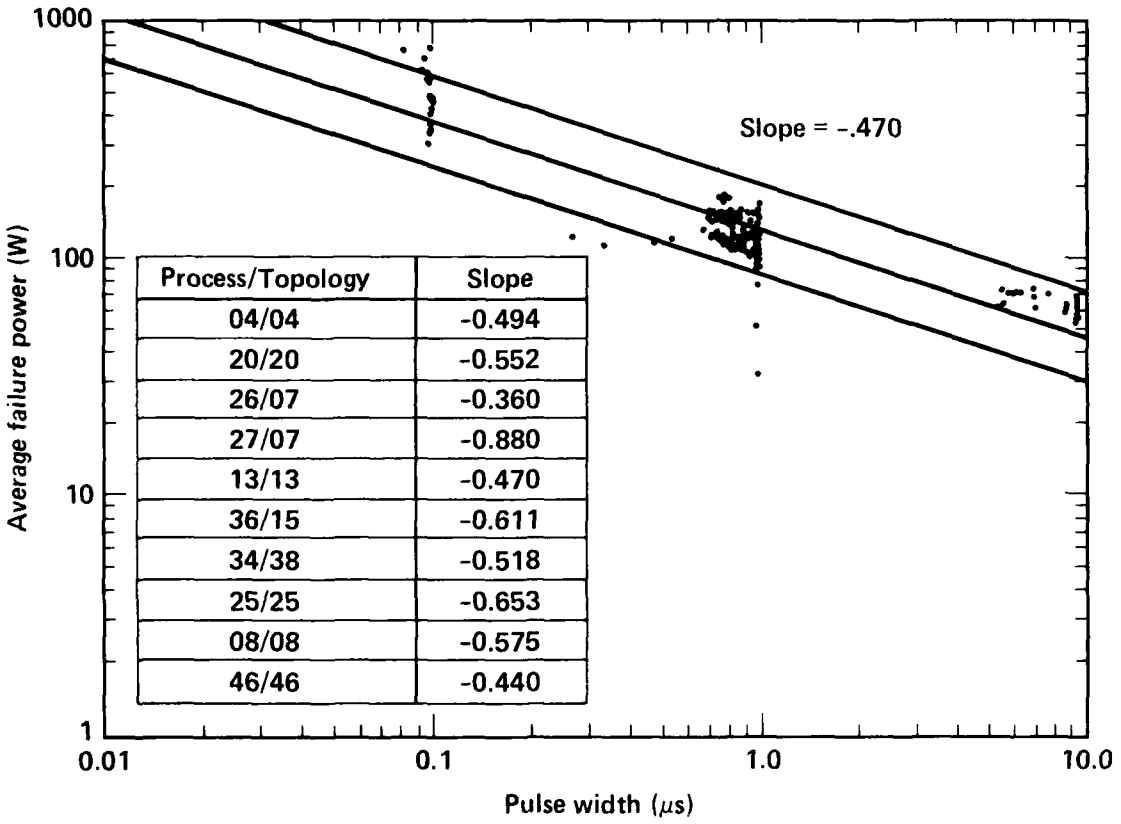

Process/Topology	Slope
04/04	-0.494
20/20	-0.552
26/07	-0.360
27/07	-0.880
13/13	-0.470
36/15	-0.611
34/38	-0.518
25/25	-0.653
08/08	-0.575
46/46	-0.440

Figure 28. Experimental results from Alexander et al. and a curve fit to that data (after Ref. 4).

the curve fit. Note that the slope of the curve (power of t) is -0.47, which is close to the theoretical value (-0.50) predicted by the Wunsch-Bell model. The upper and lower 95% confidence limits have a value of about ±0.4 of the model value. This would seem typical of the data presented in the report. The tabular listing shows the slopes for a number of other process/topology combinations. The average slope for all of these combinations is -0.56, which again compares well with the theoretical value of -0.5.

Numerical Models

For the most part, the numerical models have not been quantitatively compared with experimental data. Rather, the results have been compared qualitatively with experimental trends. The experimental thermal results of Knight and Budenstein (Ref. 48) compare well qualitatively with the numerical modeling results of Orvis and Yee (Ref. 15). Figure 29 shows the experimental heating results of Knight and Budenstein. The thin film silicon-on-sapphire diode is 200 μm wide and the n region is 100 μm long and 0.6 μm thick. The figures are darker in regions of higher temperature. Note that the heating is greatest at the p^+-n junction and at the n-n^+ junction. Figure 30, from the paper by Orvis et al. (Ref. 15), shows heating in similar regions of the device, although the modeled device is much smaller then the experimental device (10 μm compared to 100 μm).

The low-voltage characteristics of the model by Orvis are shown in Fig. 31 from Ref. 15. These characteristics are compared to the well-established analytical characteristics from Sze (Ref. 54). Note that the largest deviation is on the order of only 8%.

Metallization Models

Figure 32 shows the application of the Tasca metallization failure model to real failure data (Ref. 26). The model shows two curves calculated for the minimum and maximum cross-sectional area of the metallization, as defined by the manufacturer. As would be expected, the failure points seem to cluster about the curve for the minimum cross-sectional area (i.e., smaller wires are easier to burn out).

Figure 33 similarly compares the Pierce model of metallization failure applied to an aluminum trace over an oxide barrier (Ref. 49).

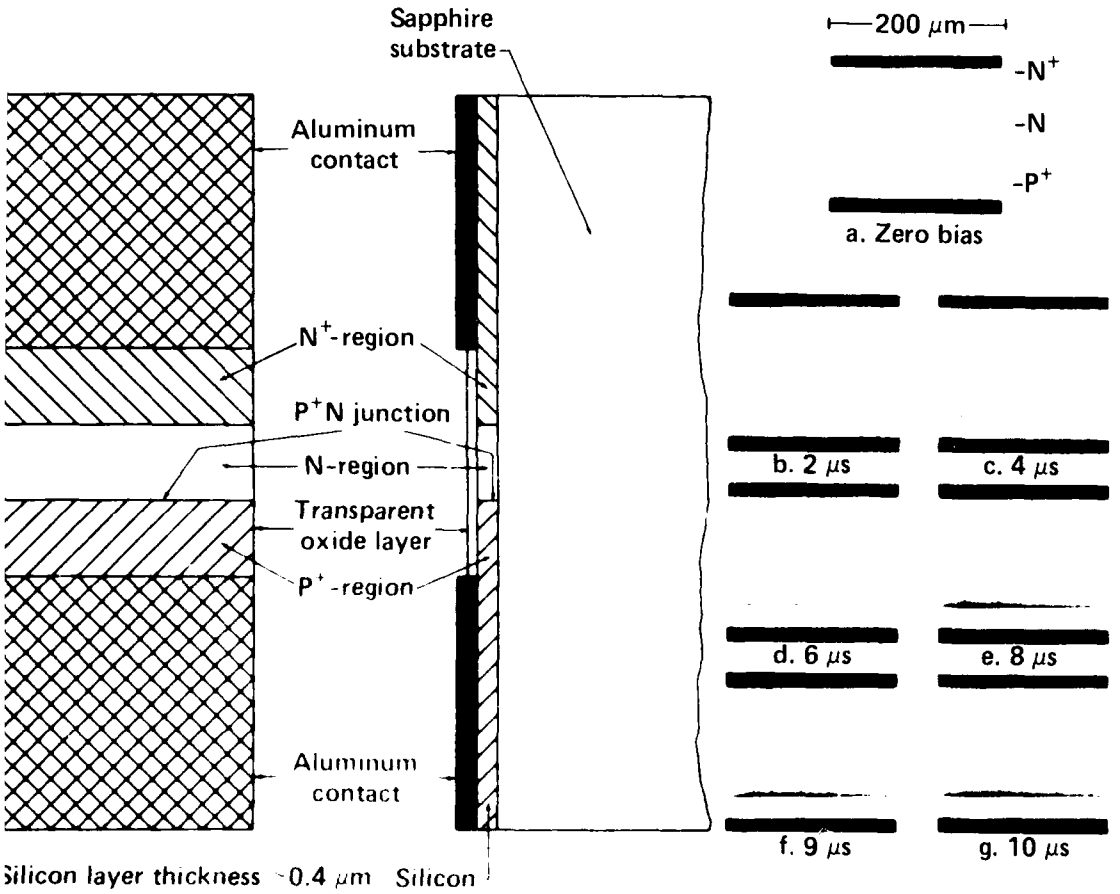

Figure 29. Experimental heating results of Knight and Bodenstein on a thin film silicon-on-sapphire diode. Darker areas in the photographs indicate higher temperatures (after Ref. 18).

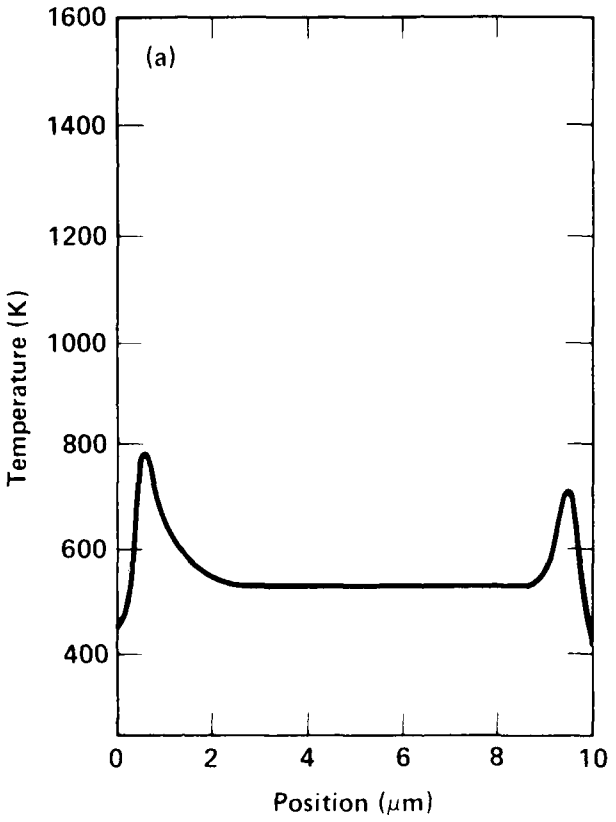

Figure 30. Numerical heating results by Orvis. The higher temperatures occur at the boundaries of the n region (Ref. 15).

50. D. C. Wunsch, "The Application of Electrical Overstress Models to Gate Protective Networks," *16th Annual Proceedings, Reliability Physics 1978* (IEEE Electron Devices Society and IEEE Reliability Group, San Diego, CA, 1978), pp. 47-55.

51. J. S. Smith, "Electrical Overstress Failure Analysis in Microcircuits," *16th Annual Proceedings, Reliability Physics 1978* (IEEE Electron Devices Society and IEEE Reliability Group, San Diego, CA, 1978), pp. 41-46.

52. B. M. Kalab, *Analysis of Failure of Electronic Circuits from EMP-Induced Signals--Review and Contribution*, Harry Diamond Laboratories, Adelphi, MD, HDL-TR-1615 (1973).

53. H. F. Wolf, *Silicon Semiconductor Devices*, 2nd ed. (Pergamon Press, New York, NY, 1969), pp. 98-99.

54. S. M. Sze, *Physics of Semiconductor Devices*, 2nd ed. (John Wiley & Sons, New York, 1981).

55. R. A. Croxall and A. K. Thomas, *Subsystem Nuclear Vulnerability Assessment Methodology*, Air Force Weapons Laboratory, Kirtland AFB, NM, AFWL-TR [illegible] (1978).

56. R. E. Thomas, "Semiconductor Device Failure Criteria for Simulated [illegible] *Electrical Overstress/Electrostatic Discharge Symposium Proceedings* (Reliability Analysis Center, RADC/RBRAC, Griffiss AFB, NY; [illegible] 1981), vol. EOS-3, pp. 139-144 (1982).

T. Misawa, "Negative Resistance in *p-n* Junctions Under Avalanche Breakdown Conditions, Part II," *IEEE Trans. Elect. Dev. ED-13*(1), pp. 143-151 (1966).

V. A. J. Van Lint, J. H. Alexander, D.K. Nichols, and P. R. Ward, "Computerized Model for Response of Transistors to a Pulse of Ionizing Radiation," *IEEE Trans. Nucl. Sci. NS-14*(6) pp. 170-178 (1967).

M. W. Muller and H. Guckel, "Negative Resistance and Filamentary Currents in Avalanching Silicon p^+-i-n^+ Junctions," *IEEE Trans. Elect. Dev. ED-15*(8), pp. 560-568 (1968).

H. C. Bowers, "Space-Charge-Induced Negative Resistance in Avalanche Diodes," *IEEE Trans. Elect. Dev. ED-15*(6), pp. 343-350 (1968).

L. R. Razouk and G. W. Neudeck, "The p^+-n^--n^+ Diode Pulsed at Extreme Current Densities--I. Numerical Techniques and Reverse Pulsed Case," *Solid State Electronics 23*, pp. 143-149 (1980).

G. W. Neudeck and L. R. Razouk, "The p^+-n^--n^+ Diode Pulsed at Extreme Current Densities--II. The Forward Pulsed Case and its Anomalous Voltage Response," *Solid State Electronics 23*, pp. 151-155 (1980).

E. M. Buturla, P. E. Cottrell, B. M. Grossman, and K. A. Salsburg, "Finite-Element Analysis of Semiconductor Devices: The FIELDAY Program," *IBM J. Res. Develop. 25*(4), pp. 216-231 (1981).

G. D. Hachtel, M. H. Mack, R. R. O'Brien, and B. Speelpenning, "Semiconductor Analysis Using Finite Elements--Part I: Computational Aspects," *IBM J. Res. Develop. 25*(4), pp. 232-245 (1981).

G. D. Hachtel, M. H. Mack, and R. R. O'Brien, "Semiconductor Analysis Using Finite Elements--Part II: IGFET and BJT Case Studies," *IBM J. Res. Develop. 25*(4), pp. 246-260 (1981).

S. P. Gaur and D. H. Navon, "Two-Dimensional Carrier Flow in a Transistor Structure Under Nonisothermal Conditions," *IEEE Trans. Elect. Dev. ED-23*(1), pp. 50-57 (1976).

K. Hane, M. Mogi, and T. Suzuki, "Influence of an External Resistor on Second Breakdown in Epitaxial Planar Transistors," *IEEE Trans. Elect. Dev. ED-26*(2), pp. 157-158 (1979).

E. R. Knight and P. P. Budenstein, "Effects of Junction Spikes and Doping Level on the Second Breakdown Susceptibility of Silicon-on-Sapphire Diodes," *Electrical Overstress/Electrostatic Discharge Symposium Proceedings, 1980* (Reliability Analysis Center, RADC/RBRAC, Griffiss AFB, NY; San Diego, CA; 1980), vol. EOS-2, pp. 122-129 (1981).

D. G. Pierce, "Modeling Metallization Burnout of Integrated Circuits, *Electrical Overstress/Electrostatic Discharge Symposium Proceedings, 1982* (Reliability Analysis Center, RADC/RBRAC, Griffiss AFB, NY; Orlando, FL; 1982), vol. EOS-4, pp. 56-61 (1983).

23. A. C. English, "Physical Investigation of the Mesoplasma in Silicon," *IEEE Trans. Elect. Dev. ED-13*(8/9), pp. 662-667 (1966).

24. R. H. Haitz, A. Goetzberger, R. M. Scarlett, and W. Shockley, "Avalanche Effects in Silicon *p-n* Junctions. I. Localized Photomultiplication Studies on Microplasmas," *J. App. Physics 34*(6), pp. 1581-1590 (1963).

25. A. Goetzberger, B. McDonald, R. H. Haitz, and R. M. Scarlett, "Avalanche Effects in Silicon *p-n* Junctions. II. Structurally Perfect Junctions," *J. App. Physics 34*(6), pp. 1591-1600 (1963).

26. D. M. Tasca, "Pulse Power Failure Modes in Semiconductors," *IEEE Trans. Nucl. Sci. NS-17*(6), pp. 364-372 (1970).

27. H. S. Carslaw and J. C. Jaeger, *Conduction of Heat in Solids*, 2nd ed., (Oxford University Press, London, 1959), pp. 348-349.

28. W. D. Raburn and W. H. Causey, *Determination of Semiconductor Junction Vulnerability to Second Breakdown*, U. S. Army Missle Research and Development Command, Redstone Arsenal, AL, EA-CR-77-1 (1977).

29. T. Misawa, "Negative Resistance in *p-n* Junctions Under Avalanche Breakdown Conditions, Part I," *IEEE Trans. on Elect. Dev. ED-13*(1), pp. 137-143 (1966).

30. D. M. Tasca and S. J. Stokes, III, *EMP Response and Damage Modeling of Diodes, Junction Field Effect Transistor Damage Testing and Semiconductor Device Failure Analysis, Final Report*, Harry Diamond Laboratories, Adelphi, MD, HDL-CR-76-090-1 (1976).

31. H. B. O'Donnell and D. M. Tasca, *Development of High Level Electrical Stress Failure Threshold and Prediction Model for Small Scale Junction Integrated Circuits*, General Electric Co., Philadelphia, PA, Report No. 77SD4252 (1977).

32. D. R. Alexander, J. B. Almassy, G. L. Brown, D. L. Durgin, C. R. Jenkins, R. N. Randall, A. Unwin, and J. J. Schwartz, *Electromagnetic Susceptibility of Semiconductor Components*, Air Force Weapons Laboratory, Kirtland Air Force Base, NM, AFWL-TR-280 (1975).

33. H. M. Olson, "DC Thermal Mode of Semiconductor Device Produces Current Filaments as Stable Current Distributions," *IEEE Trans. Elect. Dev. ED-24*(9), pp. 1177-1184 (1977).

34. N. Kusnezov and J. S. Smith, "Modeling of Electrical Overstress in Silicon Devices," *Electrical Overstress/Electrostatic Discharge Symposium Proceedings, 1979* (Reliability Analysis Center, RADC/RBRAC, Griffiss AFB, NY; Denver, CO; 1979), vol. EOS-1, pp. 133-139 (1980).

35. N. Kusnezov and J. S. Smith, "Modeling of EOS in Silicon Devices," *Electrical Overstress/Electrostatic Discharge Symposium Proceedings, 1981* (Reliability Analysis Center, RADC/RBRAC, Griffiss AFB, NY; Las Vegas, NV; 1981), vol. EOS-3, pp. 132-138 (1982).

36. K. Kano and H. J. Reich, "Forward Transient Behavior of *p-n* Junction Diodes at High Injection Levels," *IEEE Trans. Elect. Dev. ED-11*, pp. 515-523 (1964).

10. J. W. Yee, W. J. Orvis, and L. C. Martin, *Theoretical Modeling of EMP Effects in Semiconductor Junction Devices*, Air Force Weapons Laboratory, Kirtland Air Force Base, NM, AFWL-TR-82-91 (also available as Lawrence Livermore National Laboratory, Livermore, CA, UCRL-87672) (1982).

11. J. R. Black, "Electromigration--A Brief Survey and Some Recent Results," *IEEE Trans. Elect. Dev. 16*, p. 338 (1969).

12. R. L. Davies and F. E. Gentry, "Control of Electric Field at the Surface of *p-n* Junctions," *IEEE Trans. Elect. Dev. ED-11*, pp. 313-323 (1963).

13. L. L. Alston, *High-Voltage Technology* (Oxford University Press, London, 1968).

14. N. Klein, "Electrical Breakdown in Solids," *Adv. Electr. Electron Physics 26*, L. Martin, Ed., (Academic Press, New York, NY, 1969), pp. 309-424.

15. W. J. Orvis, C. F. McConaghy, J. H. Yee, G. H. Khanaka, L. C. Martin, and D. L. Lair, "Modeling and Testing for Second Breakdown Phenomena," *Electrical Overstress/Electrostatic Discharge Symposium Proceedings, 1983* (Reliability Analysis Center, RADC/RBRAC, Griffiss AFB, NY; Las Vegas, NV; 1983), vol. EOS-5 (also available as UCRL-89147, Lawrence Livermore National Laboratory, Livermore, CA, (1983)).

16. K. Koyanagi, K. Hane, and T. Suzuki, "Boundary Conditions Between Current Mode and Thermal Mode Second Breakdown in Epitaxial Planar Transistors," *IEEE Trans. Elect. Dev. ED-24*(6), pp. 672-878 (1977).

17. I. Dunn and K. I. Nuttal, "An Investigation of the Voltage Sustained by Epitaxial Bipolar Transistors in Current Mode Second Breakdown," *Int. J. Electronics 45*(4), pp. 353-372 (1978).

18. J. H. Yee, W. J. Orvis, L. C. Martin, and J. C. Peterson, "Modeling of Current and Thermal Mode Second Breakdown Phenomena," *Electrical Overstress/ Electrostatic Discharge Symposium Proceedings, 1982* (Reliability Analysis Center, RADC/RBRAC, Griffiss AFB, NY; Orlando, FL; 1982), vol. EOS-4, pp. 76-81 (1983).

19. A. L. Ward, *Calculations of Second Breakdown in Silicon Diodes*, Harry Diamond Laboratories, Adelphi, MD, HDL-TR-1978 (1982).

20. D. C. Wunsch and R. R. Bell, "Determination of Threshold Failure Levels of Semiconductor Diodes and Transistors Due to Pulse Power Voltages," *IEEE Trans. Nucl. Sci. NS-15*(6), pp. 244-259 (1968).

21. A. Baruah and P. P. Budenstein, "An Electrothermal Model for Current Filamentation in Second Breakdown of Silicon on Sapphire Diodes," *Electrical Overstress/Electrostatic Discharge Symposium Proceedings, 1979* (Reliability Analysis Center, RADC/RBRAC, Griffiss AFB, NY; Denver, CO; 1979), vol. EOS-1, pp. 76-81 (1980).

22. A. C. English, "Mesoplasmas and "Second Breakdown" in Silicon Junctions," *Solid State Electronics 6*, pp. 511-521 (1963).

VIII REFERENCES

1. D. G. Pierce and D. L. Durgin, "An Overview of Electrical Overstress Effects on Semiconductor Devices," *Electrical Overstress/Electrostatic Discharge Symposium Proceedings, 1981* (Reliability Analysis Center, RADC/RBRAC, Griffiss AFB, NY; Las Vegas, NV; 1981), vol. EOS-3, pp. 120-131 (1982).

2. D. L. Durgin, "An Overview of the Sources and Effects of Electrical Overstress," *Electrical Overstress/Electrostatic Discharge Symposium Proceedings, 1980* (Reliability Analysis Center, RADC/RBRAC, Griffiss AFB, NY; San Diego, CA; 1980), vol. EOS-2, pp. 154-160 (1981).

3. D. M. Tasca, J. C. Peden, and J. L. Andrews, *Theoretical and Experimental Studies of Semiconductor Device Degradation Due to High Power Electrical Transients*, Harry Diamond Laboratories, Washington, DC, AD-780-160 (also available as General Electric Co., Philadelphia, PA, Report No. 73SD4289) (1973).

4. D. R. Alexander, R. J. Karaskiewicz, and E. W. Enlow, *Component Statistical Characterization, Parts 1 to 4*, Air Force Weapons Laboratory, Kirtland AFB, NM, AFWL-TR-80-128, Pt. 1-4 (1981).

5. B. M. Kalab, *Damage Characterization of Semiconductor Devices for the AN/TRC-145 EMP Study*, Harry Diamond Laboratories, Adelphi, MD, HDL-TR-1915 (1980).

6. R. N. Shaw, R. D. Enoch, and R. D. Taylor, "A Versatile Mini-Computer Controlled ESD Test Equipment for Automatic Testing in Human-Body-Models," *Electrical Overstress/Electrostatic Discharge Symposium Proceedings, 1982* (Reliability Analysis Center, RADC/RBRAC, Griffiss AFB, NY; Las Vegas, NV; 1983), vol. EOS-5.

7. O. J. McAteer, R. E. Twist, and R. C. Walker, "Latent ESD Failures," *Electrical Overstress/Electrostatic Discharge Symposium Proceedings, 1982* (Reliability Analysis Center, RADC/RBRAC, Griffiss AFB, NY; Orlando, FL; 1982), vol. EOS-4, pp. 41-48 (1983).

8. E. L. Horgan, O. E. Adams, W. H. Rowan, and L. C. Templar, "EOS/ESD Failure Threshold Analysis Errors, Their Source, Size, and Control," *Electrical Overstress/Electrostatic Discharge Symposium Proceedings, 1981* (Reliability Analysis Center, RADC/RBRAC, Griffiss AFB, NY; Las Vegas, NV; 1981), vol. EOS-3, pp. 151-166 (1982).

9. D. L. Durgin, R. M. Pelzl, W. H. Thompson, and R. C. Walker, "A Survey of EOS/ESD Data Sources," *Electrical Overstress/Electrostatic Discharge Symposium Proceedings, 1982* (Reliability Analysis Center, RADC/RBRAC, Griffiss AFB, NY; Orlando, FL; 1982), vol. EOS-4, pp. 49-55 (1983).

- They have a framework that makes it possible to consider all of the relevant physics of device operation in high-voltage and high-temperature regimes.
- They predict current-mode as well as thermal-mode second breakdown.
- They allow detailed investigation into the real physical phenomena that occur during second breakdown. Because of this feature, these models are the source of much information about designing and operating devices that will maximize system survival during an EOS.

As these models become more sophisticated and reach higher dimensionality, they will probably be able to predict power-failure thresholds and pulse widths and to pinpoint where and why a device failed. At this point, simpler analytic and empirical models can be developed to reflect the information learned from the application of electrothermal models, and it will be possible to develop models useful for system analysis of larger devices.

Because metallization failure occurs at a high rate, several models for the process are described in Section III. These models are quite similar to the semiconductor-failure models, although they predict failure currents versus pulse widths rather than failure powers. Although we describe metallization failure models, no error analysis has been performed on them at this time.

VII CONCLUSIONS

In the preceeding sections, representative models for semiconductor analysis were described; these fall into two subsets:

- Models that, while useful for other types of semiconductor analysis, can be used to investigate only part of the failure process.
- Models that can investigate power-failure thresholds and pulse widths and are thus directly useful for failure analysis in our engineering environment.

The useful models are of three types: analytical thermal, empirical (based on analytical thermal), and numerical electrothermal models.

The Wunsch or Wunsch-Bell models--and variations developed by Tasca and O'Donnell--are the most widely used forms of the analytical and empirical models. In the most common analytical model, failure-power density is proportional to the inverse square root of the pulse length:

$$P/A = K_d t^{-1/2} \quad . \tag{76}$$

The damage coefficients (K_d) for many devices are tabulated in several large databases. Variations include adding terms in t^{-1} for shorter pulse lengths and replacing the constant powers with variable powers of t. For our purposes, these refinements are unnecessary because the large amount of scatter in the data completely overshadows their effects.

When sufficient experimental data are available, the empirical models are advantageous because the equation can be fitted directly to the data. With an empirical model, it is thus possible to eliminate bias errors and uncertainty that arise from unknowns about a particular device's geometry or characteristics (i.e., when manufacturer's information is lacking). On the other hand, when there are few experimental data, an analytical model should be used, if large biases in the data are allowed for.

Despite its widespread use, the Wunsch-Bell model is not without its drawbacks. The first is the large random error associated with the model, which forces engineers to considerably underestimate the failure thresholds for devices to ensure that they will survive. The problem is even more pronounced when a single unit contains device types purchased from different manufacturers (see Fig. 3). To compound these shortcomings, an engineer must beware of the fact that the Wunsch-Bell model cannot predict current-mode second breakdown. Therefore, the Wunsch-Bell model types should be used with care for pulse widths less than 100 ns, and with even more care for pulse widths less than 10 ns, to assure that current-mode second breakdown is not present.

Of the numerical models, only the electrothermal versions have sufficient details and device physics to compensate for their complexity and to warrant their use for semiconductor-failure analysis. No numerical model is now used to predict failure thresholds in real devices, and they are not really useful for engineering analysis of electronic components and systems. However, electrothermal models have several unique features that mean that these models will be quite useful as they become more sophisticated:

where

$$g_2(\lambda,\gamma) = \frac{-\lambda(1-\gamma) + [(\lambda+\gamma)^2 + \gamma^2(1-\lambda)]^{1/2}}{2\gamma} \quad . \tag{71}$$

The total-energy equivalence model equates the total energy of the positive half-sine wave with a square pulse of equal width. The frequency conversion factor is

$$K_f = \pi / g_3(\lambda,\gamma) \quad , \tag{72}$$

where

$$g_3(\lambda,\gamma) = \frac{(\gamma - 2\lambda^2)\cos^{-1}(\lambda) + (2-\gamma)\lambda\sqrt{1-\lambda^2}}{2(\gamma+\lambda)(1-\lambda)} \quad . \tag{73}$$

Finally, the thermal equivalence model equates equal temperatures generated in a device for a positive half-cycle sine wave and a square wave. The frequency conversion factor is

$$K_f = 8\pi / [g_4(\lambda,\gamma)]^2 \quad , \tag{74}$$

where

$$g_4(\lambda,\gamma) = \frac{1}{(1-\lambda)(\lambda+\gamma)} \int_{\sin^{-1}(\lambda)}^{X_f} \frac{[\gamma\sin^2(x) + \lambda(1-\gamma)\sin(x) - \lambda^2]}{\sqrt{X_f - x}}\, dx \quad . \tag{75}$$

In Eq. 75, X_f is the value of x that maximizes the integral.

According to Thomas, if these conversion factors are evaluated, they indicate adjustments in the failure power of about 10 to 20%. He therefore suggests that waveform effects are not a major source of uncertainty in EMP vulnerability assessments, since the variability of the damage coefficients is much larger then this factor.

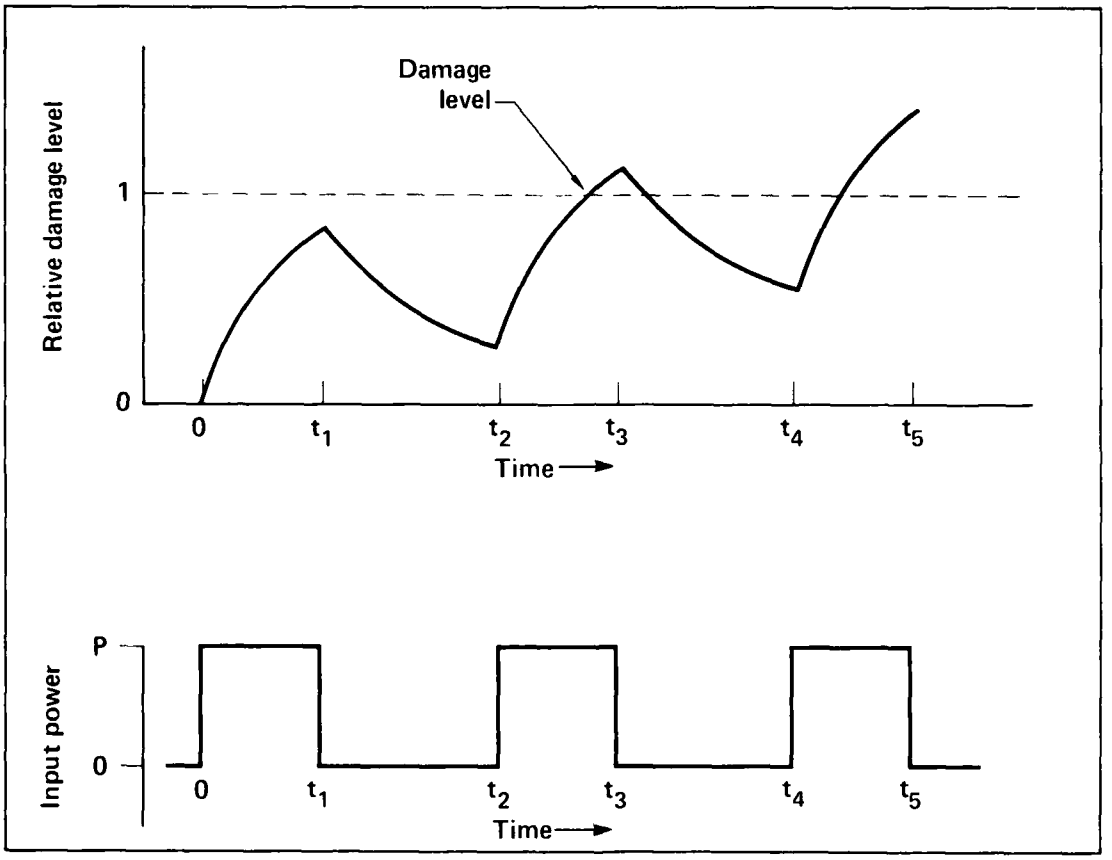

Figure 34. Tasca complex waveform damage-prediction technique. The device is assumed to be damaged when the relative damage level first exceeds 1 (after Ref. 3).

assumed to have failed. Figure 34 is an example of the value of this equation for a unipolar train of square pulses. Using this method, Tasca claims an accuracy of 20 to 50%, depending on the particular form and treatment of the square-wave damage data obtained from limited sample sizes.

R. A. Croxall and A. K. Thomas-- Croxall and Thomas have developed a factor to convert damped sine stress to square pulse; this conversion factor is used with the Wunsch-Bell model (Ref. 55). Assuming that the sine wave damps out with a Q_a of 24 (i.e., the sine wave damps as $\exp[-(\pi/Q_a\tau)t]$, where τ is the period and t is the time), they find a factor,

$$t = 1/(2.25f) \quad , \tag{66}$$

that converts the frequency f of the sine wave to a pulse length that can be inserted directly into the Wunsch-Bell model, with the same damage constant as was determined for square pulse data:

$$P/A = K_d t^{-1/2} \quad . \tag{67}$$

R. E. Thomas-- Thomas takes a much more detailed look at the methods for making sinusoidal data equivalent to square-pulse data (Ref. 56). He uses a method similar to that of Croxall and A. K. Thomas and assumes that the Wunsch-Bell damage equation and damage constant are device-dependent and not stress-dependent. He then determines a frequency conversion factor to convert sinusoidal frequency to pulse and determines an equivalent pulse length to use in the Wunsch-Bell power-failure equation (Eq. 67). This results in the equation

$$P/A = K_d(K_f f)^{1/2} \quad , \tag{68}$$

where f is the frequency of the sine wave and K_f is the frequency conversion factor.

Thomas considers four different equivalency criteria for comparing sinusoidal and square pulses: average power, equivalent half power, total energy, and thermal equivalence. Average power equivalence equates the average power of the positive half cycle of a sine wave to a square pulse of equal duration:

$$K_f = 4\pi\cos^{-1}(\lambda)\left[\frac{(1-\lambda)(\lambda+\gamma)}{(\gamma - 2\lambda^2\cos^{-1}(\lambda) + (2-\gamma)\lambda\sqrt{1-\lambda^2}}\right] , \tag{69}$$

where $\lambda = R_s/R_o$, $\gamma = V_b/V_o$, R_s is the device surge resistance, R_o is the source impedance, V_b is the breakdown voltage, and V_o is the peak open-circuit source voltage.

The half-power equivalence model equates the maximum-power point and the half-power points of the sine wave and the square wave. This results in a frequency conversion factor of

$$K_f = \frac{\pi}{\cos^{-1}g_2(\lambda,\gamma)} \quad , \tag{70}$$

VI STRESS PARAMETERS

Stress parameters are those combinations of electrical waveforms and physical environment that are incident on a semiconductor device because of a real EOS transient, rather than because of an idealized test pulse. Stress parameters include temperature, current, and voltage waveforms incident on the device. Stress parameters can also include the biasing conditions of the device before the EOS pulse is applied. Of all these parameters, second breakdown appears to be most sensitive to the applied power, while metallization failure is sensitive to the applied current. Second breakdown is also sensitive to the initial temperature of the device, although to a much lesser degree than to the applied power. Also of importance in both cases is the pulse length. If the pulse is short enough, then thermal-mode second breakdown failure or metallization failure may be averted. However, in extremely short pulses (less than 100 ns) current-mode second breakdown effects may become apparent that are not accounted for by the analytical or empirical models. The greatest difficulty is in generating a realistic comparison between the real EOS stress pulse waveforms and the square-pulse device-damage data.

While most EOS testing and modeling uses a square-pulse excitation to initiate second breakdown and cause semiconductor devices to fail, the actual stresses that a device will be expected to survive are quite different. Figure 1 compares several of these threats. Of primary importance is the EMP threat, which is generally displayed as a double exponential, with a rise time of 1 to 10 ns and a fall time of 10 to 100 ns. Another EMP pulse waveform is that shown in the figure, where it was assumed that the pulse described above was conducted to the semiconductor in question through an inductive load. This load results in a decaying sine wave. Also of importance is lightning-generated EMP (LEMP), which is generally described as a triangular shaped waveform. Note that none of these waveforms is easily compared with a square pulse.

To offset this difficulty, several authors have attempted to develop some transforms whereby the square-pulse data may be used to predict failures resulting from nonsquare-pulse stresses.

D. M. Tasca, J. C. Peden, and J. L. Andrews-- Tasca et al. experimentally and analytically compare square-pulse failure data with complex-waveform failure data. The complex waveforms consist of unipolar and bipolar square-pulse trains, triangular pulses, and damped sinusoidal waveforms (Ref. 3). They compare the complex stress waveforms with the square-wave failure data through the use of Duhamel's theorem, which relates the temperature rise in a device during the application of a time-varying pulse

$$\Delta T = \int_0^t P(\tau) H'(t - \tau)\, d\tau , \tag{64}$$

where ΔT is the temperature rise, $P(t)$ is the time-varying rate of input power versus time, and $H'(t)$ is the derivative of the square-wave thermal response function. They then modify this equation to take into account the square-pulse damage equations (such as Wunsch-Bell model),

$$1 = \int_0^t P(\tau) \left[\frac{d}{d(t-\tau)} \left(\frac{1}{P_D(t-\tau)} \right) \right] d\tau , \tag{65}$$

where $P_D(t)$ is the square-wave damage power for a pulse width t. This equation is then integrated until the right side first equals 1, at which point the device is

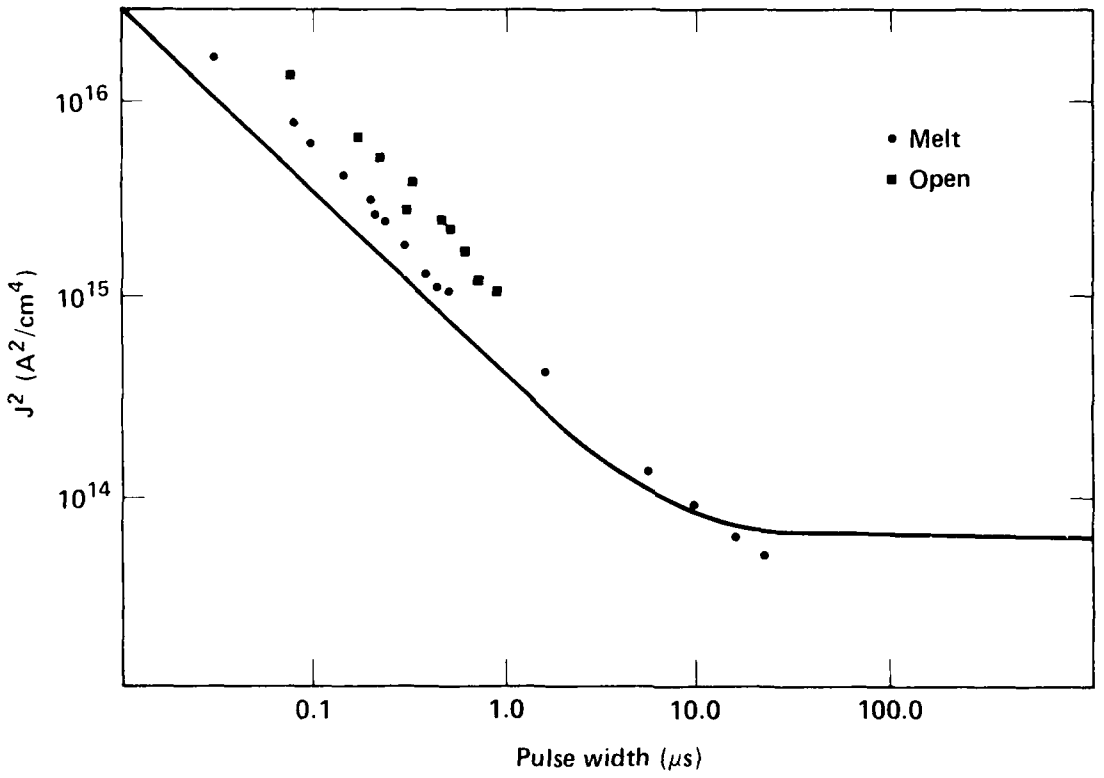

Figure 33. Pierce model of metallization failure compared with experimental data (after Ref. 49).

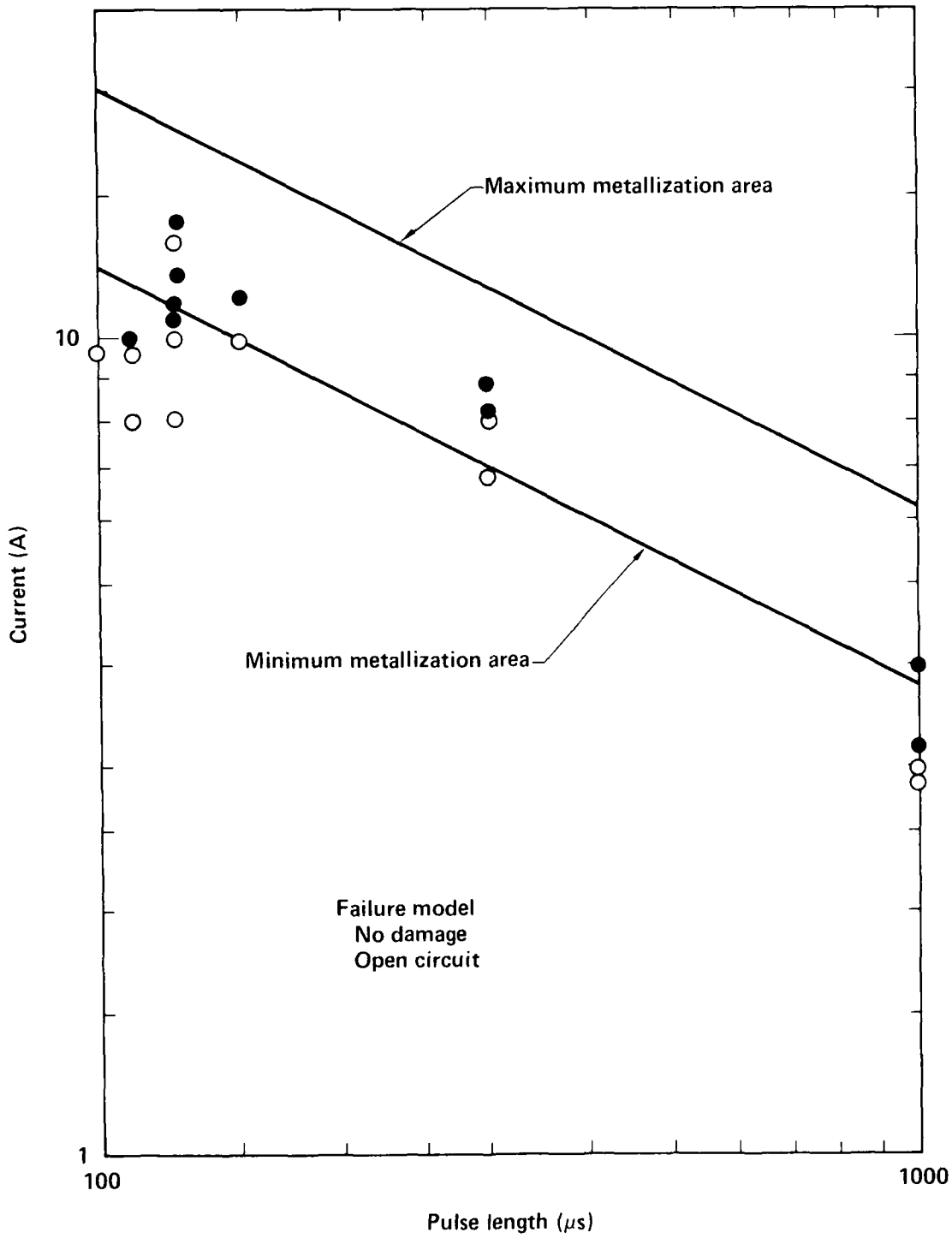

Figure 32. Tasca metallization failure model compared with experimental data (after Ref. 26).

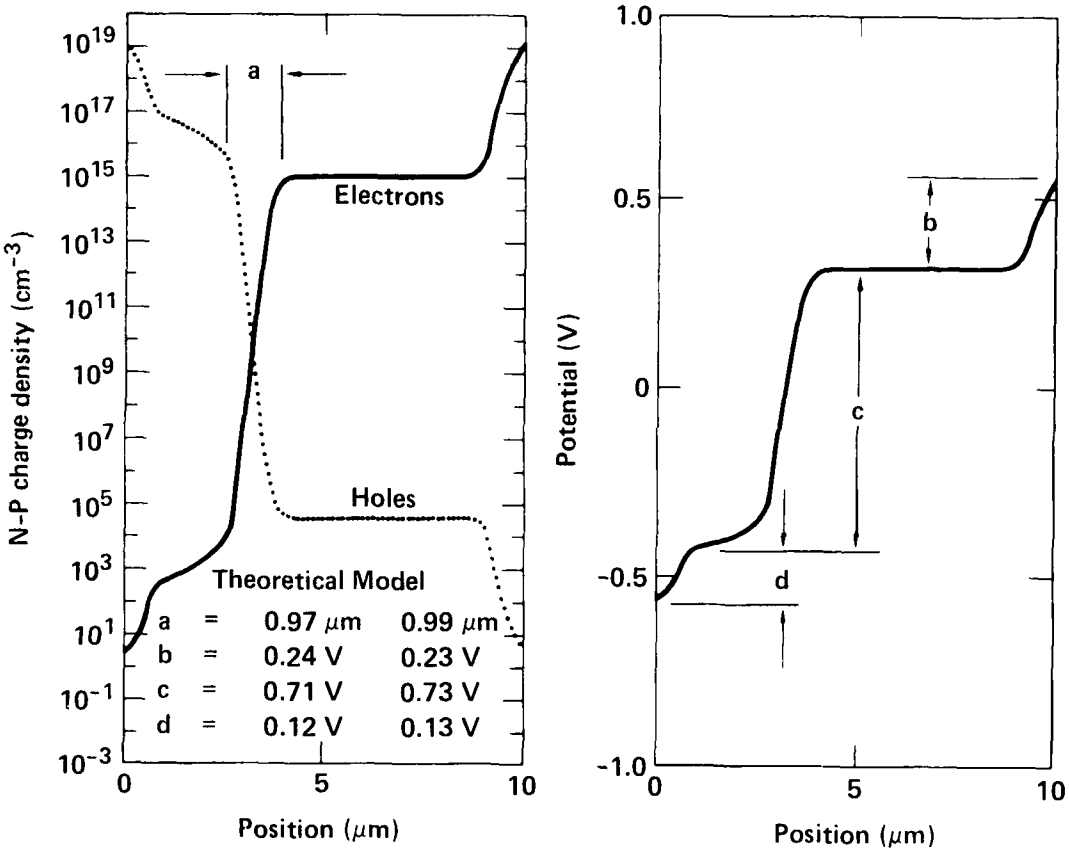

Figure 31. Low voltage results from Orvis compared with some analytical results from Sze (Ref. 15).

IX BIBLIOGRAPHY

Electronic Component Modeling and Testing Program, Pt. 1, Air Force Weapons Laboratory, Kirtland AFB, NM, AFWL-TR-73-62, (1980).

D. R. Alexander, J. B. Almassy, G. L. Brown, D. L. Durgin, C. R. Jenkins, R. N. Randall, A. Unwin, and J. J. Schwarz, *Electromagnetic Susceptibility of Semiconductor Components*, Air Force Weapons Laboratory, Kirtland AFB, NM, AFWL-TR-74-280, (1975).

D. R. Alexander, R. J. Karaskiewicz, and E. W. Enlow, *Component Statistical Characterization, Parts 1 to 4*, Air Force Weapons Laboratory, Kirtland AFB, NM, AFWL-TR-80-128, Pt. 1-4 (1981).

L. L. Alston, *High-Voltage Technology* (Oxford University Press, London, 1968).

A. Baruah and P. P. Budenstein, "An Electrothermal Model For Current Filamentation in Second Breakdown of Silicon on Sapphire Diodes," *Electrical Overstress/Electrostatic Discharge Symposium Proceedings, 1979* (Reliability Analysis Center, RADC/RBRAC, Griffiss AFB, NY; Denver, CO; 1979), vol. EOS-1, pp. 126-132 (1980).

G. Bedrosien, R. Christie, and V. Tatoian, *A Critical Review of Semiconductor Failure Modeling for Nuclear Hardening* (The Dikewood Corp., Albequerque, NM, 1980).

J. R. Black, "Electromigration--A Brief Survey and Some Recent Results, *IEEE Trans. Elect. Dev. 16*, p. 338 (1969).

D. L. Blackburn and D. W. Berning, "Reverse-Bias Second Breakdown in Power Transistors," *Electrical Overstress/Electrostatic Discharge Symposium Proceedings, 1979* (Reliability Analysis Center, RADC/RBRAC, Griffiss AFB, NY; Denver, CO; 1979), vol. EOS-1, pp. 116-121 (1980).

H. C. Bowers, "Space-Charge-Induced Negative Resistance in Avalanche Diodes," *IEEE Trans. Elect. Dev. ED-15*(6), pp. 343-350 (1968).

P. P. Budenstein et al., *Second Breakdown and Damage in Semiconductor Junction Devices*, U. S. Army Missle Research and Development Command, Redstone Arsenal, AL, RG-TR-72-15 (1972).

E. M. Buturla, P. E. Cottrell, B. M. Grossman, and K. A. Salsburg, "Finite-Element Analysis of Semiconductor Devices: The FIELDAY Program," *IBM J. Res. Develop. 25*(4), pp. 216-231 (1981).

H. B. Cook, *High Power Pulse Testing of Integrated Circuits*, U. S. Army Missle Research and Development Command, Redstone Arsenal, AL, RG-72-22, (1972).

R. L. Davies and F. E. Gentry, "Control of Electric Field at the Surface of *p-n* Junctions," *IEEE Trans. Elect. Dev. ED 11*, pp. 313-323 (1963).

J. Donn and K. I. Nuttal, "An Investigation of the Voltage Sustained by Epitaxial Bipolar Transistors in Current Mode Second Breakdown," *Int. J. Electronics* 45(4), pp. 353-372 (1978).

D. L. Durgin, "An Overview of the Sources and Effects of Electrical Overstress," *Electrical Overstress/Electrostatic Discharge Symposium Proceedings, 1980* (Reliability Analysis Center, RADC/RBRAC, Griffiss AFB, NY; San Diego, CA; 1980), vol. EOS-2, pp. 151-160 (1981).

D. L. Durgin, R. M. Pelzl, W. H. Thompson, and R. C. Walker, "A Survey of EOS/ESD Data Sources," *Electrical Overstress/Electrostatic Discharge Symposium Proceedings, 1982* (Reliability Analysis Center, RADC/RBRAC, Griffiss AFB, NY; Orlando, FL; 1982), vol. EOS-4, pp. 49-55 (1983).

A. C. English, "Mesoplasmas and "Second Breakdown" in Silicon Junctions," *Solid State Electronics 6*, pp. 511-521 (1963).

A. C. English, "Physical Investigation of the Mesoplasma in Silicon," *IEEE Trans. Elect. Dev. ED-13*(8/9), pp. 662-667 (1966).

S. P. Gaur and D. H. Navon, "Two-Dimensional Carrier Flow in a Transistor Structure Under Nonisothermal Conditions," *IEEE Trans. Elect. Dev. ED-23*(1), pp. 50-57 (1976).

A. Goetzberger, B. McDonald, R. H. Haitz, and R. M. Scarlett, "Avalanche Effects in Silicon *p-n* Junctions. II. Structurally Perfect Junctions," *J. App. Physics 34*(6), pp. 1591-1600 (1963).

I. V. Grekhov and A. F. Kardo-Sysoev, "Subnanosecond Current Drops in delayed Breakdown of Silicon *p-n* Junctions," *Sov. Tech. Phys. Lett. 5*(8), pp. 395-396 (1979).

I. V. Grekhov, A. F. Kardo-Sysoev, and L. S. Kostina, "Breakdown Delay and Excitation of Ionization Waves in *p-n* Junctions, " *Sov. Tech. Phys. Lett. 5*(8), pp. 399-400 (1979).

I. V. Grekhov, A. F. Kardo-Sysoev, L. S. Kostina, and S. V. Shenderey, "High-Power Subnanosecond Switch," *Electronics Letters 17*(12), pp. 421-422 (1981).

H. B. Grutchfield and T. J. Montoux, "Current Mode Second Breakdown in Epitaxial Planar Transistors," *IEEE Trans. Elect. Dev. ED-13*(11), p. 743 (1966).

G. D. Hachtel, M. H. Mack, R. R. O'Brien, and B. Speelpenning, "Semiconductor Analysis Using Finite Elements--Part I: Computational Aspects," *IBM J. Res. Develop. 25*(4), pp. 232-245 (1981).

G. D. Hachtel, M. H. Mack, and R. R. O'Brien, "Semiconductor Analysis Using Finite Elements--Part II: IGFET and BJT Case Studies," *IBM J. Res. Develop. 25*(4), pp. 246-260 (1981).

R. H. Haitz, A. Goetzberger, R. M. Scarlett, and W. Shockley, "Avalanche Effects in Silicon *p-n* Junctions. I. Localized Photomultiplication Studies on Microplasmas," *J. App. Physics 34*(6), pp. 1581-1590 (1963).

K. Hane, M. Mogi, and T. Suzuki, "Influence of an External Resistor on Second Breakdown in Epitaxial Planar Transistors," *IEEE Trans. Elect. Dev. ED-26*(2), pp. 157-158 (1979).

E. L. Horgan, O. E. Adams, W. H. Rowan, and L. C. Templar, "EOS/ESD Failure Threshold Analysis Errors, Their Source, Size, and Control," *Electrical Overstress/Electrostatic Discharge Symposium Proceedings, 1981* (Reliability Analysis Center, RADC/RBRAC, Griffiss AFB, NY; Las Vegas, NV; 1981), vol. EOS-3, pp. 151-166 (1982).

E. L. Horgan and T. S. Lin, "Failure Analysis of Semiconductor Devices in EOS/ESD Testing," presented at the 1982 Nuclear Electromagnetic Pulse Meeting (NEM), Univ. of New Mexico, Albequerque, May 24-28, 1982.

P. L. Hower and P. K. Govil, "Comparison of One- and Two-Dimensional Models of Transistor Thermal Instability," *IEEE Trans. Elect. Dev. ED-21*(10), p. 617 (1974).

P. L. Hower, D. L. Blackburn, F. F. Oettinger, and S. Rubin, "Stable Hot Spots and Second Breakdown in Power Transistors," *PESC 76 Record*, 1976 (IEEE Power Electronics Specialists Conference, Cleveland, OH, 1976), pp. 234-246.

R. L. Huffman and D. L. Coleman, *Final Report EMP Characteristics of Sprint Autopilot Components*, Martin Marietta Corp., Orlando, FL, CREG-69-2 (1969).

C. R. Jenkins and D. L. Durgin, "EMP Susceptibility of Integrated Circuits," *IEEE Trans. Nucl. Sci. NS-22*(6), pp. 2494-2499 (1975).

B. M. Kalab, *Analysis of Failure of Electronic Circuits from EMP-Induced Signals--Review and Contribution*, Harry Diamond Laboratories, Adelphi, MD, HDL-TR-1615 (1973).

B. M. Kalab, *Damage Characterization of Semiconductor Devices for the AN/TRC-145 EMP Study*, Harry Diamond Laboratories, Adelphi, MD, HDL-TR-1915 (1980).

K. Kano and H. J. Reich, "Forward Transient Behavior of *p-n* Junction Diodes at High Injection Levels," *IEEE Trans. Elect. Dev. ED-12*, pp. 515-523 (1964).

N. Klein, "Electrical Breakdown in Solids," *Adv. Electr. Electron Physics 26*, L. Martin, Ed., (Academic Press, New York, NY, 1969), pp. 309-424.

C. Kleiner, J. Nelson, F. Vassallo, and E. Heaton, "Integrated Circuit Model Development for EMP," *IEEE Trans. Nucl. Sci. NS-21*, pp. 323-331 (1974).

E. R. Knight and P. P. Budenstein, "Effects of Junction Spikes and Doping Level on the Second Breakdown Susceptibility of Silicon-on-Sapphire Diodes," *Electrical Overstress/Electrostatic Discharge Symposium Proceedings, 1980* (Reliability Analysis Center, RADC/RBRAC, Griffiss AFB, NY; San Diego, CA; 1980), vol. EOS-2, pp. 122-129 (1981).

K. Koyanagi, K. Hane, and T. Suzuki, "Boundary Conditions Between Current Mode and Thermal Mode Second Breakdown in Epitaxial Planar Transistors," *IEEE Trans. Elect. Dev. ED-24*(6), pp. 672-678 (1977).

N. Kusnezov and J. S. Smith, "Modeling of Electrical Overstress in Silicon Devices," *Electrical Overstress/Electrostatic Discharge Symposium Proceedings, 1979* (Reliability Analysis Center, RADC/RBRAC, Griffiss AFB, NY; Denver, CO; 1979), vol. EOS-1, pp. 133-139 (1980).

N. Kusnezov and J. S. Smith, "Modeling of EOS in Silicon Devices," *Electrical Overstress/Electrostatic Discharge Symposium Proceedings, 1981* (Reliability Analysis Center, RADC/RBRAC, Griffiss AFB, NY; Las Vegas, NV; 1981), vol. EOS-3, pp. 132-138 (1982).

H. P. D. Lanyon, "Electron Transport and Ionization in Silicon at High Fields," *Solid State Electronics 21*, p. 291 (1979).

O. J. McAteer, R. E. Twist, and R. C. Walker, "Latent ESD Failures," *Electrical Overstress/Electrostatic Discharge Symposium Proceedings, 1982* (Reliability Analysis Center, RADC/RBRAC, Griffiss AFB, NY; Orlando, FL; 1982), vol. EOS-4, pp. 41-48 (1983).

M. W. Muller and H. Guckel, "Negative Resistance and Filamentary Currents in Avalanching Silicon p^+-i-n^+ Junctions," *IEEE Trans. Elect. Dev. ED-15*(8), pp. 560-568 (1968).

G. W. Neudeck and L. R. Razouk, "The p^+-n^--n^+ Diode Pulsed at Extreme Current Densities--II. The Forward Pulsed Case and its Anomalous Voltage Response," *Solid State Electronics 23*, pp. 151-155 (1980).

H. B. O'Donnell and D. M. Tasca, *Development of high Level Electrical Stress Failure Threshold and Prediction Model for Small Scale Junction Integrated Circuits*, General Electric Co., Philadelphia, PA, Report No. 77SD4252 (1977).

H. M. Olson, "DC Thermal Mode of Semiconductor Device Produces Current Filaments as Stable Current Distributions," *IEEE Trans. Elect. Dev. ED-24*(9), pp. 1177-1184 (1977).

W. J. Orvis, C. F. McConaghy, J. H. Yee, G. H. Khanaka, L. C. Martin, and D. L. Lair, "Modeling and Testing for Second Breakdown Phenomena," *Electrical Overstress/Electrostatic Discharge Symposium Proceedings, 1983*, (Reliability Analysis Center, RADC/RBRAC, Griffiss AFB, NY; Las Vegas, NV; 1983), vol. EOS-5 (also available as Lawrence Livermore National Laboratory, Livermore, CA, UCRL-89147).

D. G. Pierce, "Modeling Metallization Burnout of Integrated Circuits, *Electrical Overstress/Electrostatic Discharge Symposium Proceedings, 1982* (Reliability Analysis Center, RADC/RBRAC, Griffiss AFB, NY; Orlando, FL; 1982), vol. EOS-4, pp. 56-61 (1983).

D. G. Pierce and D. L. Durgin, "An Overview of Electrical Overstress Effects on Semiconductor Devices," *Electrical Overstress/Electrostatic Discharge Symposium Proceedings, 1981* (Reliability Analysis Center, RADC/RBRAC, Griffiss AFB, NY; Las Vegas, NV; 1981), vol. EOS-3, pp. 120-131 (1982).

M. D. Pocha and J. C. Koo, *Avalanche Diode Studies*, Lawrence Livermore National Laboratory, Livermore, CA, unpublished report (1982).

W. M. Portnoy, Investigation of the Physics of Failure in Semiconductors Resulting from Electrical transients, Texas Tech. Univ., Lubbock, TX, Interim report for the Air Force Weapons Laboratory (1982).

W. D. Raburn and W. H. Causey, *Determination of Semiconductor Junction Vulnerability to Second Breakdown*, U. S. Army Missle Research and Development Command, Redstone Arsenal, AL, EA-CR-77-1 (1977).

L. R. Razouk and G. W. Neudeck, "The p^+-n^--n^+ Diode Pulsed at Extreme Current Densities--I. Numerical Techniques and Reverse Pulsed Case," *Solid State Electronics 23*, pp. 143-149 (1980).

L. W. Ricketts, J. E. Bridges, and J. Miletta, *EMP Radiation and Protective Techniques* (Wiley, New York, NY, 1976), Chapter 3.

D. F. Rutherford and J. F. Perkins, Effects of Electrical Overstress o Digital Bipolar Microcircuits and Analysis Techniques for Failure Site Location," *Electrical Overstress/Electrostatic Discharge Symposium Proceedings, 1979* (Reliability Analysis Center, RADC/RBRAC, Griffiss AFB, NY; Denver, CO; 1979), vol. EOS-1, pp. 64-77 (1980).

R. M. Scarlett and W. Shockley, "Secondary Breakdown and Hot Spots in Power Transistors," 1963 *IEEE International Convention Record, Pt. 3, 1963* (IEEE Electron Devices Society and IEEE Reliability Group, , 1963), pp. 3-13.

R. N. Shaw, R. D. Enoch, and R. D. Taylor, "A Versatile Mini-Computer Controlled ESD Test Equipment for Automatic Testing in Human-Body-Models," *Electrical Overstress/Electrostatic Discharge Symposium Proceedings*, (Reliability Analysis Center, RADC/RBRAC, Griffiss AFB, NY; Las Vegas, NV; 1983), vol. EOS-5.

A. H. M. Shousha, "Negative Differential Conductivity Due to Electrothermal Instabilities in Thin Amorphous Films," *J. Appl. Phys. 42*(12), p. 5131 (1971).

J. S. Smith, "Electrical Overstress Failure Analysis in Microcircuits," *16th Annual Proceedings, Reliability Physics 1978* (IEEE Electron Devices Society and IEEE Reliability Group, San Diego, CA, 1978), pp. 41-46.

D. M. Tasca, "Pulse Power Failure Modes in Semiconductors," *IEEE Trans. Nucl. Sci. NS-17*(6), pp. 364-372 (1970).

D. M. Tasca, J. C. Peden, and J.L. Andrews, *Theoretical and Experimental Studies of Semiconductor Device Degradation Due to High Power Electrical Transients*,, Harry Diamond Laboratories, Washington, DC, AD-780-160 (also available as General Electric Co., Philadelphia, PA, Report No. 73SD4289) (1973).

D. M. Tasca, J.C. Peden, and J. Miletta, "Non-Destructive Screening for Second Breakdown," *IEEE Trans. on Nucl. Sci. NS-19*, pp. 57-67 (1972).

D. M. Tasca and S. J. Stokes, III, *EMP Response and Damage Modeling of Diodes, Junction Field Effect Transistor Damage Testing and Semiconductor Device Failure Analysis, Final Report*, Harry Diamond Laboratories, Adelphi, Md, HDL-CR-76-090-1 (1976).

R. E. Thomas, "Semiconductor Device Failure Criteria for Sinusoidal Stresses," *Electrical Overstress/Electrostatic Discharge Symposium Proceedings, 1981* (Reliability Analysis Center, RADC/RBRAC, Griffiss AFB, NY; Las Vegas, NV; 1981), vol. EOS-3, pp. 139-144 (1982).

V. A. J. Van Lint, J. H. Alexander, D.K. Nichols, and P. R. Ward, "Computerized Model for Response of Transistors to a Pulse of Ionizing Radiation," *IEEE Trans. Nucl Sci. NS-14*(6) pp. 170-178 (1967).

A. L. Ward, "Studies of Second Breakdown in Silicon Diodes," *IEEE Trans. on Parts, Hybrids and Packaging PHP-13*(4), pp. 361-368 (1977).

A. L. Ward, "Doping Profiles and Second Breakdown," *Electrical Overstress/Electrostatic Discharge Symposium Proceedings, 1979* (Reliability Analysis Center, RADC/RBRAC, Griffiss AFB, NY; Denver, CO; 1979), vol. EOS-1, pp. 109-115 (1980).

A. L. Ward, *Calculations of Second Breakdown in Silicon Diodes*, Harry Diamond Laboratories, Adelphi, MD, HDL-TR-1978 (1982).

D. C. Wunsch, "The Application of Electrical Overstress Models to Gate Protective Networks," *16th Annual Proceedings, Reliability Physics 1978* (IEEE Electron Devices Society and IEEE Reliability Group, San Diego, CA, 1978), pp. 47-55.

D. C. Wunsch and R. R. Bell, "Determination of Threshold Failure Levels of Semiconductor Diodes and Transistors Due to Pulse Power Voltages," *IEEE Trans. Nucl. Sci. NS-15*(6), pp. 244-259 (1968).

J. H. Yee, W. J. Orvis, L. C. Martin, and J. C. Peterson, "Modeling of Current and Thermal Mode Second Breakdown Phenomena," *Electrical Overstress/Electrostatic Discharge Symposium Proceedings, 1982* (Reliability Analysis Center, RADC/RBRAC, Griffiss AFB, NY; Orlando, FL; 1982), vol. EOS-4, pp. 76-81 (1983).

J. H. Yee, W. J. Orvis, and L. C. Martin, *Theoretical Modeling of EMP Effects in Semiconductor Junction Devices*, Air Force Weapons Laboratory, Kirtland Air Force Base, NM, AFWL-TR-82-91 (also available as Lawrence Livermore National Laboratory, Livermore, CA, UCRL-87672) (1982).

X TABLE OF SYMBOLS

A	Cross-sectional area
C_A	Junction capacitance
$D_n(\|E\|,T,N)$	Electron diffusion coefficient
$D_p(\|E\|,T,N)$	Hole diffusion coefficient
E	Electric field
$G(\|E\|,T,n,p)$	Avalanche generation term
H	Heat of fusion
I	Current
$J = J_n + J_p$	Total carrier current density
J'	DC part of the total current
J_n	Electron current density
J_{ns}	Injection current density, n side
J_p	Hole current density
J_{ps}	Injection current density, p side
$K(T)$	Thermal conductivity
K_d	Damage constant
K_f	Frequency conversion factor
K_m	Thermal conductivity of the metallization
K_{ox}	Thermal conductivity of the oxide
$N = N_D - N_A$	Net positive doping density
N_D	Donor density
N_A	Acceptor density
P	Power
P_D	Square wave damage power
Q	Heat generation per unit time per uint volume
Q_a	Quality factor
Q_f	Final heat; heat required for melting
R	Radius of the cylindrical hot-spot
R_o	Source Impedance
R_s	Surge resistance
T	Absolute temperature
T_j	Ambient temperature
T_m	Final or failure or melting temperature
$U(T,n,p)$	Recombination term
V	Volume
V_0	Peak open-circuit voltage
V_b	Breakdown voltage
W	Depletion width
Z	Impedance
a	Radius of the spherical hot spot
c	Heat capacity
f	frequency
g	Wave vector
k	Thermal diffusivity
k_m	Thermal diffusivity of the metallization
$k_o x$	Thermal diffusivity of the oxide
l	Metallization thickness
n	Electron density
p	Hole density
q	Magnitude of the charge on an electron

r	Radial distance
r_e	Resistivity
r_m	Resistivity at melting point
r_t	Temperature coefficient of the resistivity
s	Surface area
t	Time
$t_p d$	Propagation delay
w	Length of metal wire
x	Distance
α	Avalanche coefficient
$\alpha' = \partial\alpha/\partial E$	Rate of change of α with electric field
$\gamma = R_s/R_0$	
δ	Oxide thickness
ε	Permittivity
θ_{JA}	Thermal resistance of a junction
$\lambda = V_b/V_0$	
$\mu_n(\lvert E\rvert, T, N)$	Electron mobility
$\mu_p(\lvert E\rvert, T, N)$	Hole mobility
ρ	Mass density
τ	Period
φ	Electrostatic potential
ω	Angular frequency

END

FILMED

7-85

DTIC